BERICHTE
aus dem Fachbereich Geowissenschaften
der Universität Bremen

No. 170

Budziak, D.

LATE QUATERNARY MONSOONAL CLIMATE AND RELATED VARIATIONS IN PALEOPRODUCTIVITY AND ALKENONE-DERIVED SEA-SURFACE TEMPERATURES IN THE WESTERN ARABIAN SEA

Berichte, Fachbereich Geowissenschaften, Universität Bremen, No. 170,
114 pages, Bremen 2001

ISSN 0931-0800

The "Berichte aus dem Fachbereich Geowissenschaften" are produced at irregular intervals by the Department of Geosciences, Bremen University.

They serve for the publication of experimental works, Ph.D.-theses and scientific contributions made by members of the department.

Reports can be ordered from:

Gisela Boelen

Sonderforschungsbereich 261

Universität Bremen

Postfach 330 440

D 28334 BREMEN

Phone: (49) 421 218-4124

Fax: (49) 421 218-3116

e-mail: boelen@uni-bremen.de

Citation:

Budziak, D.

Late Quaternary monsoonal climate and related variations in paleoproductivity and alkenone-derived sea-surface temperatures in the western Arabian Sea.

Berichte, Fachbereich Geowissenschaften, Universität Bremen, No. 170, 114 pages, Bremen, 2001.

ISSN 0931-0800

Late Quaternary monsoonal climate and related variations in paleoproductivity and alkenone-derived sea-surface temperatures in the western Arabian Sea

Dissertation

zur Erlangung des

Doktorgrades der Naturwissenschaften

im Fachbereich 5

der Universität Bremen

vorgelegt von

Dörte Budziak

Bremen

2000

Tag des Kolloquiums: 20. Oktober 2000

Gutachter:

1. Herr Prof. Dr. G. Wefer

2. Herr Prof. Dr. V. Ittekkot

Prüfer:

1. Herr Prof. Dr. C. Devey

2. Herr Dr. habil. R. R. Schneider

Table of Contents

ACKNOWLEDGEMENTS

First of all, I wish to express my gratitude to Prof. Dr. Gerold Wefer, who gave me the opportunity for this dissertation, for his advice and support, and to Prof. Dr. Venugopalan Ittekkot for taking on the job of doing the second expert report.

For their encouragement and the many discussions, which greatly improved my knowledge and the quality of this thesis, I am very grateful to Drs. Ralph R. Schneider and Peter J. Müller.

Drs. Lydie Dupont, Henning Kuhnert, Carsten Rühlemann, Stefan Mulitza, H.-Stefan Niebler, Oscar Romero and Gerhard Fischer were always willing to listen to my problems and willing to help me. I would also like to thank my office mates, Drs. Tobias Wolff, Elizabeth M. Holmes and especially Martin Cepek for the quiet working atmosphere. Chris Moos' perpetual scepticism led me to think over my theories.

For their great help and patience during my laboratory work, I am indebted to Hella Buschhoff, Ralph Kreutz and Dietmar Grotheer. Mrs. Carmen Murken, Gisela Boelen, Britta Schilder-Lübben and Adelheid Grimm-Geils were always willing to assist me.

My family and friends provided consistent support and were always there for me. For the excellent IT assistance I am especially thankful to Dipl. Inf. Olaf Bergst.

This research was funded by the Deutsche Forschungsgemeinschaft (Mu 788/2-2) and the Sonderforschungsbereich 261 „Der Südatlantik im Spätquartär".

Zusammenfassung

Die heutige Oberflächenwasser-Hydrographie des Arabischen Meeres wird im wesentlichen bestimmt von der saisonalen Variation der atmosphärischen Zirkulation und deren Intensität. Im Sommer bestimmen starke SW Monsunwinde die Region, während im Winter kalte NE Monsunwinde vorherrschen.

Sedimentkerne der *Meteor*-Reise M31-3 aus dem westlichen Arabischen Meer wurden im Hinblick auf die Gehalte an Alkenonen und organischem Kohlenstoff (TOC) und die Zusammensetzung stabiler Isotope ($\delta^{18}O$, $\delta^{13}C$) untersucht. Ziel dieser Arbeit war es, die Intensität des indischen Monsunsystems und dadurch bedingte Produktivitäts- und Temperaturänderungen im Auftriebsgebiet des westlichen Arabischen Meeres während des Spätquartärs zu rekonstruieren. Alkenon/TOC-Zeitreihen von Kern GeoB 3005 aus dem küstenfernen Auftriebsgebiet in der Nähe des Golfs von Aden wurden verglichen mit Daten von Kern GeoB 3007 vom Owen Rücken, dem 'Ocean Drilling Program' (ODP) Site 723 aus dem küstennahen Auftriebsgebiet vor Oman und mit Kern MD 900963 aus dem östlichen, äquatorialen Arabischen Meer.

Die Alkenon/TOC-Variationen deuten im gesamten Arabischen Meer auf Perioden höherer Produktivität im Einklang mit dem orbitalen Präzessionssignal hin. Betrachtet man allerdings die zeitliche Abfolge der Produktivitätsänderungen in Relation mit der borealen Sommerinsolation, ergeben sich signifikante Unterschiede sowohl zwischen dem westlichen und östlichen Arabischen Meer, als auch zwischen dem Alkenon/TOC-Signal und Auftriebsindikatoren im westlichen Arabischen Meer. Die Alkenon/TOC-Zeitreihen aus dem westlichen Arabischen Meer eilen den aus anderen Arbeiten als Auftriebsindikatoren bekannten Proxies um etwa 5 kyr nach. Im Gegensatz dazu finden Maxima in den Alkenon/TOC-Zeitreihen im westlichen Arabischen Meer etwa 3 kyr vor Produktivitätsmaxima im östlichen Arabischen Meer statt.

Diese Unterschiede in den Phasenbeziehungen zwischen den Produktivitäts- und Auftriebsindikatoren im westlichen und östlichen Arabischen Meer lassen auf unterschiedliche Steuerungsmechanismen schließen. Im westlichen Arabischen Meer scheinen die Alkenon/TOC-Zeitreihen ein kombiniertes Signal aus verminderter SW Monsun gesteuerter Auftriebsintensität und verstärkter Durchmischung infolge von stärkeren und länger andauernden NE Monsunwinden zu dokumentieren. Hingegen im östlichen Arabischen Meer scheint die Produktivität vorwiegend von der Intensität der NE Monsunwinde abhängig zu sein, die sich möglicherweise auch in Phase mit dem globalen Eisvolumen im Frequenzbereich der Präzession verstärken, bzw. abschwächen.

Am Owen Rücken zeigen sich Produktivitätsmaxima während der glazialen Substadien 8.2, 6.2 und 2.2, wobei die präzessionsbezogenen Änderungen an dieser Lokation von nur untergeordneter

Bedeutung sind. Eine mögliche Erklärung hierfür findet sich in der periodischen NW-SE Verlagerung der Findlater Jet Achse, die die Region des küstenfernen Auftriebs im NW von der Konvergenzzone im SE trennt.

Mit Hilfe von Kohlenstoffisotopen planktischer Foraminiferen lassen sich nährstoffabhängige $\delta^{13}C$ Variationen von gelöstem anorganischen Kohlenstoff rekonstruieren. So wurde die Differenz von *Globigerinoides ruber* (w) und der tiefer in der Wassersäule lebenden Art *Neogloboquadrina dutertrei* ($\Delta\delta^{13}C_{r\text{-}d}$) des Kerns GeoB 3005 als Anzeiger von Nährstoffänderungen im Auftriebsgebiet in der Nähe des Golfs von Aden benutzt. Die Resultate der Kreuz-Spektralanalysen zwischen dem $\Delta\delta^{13}C_{r\text{-}d}$ Signal des Kerns GeoB 3005 und anderen Proxies, die zur Rekonstruktion der Auftriebsintensität verwendet werden, deuten darauf hin, daß Produktivitätsmaxima nicht gleichzusetzen sind mit maximalem Auftrieb im westlichen Arabischen Meer. Wichtiger noch als die Intensität des Auftriebs an sich, scheint die Verfügbarkeit von Nährstoffen in den lichtdurchfluteten Wasserschichten zu sein.

Neben der Produktivität wurden auch Oberflächenwassertemperaturen (SSTs) auf der Basis des Untersättigungsgrades der C_{37} Alkenone (UK'37) rekonstruiert. Das Alkenontemperatursignal spiegelt trotz der im westlichen Arabischen Meer so stark ausgeprägten Saisonalität eher Temperaturen des Jahresmittels wider und nicht die der Auftriebssaison während des SW Monsuns. Dies wurde in einem Vergleich der Alkenon-Temperaturen von Oberflächensedimentproben mit rezenten SSTs deutlich.

Die Zeitreihen der Alkenon-Temperaturen der Kerne GeoB 3005 und GeoB 3007 zeigen gleiche Variationen mit warmen SSTs in den Interglazialen und kalten SSTs in den Glazialzeiten. Eine Ausnahme bildet das glaziale Stadium 6, das im Vergleich relativ warm bleibt. Ähnliche Temperaturmuster wurden auch für den Bereich des Küstenauftriebs vor Oman für ODP Site 723 und für das östliche Arabische Meer für Kern MD 900963 rekonstruiert. Diese SST Änderungen verlaufen in guter Übereinstimmung mit der Modulation der borealen Sommerinsolation in den niederen Breiten durch die Ekzentrizität. Ein ausgeprägtes Präzessionssignal, wie es für die Paläoproduktivität im Arabischen Meer charakteristisch zu sein scheint, konnte für die SST-Zeitreihen nicht bestätigt werden.

Obwohl die allgemeinen Temperaturvariationen sehr ähnlich verlaufen, zeigt ein detaillierter Vergleich zwischen dem westlichen und dem östlichen Arabischen Meer signifikante Unterschiede vor allem während kalter Perioden. Möglicherweise kühlten die NE Monsunwinde das westliche Arabische Meer während der Glazialzeiten stärker ab als das östliche Arabische Meer.

Summary

Records of total organic carbon (TOC) and C_{37} alkenones were used as indicators for past primary productivity in the western and eastern Arabian Sea. Data from GeoB 3005, an open ocean site in the western Arabian Sea upwelling area, are compared with similar records of GeoB 3007 from the Owen Ridge, Ocean Drilling Program (ODP) Site 723 from the continental margin off Oman and MD 900963 from the eastern Arabian Sea. TOC/C_{37} alkenone records together with other proxies used to reconstruct upwelling intensity, indicate periods of high productivity in tune with precessional forcing all over the Arabian Sea. Based on their phase-relationship to variations in boreal summer insolation they can be divided into three groups. In the western Arabian Sea the precession-related phasing is different between productivity proxies and those for summer monsoon wind strength and upwelling intensity. TOC and C_{37} alkenone records from the western Arabian Sea lag the other monsoonal indicators by about 5 kyr, but lead productivity indicators from the eastern Arabian Sea by 3 kyr. Based on the differences in phase relationships associated with the precessional cycling between productivity and monsoonal proxies in the western Arabian Sea it is proposed that the TOC/C_{37} alkenone signal in the western Arabian Sea document a combined signal of moderate SW monsoon winds and of strengthened and prolonged NE monsoon winds. In the eastern Arabian Sea the phasing hints to coincidence between maximum productivity and stronger NE monsoon winds associated with precession-related maxima in ice volume.

In contrast, variations in paleoproductivity at site GeoB 3007 from the Owen Ridge indicate productivity maxima during glacial substages 8.2, 6.2 and 2.2, whereas precession-related changes are of only minor importance at this location. The results of frequency analyses confirm that productivity at site GeoB 3007 responds predominantly to glacial-interglacial climate changes, while site GeoB 3005 from the open ocean upwelling region near the Gulf of Aden is dominated by precessional insolation. A possible explanation for the pattern revealed at the Owen Ridge is the periodic NW-SE displacement of the Findlater Jet axis, which separates the region of open ocean upwelling to the northwest from downwelling to the southeast of the jet.

The carbon isotopes of planktic foraminifera reflect nutrient related $\delta^{13}C$ variations of dissolved inorganic carbon. The difference between the planktic foraminifera *Globigerinoides ruber* (w), living in the upper 50 m of the water column, and the deeper living *Neogloboquadrina dutertrei* ($\Delta\delta^{13}C_{r\text{-}d}$) of core GeoB 3005 displays nutrient variations in the

upwelling area near the Gulf of Aden. The results of cross-spectral analyses between $\Delta\delta^{13}C_{r\text{-}d}$ of GeoB 3005 and proxies for SW monsoon intensity indicate, too, a dissociation of productivity from monsoonal upwelling intensity. Instead, productivity depends mainly on the availability of nutrients, while upwelling intensity of sub-surface water masses seems to be of only secondary importance.

Additionally, sea surface temperatures (SSTs) were reconstructed using the unsaturation ratio of C_{37} alkenones. Alkenone SSTs reflect annual mean temperatures rather than explicitly the season of upwelling. This is evident from alkenone SSTs in a transect of surface sediments extending from the inner Gulf of Aden into the western Arabian Sea. The alkenone-derived SST records of GeoB 3005 from the open ocean upwelling region near the Gulf of Aden and GeoB 3007 from the Owen Ridge reveal similar variations with high SSTs during interglacial and low SSTs during glacial periods. The glacial marine oxygen isotope stage (MIS) 6 remains relatively warm and was not as cold as MIS 3 to 4 and 8 according to the alkenone SST. Similar variation-patterns were reconstructed in the coastal upwelling area off Oman for ODP Site 723 as well as in the eastern Arabian Sea for MD 900963, where upwelling is not as pronounced as in the western Arabian Sea. Spectral-analyses indicate that SST changes are in good agreement with the modulation of low-latitude precessional insolation changes by eccentricity. However, they do not show the pronounced cyclicity in the precessional frequency band, which is characteristic for variations in paleoproductivity.

Although the overall variation pattern is very similar, a close comparison between the western (GeoB 3005) and the eastern Arabian Sea (MD 900963) shows larger differences between both sites during cold intervals than during periods of warm SSTs. This is attributed to a more effective cooling of surface waters in the western Arabian Sea by prolonged NE monsoon winds during times of expanded Northern Hemisphere ice-sheets, thereby lowering the annual mean SSTs stronger than in the eastern Arabian Sea.

1. Introduction

1.1 Climate Changes

The Late Quaternary, spanning the past 2 Million years, is characterised by the alternation of glacial and interglacial times. A principle influence on the periodical spreading and retreat of continental ice sheets of the northern and southern Hemispheres are the variations in the Earth's orbit around the sun. These so called Milankovitch cycles have periodicities of 100, 41, 23 and 19 kyr, corresponding to Earth's eccentricity, obliquity and precession, respectively, which in combination control the amount of incoming solar energy.

Detailed studies on the oxygen isotope composition of planktonic foraminifera from oceanic sediment cores confirmed this correspondence between ice volume and variations in the Earth's orbit [*Hays et al.*, 1976]. Thus, deep-sea sediments provide insights into the dynamics of climate changes on time-scales of hundreds to thousands of years. These sediments are studied to understand the complex interactions between atmosphere, ocean, continents and external forcing mechanisms in order to predict future climate changes, which are probably triggered by anthropogenic influences.

Earth's heat budget is controlled by the amount of incoming solar energy and its absorption at the planet's surface. In addition, the amount of outgoing radiation is influenced by greenhouse gases in the atmosphere, e.g. water vapour, carbon dioxide (CO_2) and methane (CH_4). Investigations of the Vostok ice-cores confirmed that global temperature changes went along with variations in CO_2 concentrations [*Petit et al.*, 1999]. Since the beginning of the Industrial Revolution in the 18^{th} century, the atmospheric content of CO_2 increased steadily [*Gross & Gross*, 1996]. Thus, human activities like deforestation of woodlands on the one hand and the burning of fossil carbon resources on the other, may alter the sensitive balance of incoming and outgoing energy.

The oceans play an important role in the withdrawal of CO_2 from the atmosphere. In the seawater the total amount of CO_2 is about 60 times the amount contained in the atmosphere, because CO_2 is highly soluble especially in cold water. Thus, small changes in the ocean's chemistry and temperature may have large effects on the atmosphere. Dissolved CO_2 is organically fixed predominantly by photosynthesising algae (primary production) forming a variety of carbohydrates (CH_2O) and secreting carbonate ($CaCO_3$) shells. Among other factors sunlight and the availability of nutrients in the photic zone determine the growth and distribution of these organisms. Dead organic matter is recycled by respiration or accumulated

in sediments (export production) (Figure 1). These processes, taking place for millions of years, have turned the oceans into major carbon reservoirs [*Berger et al., 1989*; *Gross & Gross*, 1996].

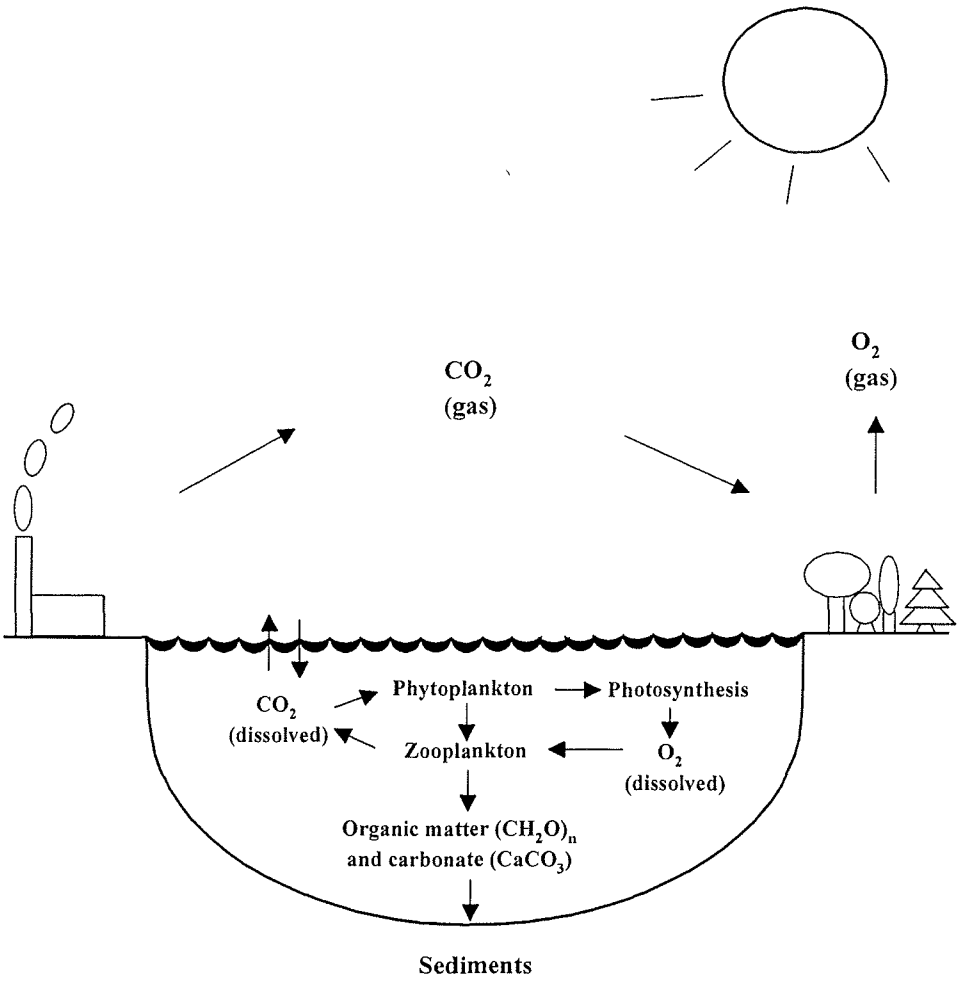

Figure 1: Schematic picture of the biological pump and related withdrawal of atmospheric CO_2 by oceanic processes

Climatic changes are important factors controlling fluctuations of primary productivity in surface waters [*Berger et al.,* 1989]. Hence, the distribution of biogenic particles, total organic carbon (TOC), microfossil assemblages as well as the elemental and isotopic composition of fossil carbonate shells contains information on paleoclimatological conditions [*Pisias et al.*, 1995]. These so called proxies are used to reconstruct e.g. past productivity, sea-surface temperatures (SSTs) and nutrient contents of surface water masses [*Wefer et al.*, 1999].

1.1.1 Productivity Estimates Using Total Organic Carbon and C_{37} Alkenones

Although only a fraction of the organic matter produced in the surface waters is buried in sediments, relative variations in the sedimentary TOC content reflect the intensity of past surface water productivity [e.g. *Müller & Suess*, 1979]. In addition, several organic biomarker compounds can be used to discriminate between different plankton groups and their relative contribution to the sedimentary signal of TOC [*Schubert et al.,* 1998].

One of these biomarkers are alkenones, which are produced by surface dwelling prymnesiophyte algae. Alkenones are long-chain methyl and ethyl ketones and have chain lengths of 37 to 39 carbon atoms (C_{37} to C_{39}) and two or three double bonds in one molecule [*De Leeuw et al.*, 1980; *Brassell*, 1993]. The sedimentary concentration of alkenones has previously been used as productivity indicator by *Rostek et al.* [1994]. Also appearing in older sedimentary rocks [*Farrimond et al.*, 1987], alkenones seem to be relatively stable with regard to diagenetic processes [*Volkman et al.*, 1980].

1.1.2 Temperature Estimates Using C_{37} Alkenones

Another, more popular, area of application for alkenones is their use as paleothermometer in order to reconstruct past SSTs because the ratio of di- and tri-unsaturated C_{37} alkenones changes as a function of temperature [e.g. *Brassell et al.,* 1986; *Prahl & Wakeham,* 1987]. The growth temperature of the alkenone producers, namely *Emiliania huxleyi* and *Gephyrocapsa oceanica* [*Volkman et al.*, 1980], can be estimated by determining this ratio expressed by the keton-unsaturation index UK'37 [*Prahl et al.,* 1988]: UK'37 = ([37:2] / [37:3 + 37:2). This UK'37 index is then to be converted into temperatures applying an empirical formula, e.g. after *Müller et al.*, [1998]: SST (°C) = (UK'37 - 0.044) / 0.033.

1.1.3 Estimates of Nutrient Contents Using Carbon Isotopes

The availability of nutrients in surface waters is one limiting factor on primary productivity. One marker reflecting nutrient availability is the ratio of the stable carbon isotopes ^{13}C and ^{12}C, expressed as $\delta^{13}C$ of carbonate secreting organisms, such as planktonic foraminifera. In photosynthesising organisms ^{12}C is more readily incorporated into the organism than ^{13}C, resulting in an ^{13}C-enrichment in surface waters, relative to deep waters. Thus, $\delta^{13}C$ reflects the intensity of primary productivity, depending in turn on the nutrient content within the ocean's photic zone [*Seibold & Berger,* 1993].

1.2 The Indian Monsoon System

1.2.1 Meteorological Characteristics

Monsoon systems in general, are atmospheric circulation systems characterised by seasonally reversing winds, which result from differential heating of land and ocean. While solar insolation causes large seasonal temperature differences on the continents, the temperature changes in the oceans are comparatively small [*Young*, 1987].

As the summer begins, the Indian continent warms faster than the ocean, heating the overlying air and making it less dense than the surrounding atmosphere (Figure 2a). The warmed air starts to rise and forms a low-pressure area above the Tibetan Plateau. In contrast, the air above the southern Indian Ocean is cooler and forms a high-pressure area. To compensate this pressure gradient, low-level southwesterly winds blow from the sea to the

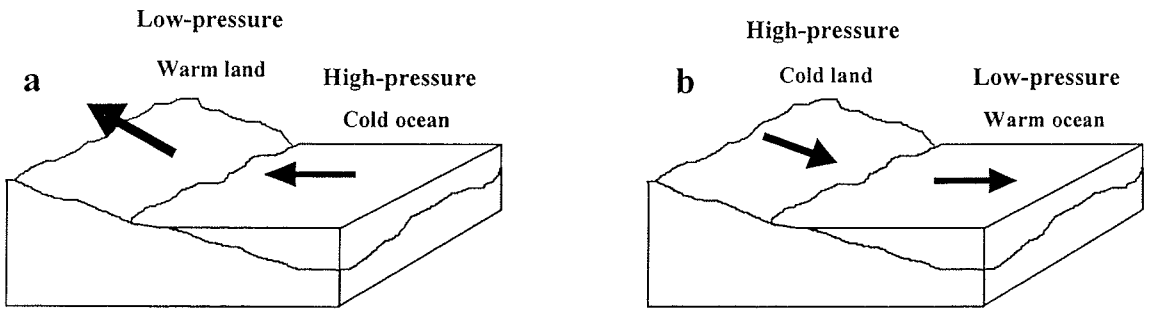

Figure 2: The principle of differential heating and related monsoonal air-flow during the SW and NE monsoon seasons in summer (a) and winter (b), respectively, after *Gross & Gross* [1996].

land in a layer from near the ocean's surface up to a few hundred metres in height, bringing much of the summer rainfall to the Asian continent. In winter, the situation reverses, because the surface water masses of the Indian Ocean retain their warmth relative to the rapidly cooling continent (Figure 2b). Cool, NE monsoon winds blow down from the now snow-covered Tibetan Plateau onto the Arabian Sea. Compared to other monsoon systems of e.g. Africa and Australia the Indian monsoon is particularly strong because of the elevated position of the Tibetan Plateau, which supports the formation of the summer and winter pressure gradients between land and ocean [*Webster*, 1987; *Bigg*, 1996; *Gross & Gross*, 1996].

1.2.2 Establishment of Monsoon-Meteorology

Like no other meteorological phenomenon monsoons played, and still play, an important role on culture, economy and religion of more than half of the world's people, especially in China and India. Since ancient times merchandising seamen, populating the coasts of the northern Indian Ocean, used these seasonally changing winds. The oldest known reports came from lower Mesopotamia and are dated about 2300 B.C. [*Warren*, 1987]. After the pioneering voyage of the Portuguese sailor Vasco da Gama (1468-1524) around Africa in May 1498, regular European trade routes were established between the western and eastern civilisations using the monsoon winds to reach India [*Gross & Gross*, 1996].

It took almost another two centuries before the astronomer Edmund Halley (1656-1742) developed the first descriptive model of the monsoonal system in general in 1686. He used the principle of differential heating in order to explained the origins of the monsoon winds. A second essential driving mechanism was identified by George Hadley (1685-1758) in 1735, who incorporated the effect of Earth's rotation (Coriolis force) on the winds in order to explain the southwesterly or northeasterly orientation observed at the east-west coastlines of the major continents [*Webster*, 1987].

Since then, the knowledge and understanding of Earth's atmosphere has been increased by close observations as well as theory. The lower troposphere, extending from sea-level to an altitude of about 11 km, is heated predominantly by the release of latent heat due to the condensation of water vapour [*Gross & Gross*, 1996]. Thus, the transport and release of latent heat, too, determines the strength and location of the monsoon and its precipitation by storage, redistribution and release of solar energy [*Webster*, 1987].

One of the first attempts to forecast monsoon intensity and associated rainfall variability on the basis of systematic investigations were made by Sir Gilbert Walker (1868-1958), third director of the India Meteorological Department, using among others, historical Nile records [*Kutzbach*, 1987]. Today, there is still need to improve monsoon forecasts based on long-term observations in order to improve agricultural production in countries depending on the monsoonal rainfalls.

1.3 The Arabian Sea: Oceanographic Setting

Although one of the smallest ocean basins, the Arabian Sea provides a high diversity of eutrophic, oligotrophic, upwelling and oxygen-reduced environments. Additionally, a complete semi-annual reversal of wind-induced surface currents is caused by the Indian

monsoon system, making the Arabian Sea an attractive area to study the history of monsoonal climate and related biogeochemical processes.

The oceanic surface circulation of the Arabian Sea is largely determined by the atmospheric flow pattern of the monsoonal winds. With the onset of the SW monsoon winds in April and May, the coastal, northward directed Somali Current develops [*Wyrtki,* 1973]. While the SW monsoon winds prevail, the Somali Current, consists of two gyres, the Southern Gyre and the Great Whirl in the north. By mid-May the East Arabian Current (Figure 3) is established off Arabia [*Tomczak & Godfrey,* 1994]. At the end of August to September the two gyre-system diminishes rapidly and the Somali Current appears as a continuous western boundary current [*Schott,* 1983; *Swallow & Fieux,* 1982].

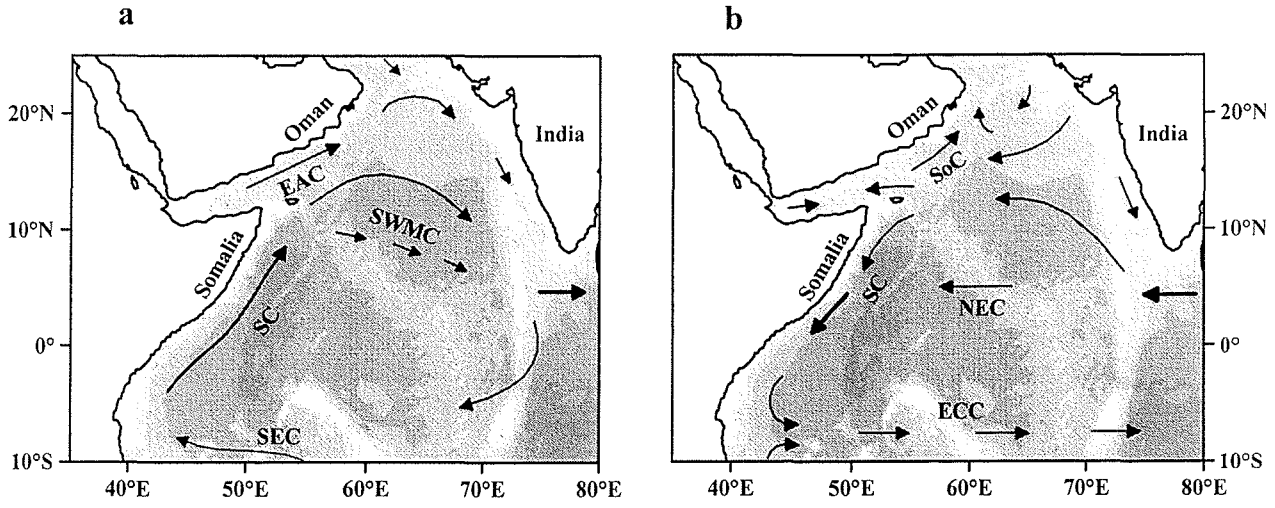

Figure 3: Circulation pattern of the main surface currents in the Arabian Sea during summer (a) and winter (b) after *Brown et al.* [1998]: East Arabian Current (EAC), Equatorial Counter Current (ECC), North Equatorial Current (NEC), Somali Current (SC), Socotra Current (SoC), and South West Monsoon Current (SWMC).

On the basis of Ekman transport coastal upwelling develops off the Somali and Oman coasts during the summer season [*Wyrtki,* 1973]. The SW monsoon winds blow parallel to the coast and drive the ocean circulation: surface water is transported offshore and replaced by colder, nutrient-rich subsurface water masses within a narrow band (100 km) along the coast. Farther offshore, an open ocean type upwelling develops in a broad region (400 km) due to the positive curl in the wind stress [*Swallow,* 1984; *Luther et al.,* 1990; *Brock & McClain,* 1992]. Along the west coast of India weak upwelling may occasionally occur [*Wyrtki,* 1973]. Long-time sediment trap studies report an increase in biogenic and lithogenic particle fluxes with the onset of the summer monsoon in correlation with higher wind speeds and decreasing sea-

surface temperatures (SST) in the western and eastern Arabian Sea [*Nair et al.,* 1989; *Ittekkot et al.,* 1992; *Haake et al.* 1993].

With the onset of the NE monsoon winds in November the Somali Current turns to the south, crosses the equator and flows eastward with the Equatorial Counter Current [*Wyrtki,* 1973]. During this time of the year, the surface circulation of the Indian Ocean resembles the circulation patterns in the Atlantic and Pacific Oceans with characteristic North and South Equatorial Currents and an Equatorial Counter Current (Figure 3). At the peak of the NE monsoon season a weak westward flow, an extension of the North Equatorial Current, dominates the Arabian Sea [*Tomczak & Godfrey,* 1994]. With the exception of moderate upwelling south of Arabia due to the Socotra Current, which flows against the NE monsoon winds [*Swallow,* 1984], the NE monsoon does not induce upwelling but a deepening of the mixed layer. This enhances the primary production and particle fluxes, and lowers the SST in the western Arabian Sea [*Nair et al.,* 1989].

During the NE monsoon season, low salinity water is transported from the Bay of Bengal around the southern tip of India into the eastern Arabian Sea, where it splits into two branches: one continues westward along 5° N, while the other flows along the Indian west coast against the prevailing NE monsoon winds [*Wyrtki,* 1973]. In April the westward flow pattern is reduced, less defined and finally changes into a weak anticyclonic pattern with the onset of the SW monsoon winds [*Tomczak & Godfrey,* 1994].

2. Objectives and Presentation of Results

The main objectives of this dissertation are:

1. To determine the temporal as well as spatial variability of past surface-water productivity in the Arabian Sea, which is recorded in the sedimentary TOC/C_{37} alkenone concentrations.
2. To assess and interpret the different phasing of past variations in surface-water productivity in the Arabian Sea with respect to the primary orbital parameters of eccentricity, obliquity and precessional insolation, as compared to indicators of monsoonal upwelling intensity.
3. To evaluate the temperature signal reflected by the unsaturation ratio of C_{37} alkenones in the western Arabian Sea, where strong seasonal upwelling and concomitant high biogenic fluxes occur.
4. To compare past SST variations in the open-ocean and coastal upwelling regions of the western Arabian Sea with temperature patterns from the eastern Arabian Sea, where upwelling is not as pronounced.

The results corresponding to manuscripts published, submitted or in preparation are presented in chapter 4 as follows:

1. *Late Quaternary insolation forcing on total organic carbon and C_{37} alkenone variations in the Arabian Sea*

D. Budziak, R. R. Schneider, F. Rostek, P. J. Müller, E. Bard and G. Wefer (*Paleoceanography, 15*, 307-321)

Records of TOC and C_{37} alkenones are used as indicators for past primary productivity. New data of GeoB 3005 from the open ocean upwelling region near the Gulf of Aden are compared with similar records from ODP Site 723 from the continental margin off Oman and MD 900963 from the eastern Arabian Sea. These records together with other proxies used to reconstruct upwelling intensity indicate periods of high productivity in tune with precessional forcing. The phase relationship to boreal summer insolation reveals significant differences between proxies for monsoon intensity, productivity in the western Arabian Sea and productivity in the eastern Arabian Sea.

2. *Variations of alkenone-derived sea surface temperatures and productivity patterns of C_{37} alkenones in the Arabian Sea during the Late Quaternary*

D. Budziak, R. R. Schneider, F. Rostek, P. J. Müller, E. Bard and G. Wefer (to be submitted to *Earth and Planetary Science Letters*)

The alkenone SST signal of surface sediments was related to modern SST conditions revealing that alkenone-derived SSTs reflect rather annual mean temperatures than preferentially the season of upwelling. Variations in alkenone-SSTs were reconstructed for GeoB 3005 from the open ocean upwelling region near the Gulf of Aden and compared with SST records from the coastal upwelling region off Oman (ODP Site 723) and from the eastern Arabian Sea (MD 900963). All SST records show similar variation patterns with high SSTs during interglacial and low SSTs during glacial periods. Marine oxygen isotope stage (MIS) 6 differs from this pattern for it remained relatively warm. These SST changes are in good agreement with the modulation of precessional insolation changes by eccentricity. However, they do not show the pronounced cyclicity in the precessional frequency band, which is characteristic for proxies of past variations in primary productivity.

3. *Late Quaternary productivity variations in the Arabian Sea induced by meridional movements in Findlater Jet position*

D. Budziak, C. A. Moos, R. R. Schneider, P. J. Müller and G. Wefer (to be submitted to *Palaeogeography, Palaeoclimatology, Palaeoecology*)

At the Owen Ridge (GeoB 3007) the records of TOC and C_{37} alkenones indicate productivity maxima during glacial substages 8.2, 6.2 and 2.2. In contrast, highest productivity occurred every 20 to 25 kyr at the open ocean upwelling site GeoB 3005. The productivity pattern at the Owen Ridge is attributed to periodic NW-SE displacements of the Findlater Jet axis in tune with glacial-interglacial changes. This axis separates the region of open ocean upwelling to the northwest from downwelling to the southeast of the jet. Site GeoB 3005 lies well within the open ocean upwelling region and therefore is insensitive to changes in the position of the Findlater Jet.

4. *Carbon isotopes of planktic foraminifera recording nutrient and productivity variations in the northwestern Arabian Sea during the past 300,000 yr*

C. A. Moos, D. Budziak, R. R. Schneider and G. Wefer (to be submitted to *Geology*)

Carbon isotopes of planktic foraminifera display nutrient related $\delta^{13}C$ variations of dissolved inorganic carbon ($\delta^{13}C_{\Sigma CO2}$). The difference between the carbon isotope records of the planktic foraminifera *Globigerinoides ruber* (w) and *Neogloboquadrina dutertrei* ($\Delta\delta^{13}C_{r\text{-}d}$) of core GeoB 3005 suggests nutrient availability in surface waters in tune with Earth's orbital parameters of eccentricity and precession, as well as at periods of 12.5 and 7.7 kyr. The results of cross-spectral analyses between $\Delta\delta^{13}C_{r\text{-}d}$ of GeoB 3005 and proxies for SW monsoon intensity indicate that productivity depends mainly on the availability of nutrients, while upwelling intensity of sub-surface waters seems to be of only secondary importance.

The data, which form the basis of this thesis, is archived in the Pangaea database (www.pangaea.de).

3. Material and Methods

3.1 Material

The sediment cores GeoB 3005 and GeoB 3007 as well as the multicorer core-tops presented in this study were recovered during R/V *Meteor* cruise M31/3, reaching from the inner Gulf of Aden into the western Arabian Sea [*Hemleben et al.*, 1996]. The sampling sites are summarised in Table 1. The sediments consist of foraminifera-bearing carbonate ooze with clay [*Hemleben et al.*, 1996] and are intensely bioturbated, which indicate oxygenated conditions of the oceanic bottom waters. No indications for sediment disturbances (hiatus, slumps, etc.) have been detected, except for two sandy foraminiferal layers in core GeoB 3007, which might indicate some winnowing of the fine fraction [*Hemleben et al.*, 1996].

Device	Site GeoB	Station-Nr. [*Hemleben et al.*, 1996]	Lat. (°N)	Long. (°E)	Water depth (m)
MC	3002-1	105	12° 17.3	44° 38.2	752
MC	3003-5	106	13° 29.6	50° 17.7	2013
MC	3004-4	107	14° 36.3	52° 55.2	1801
SL	3005-1	108	14° 58.3	54° 22.2	2316
KL	3005-2	108	14° 58.3	54° 22.0	2309
MC	3005-3	108	14° 58.2	54° 22.2	2313
MC	3006-2	109	15° 49.7	56° 59.7	3521
SL	3007-1	111-1	16° 10.2	59° 45.3	1920
MC	3007-3	111-1	16° 10.2	59° 46.2	1914
MC	3008-5	111-2	16° 05.4	59° 41.0	2223
MC	3009-2	110	16° 12.6	60° 16.8	4071
MC	3010-3	112	17° 45.0	58° 09.0	3165
MC	3011-3	113	16° 31.9	55° 19.9	2624
MC	3012-1	114	14° 32.4	51° 44.9	1538
MC	3013-2	115	13° 18.6	48° 47.0	1731
MC	3014-2	116	12° 51.7	47° 26.1	1626

Table 1: Description of sampling sites during R/V *Meteor* cruise M31/3. Devices used are multicorer cores (MC), gravity cores (SL) and piston cores (KL).

3.2 Methods

The methods used in this study are described in detail in the following manuscripts in chapter 4. Therefore, only a brief overview is given here.

3.2.1 Isotopes and Stratigraphy

The planktonic foraminiferal species *Neogloboquadrina dutertrei* (d'Orbigny) was used for stable oxygen ($\delta^{18}O$) and carbon ($\delta^{13}C$) isotope measurements on GeoB 3005 and GeoB 3007. A Finnigan MAT 251 micromass-spectrometer coupled with a Finnigan automated carbonate device was used to analyse the samples.

The stratigraphic framework of GeoB 3005 was derived from graphic correlation with the SPECMAP $\delta^{18}O$ stack of *Imbrie et al.* [1984]. The age model of GeoB 3007 is based on the correlation of the $\delta^{18}O$ record of the planktonic foraminifera *N. dutertrei* with the $\delta^{18}O$ timescale of the same foraminiferal species in GeoB 3005 using the software package AnalySerie 1.0a7 of *Paillard et al.* [1996]. Sedimentation rates were calculated on the basis of the depth-age model between stratigraphic tie-points.

3.2.2 Organic Carbon and C_{37} Alkenones

A second sample series was freeze dried, ground in an agate mortar and used for carbon and alkenone analyses. Organic carbon was determined on decalcified samples by combustion at 1050 °C using a Heraeus CHN-O-Rapid elemental analyser [*Müller et al.*, 1994]. The concentrations of long-chain unsaturated ketones (alkenones) were determined in 2 g and 5 g aliquots of freeze dried samples [*Müller et al.*, 1994; 1998] in cores GeoB 3005 and GeoB 3007, respectively. The extraction procedure was kept similar for both cores, except for cleaning of every sample of GeoB 3007 and sediment-surface samples by alkaline hydrolysis (saponification) before being analysed by gas chromatography in order to remove possibly interfering fatty methyl esters.

Mass accumulation rates were calculated by multiplying the sedimentary concentrations of TOC and C_{37} alkenones with the dry bulk density of the sediments and the linear sedimentation rates between stratigraphic tie points.

3.2.3 Sea-Surface Temperatures

The ketone unsaturation index UK'37 was calculated according to *Prahl et al.* [1988: UK'37 = (37:2) / (37:2 + 37:3)] and converted to temperature values using the global core top calibration of *Müller et al.* [1998: UK'37 = 0.033 T + 0.044].

3.2.4 Time Series Analyses

The software program SPECTRUM developed by *Schulz & Stattegger* [1997] was used to identify the dominant frequencies in the time series of $\delta^{18}O$, SST and TOC/C_{37} alkenone concentrations as well as mass accumulation rates and to carry out cross-spectral analyses. The latter method does not only include an estimation of coherency, a linear correlation coefficient in the spectral domain, but also estimates the lead or lag reported as positive or negative phase angles, respectively, between records sharing a similar variance at a given frequency [*Jenkins & Watts*, 1968; *Imbrie et al.*, 1989]. Changes in eccentricity, obliquity and precession index (21st of June, northern hemisphere, SPECMAP convention) were calculated after *Berger* [1978] using the AnalySeries 1.0a7 software package of *Paillard et al.* [1996], normalised and summed in an orbital record referred to as ETP [*Imbrie et al.*, 1989].

4. Manuscripts published, submitted or in preparation

4.1 Late Quaternary insolation forcing on total organic carbon and C_{37} alkenone variations in the Arabian Sea

(*Paleoceanography, 15*, 307-321)

Late Quaternary insolation forcing on total organic carbon and C_{37} alkenone variations in the Arabian Sea

Dörte Budziak[1], Ralph R. Schneider[1], Frauke Rostek[2], Peter J. Müller[1], Edouard Bard[2], and Gerold Wefer[1]

[1]Fachbereich Geowissenschaften, Universität Bremen, Postfach 330 440, 28334 Bremen, Germany

[2]Centre Européen de Reserche et d'Enseignement en Géosciences de l'Environment, Université d'Aix-Marseille III et CNRS-UMR-6635, Europôle de l'Arbois, BP80, 13545 Aix-en-Provence Cedex 4, France

Abstract

We here present records of total organic carbon (TOC) and C_{37} alkenones, used as indicators for past primary productivity, from the western (WAS) and eastern Arabian Sea (EAS). New data from an open ocean site of the WAS upwelling area are compared with similar records from Ocean Drilling Program (ODP) Site 723 from the continental margin off Oman and MD 900963 from the EAS. These records together with other proxies used to reconstruct upwelling intensity, indicate periods of high productivity in tune with precessional forcing. On the basis of their phase relationship to boreal summer insolation they can be divided into three groups: in the WAS differences between monsoonal proxies (1) and productivity (2) document a combined signal of moderate SW monsoon winds and of strengthened and prolonged NE monsoon winds, whereas in the EAS phasing indicates maximum productivity (3) at times of stronger NE monsoon winds associated with precession-related maxima in ice volume.

Introduction

Deep-sea sediment records from the Arabian Sea document the history of the monsoonal circulation in the Indian Ocean. Various studies on wind-transported material such as land-derived pollen spectra [*Van Campo et al.,* 1982] and dust input [*Clemens and Prell,* 1990, 1991; *Sirocko et al.,* 1993] from adjacent landmasses, as well as proxy records of surface water productivity [e.g., *Prell and Kutzbach,* 1987; *Naidu and Malmgren,* 1996; *Reichart et*

al., 1998] revealed a strong link between precessionally driven insolation changes and monsoon intensity. This is in agreement with results from general circulation models (GCM) [e.g., *Prell and Kutzbach,* 1987, 1992; *DeMenocal and Rind,* 1993] pointing to an intensification of SW monsoon winds and enhanced upwelling with increased boreal summer insolation. Additionally, in the precessional frequency band, *Clemens et al.* [1991] documented a time lag of ~ 8 kyr (about -120° on average) between maximum boreal summer insolation (referenced to June 21) and various indicators of SW monsoon winds and related upwelling intensity. Thus radiative forcing alone cannot account for the timing of strong monsoons. *Clemens et al.* [1991] concluded that this time lag is phase-locked to the cross-equatorial transport and release of latent heat over the Tibetan Plateau resulting in intensified summer monsoon winds.

In the northern Arabian Sea, *Reichart et al.* [1998] used a variety of productivity proxies, e.g., variations of total organic carbon (TOC), to examine variations in the Indian monsoon system, applying an age model independent of the Spectral Mapping Project (SPECMAP) reference stack [*Imbrie et al.,* 1984]. Their results indicate that precession-related productivity maxima lag boreal summer insolation maxima by ~ 6 kyr (about -94°) on average. This lag is attributed to a prolonged summer monsoon season linked to late instead of early summer insolation [*Reichart et al.,* 1998].

In contrast, sediments from shallower sites at the continental slope off Oman seem to be more influenced by changes in climatic boundary conditions associated with glacial-interglacial cycles due to sea level changes and resulting sea-landward shifts of the coastal upwelling cells [*Emeis,* 1993]. Accordingly, data from Ocean Drilling Program (ODP) Site 723 suggested that the SW monsoon was weakened during glacial times as compared to the interglacials [*Niitsuma et al.,* 1991; *Anderson and Prell,* 1993]. This was interpreted to result from a glacial reduction of the pressure gradient between the ice-covered Tibetan Plateau and the Indian Ocean [*Prell,* 1984]. Consequently, the authors concluded that upwelling and the resulting primary production were reduced during cold climate periods.

In addition, paleoproductivity records revealed a different phasing with respect to boreal summer insolation between the western (WAS) and eastern Arabian Sea (EAS). *Emeis* [1993] used TOC accumulation rates to reconstruct paleoproductivity at ODP Site 723. The precessional component in this record, though of minor importance at this site, indicates a rather opposite phasing +10.7 kyr (+167°) [*Emeis,* 1993], while in the EAS a paleoproductivity reconstruction based on the coccolithophorid *Florisphaera profunda* showed a lead of +7.7 kyr (+120°) with respect to maximum summer insolation [*Beaufort et*

al., 1997]. Therefore these former studies raise two questions: (1) How important is the 100 kyr cycle, and (2) what is the reason for the difference in the phasing of primary productivity records relative to precession and insolation changes?

In order to reassess the different phasing of TOC variations and related paleoproductivity in the Arabian Sea, we here present new data of TOC and C_{37} alkenone (C_{37}) variations of core GeoB 3005, an open ocean site from within the upwelling area of the WAS (14°58.3'N, 54°22.2'E; 2310 m), in combination with ODP Site 723 (18°03.079'N, 57°36.561'E; 816 m) [*Emeis,* 1993*; Emeis et al.,* 1995] and MD 900963 from the EAS (05°04'N, 73°53'E; 2450 m) [*Rostek et al,* 1994, 1997].

Monsoon Meteorology and Hydrographic Setting

The dominant component of tropical climate variability in the Arabian Sea is the seasonal reversal of atmospheric circulation and precipitation associated with the Asian monsoon system. The distribution of a continental landmass in the north and a large ocean in the south leads to this reversal of air flow [*Cadet,* 1979]. During the Northern Hemisphere's Summer the southern Asian continent heats up more than the Indian Ocean. This extra heating causes a low-pressure cell over the Tibetan Plateau and a pressure high above the Indian Ocean. The formation of a strong, low-level jet stream known as the Findlater Jet [*Findlater,* 1969] is the result. Latent heat, absorbed over the southern subtropical ocean, transported northward across the equator, and released by precipitation over the Indian continent, controls the intensity of this jet [e.g., *Webster,* 1987].

The strong coupling between atmosphere and ocean and the seasonal changes in wind direction as well as wind intensities cause a complete semiannual reversal of surface currents in the Arabian Sea basin affecting primary productivity. *Haake et al.* [1993] described enhanced fluxes during both the SW and NE monsoon seasons. Lower fluxes were observed during the intermonsoon seasons in the WAS and central Arabian Sea (CAS), whereas peak fluxes in the EAS do not start until the late SW monsoon period, which lasts until the end of October [*Haake et al.,* 1993]. Here particle fluxes are more variable during the rest of the year. On average, highest biogenic flux rates occur in the WAS, and lower fluxes occur in the CAS and EAS. *Rixen et al.* [1996] observed that at least in the WAS, particle fluxes are controlled not only by the intensity of the upwelling systems but additionally by the amount of cold, nutrient-poor water masses which are transported from south of the equator into the

upwelling region off Oman, where highest fluxes occur during SW monsoons with moderate wind speeds.

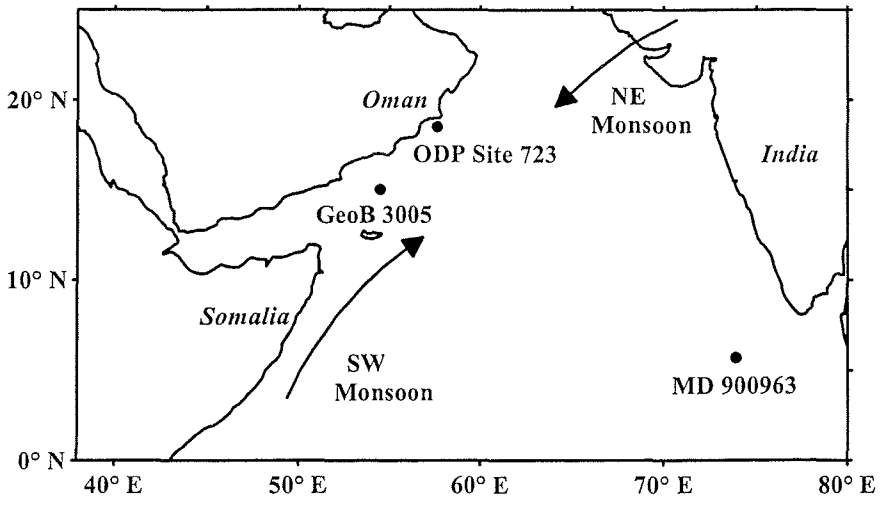

Figure 1: Map of the Indian Ocean north of the equator. Indicated are the locations of cores GeoB 3005, Ocean Drilling Program (ODP) Site 723, and MD 900963. Arrows show major wind directions of the Indian monsoon system during summer (SW monsoon) and winter seasons (NE monsoon).

During the summer season, coastal upwelling develops off the Somali and Oman coasts [*Wyrtki,* 1973] because of Ekman transport. As the SW monsoon winds, blowing parallel to the coast with the coast on its left (Figure 1), drive the ocean circulation, surface water is transported offshore and replaced by colder, nutrient-rich subsurface water masses within a narrow band (100 km) along the coast. Farther offshore, an open ocean-type upwelling develops in a broad region (400 km) because of the positive curl in the wind stress [*Swallow,* 1984; *Luther et al.,* 1990; *Brock and McClain,* 1992]. Along the west coast of India, weak upwelling may occur under favorable conditions [*Wyrtki,* 1973]. Long-time sediment trap studies report an increase in biogenic and lithogenic particle fluxes with the onset of the summer monsoon in correlation with higher wind speeds and decreasing sea surface temperatures in the WAS and EAS [*Nair et al.,* 1989; *Ittekkot et al.,* 1992; *Haake et al.,* 1993].

With the cooling of the Tibetan Plateau the atmospheric pressure gradient reverses and initiates the winter monsoon. A moderate, cool NE monsoon wind (Figure 1) compensates the pressure gradient between a now persisting high-pressure cell above the snow-covered Tibetan Plateau and a pressure low over the Indian Ocean [e.g., *Hastenrath and Lamb,* 1979]. During

the 1995 U.S. Joint Global Ocean Flux Study (JGOFS) Arabian Sea Process Study, *Hansell and Peltzer* [1998] examined TOC concentrations in the upper ocean. They described highest TOC concentrations in the mixed layer during the NE monsoon period remaining through to mid summer, while lowest TOC concentrations in the mixed layer occurred in late summer.

Material and Methods

Material

During *R/V Meteor* cruise M31/3 a gravity core (GeoB 3005-1, water depth 2316 m), a piston core (GeoB 3005-2, water depth 2309 m), and a multicorer core (GeoB 3005-3, water depth 2316 m) were recovered from a station within the upwelling area in the WAS (14°58.3´N, 54°22.2´E, site 108 in the work of *Hemleben et al.* [1996]). To minimize possible effects caused by lateral sediment transport from the continental margin, the site was positioned on a submarine plateau. GeoB 3005-1 was sampled over its entire length (1098 cm) at 5 cm intervals with 10 mL syringes and GeoB 3005-2 only between 748 and 1948 cm. These samples were stored at 4°C. GeoB 3005-3 was sampled in 1 cm slices on board, and the samples were stored frozen.

Methods

One sample series of the cores from station GeoB 3005 was wet sieved to obtain the coarse fraction (> 63 μm) which was used to pick the planktonic foraminiferal species *Neogloboquadrina dutertrei* (d'Orbigny) for stable oxygen isotope ($\delta^{18}O$) measurements. The samples were analyzed using a Finnigan MAT 251 micromass spectrometer coupled with a Finnigan automated carbonate device. The carbonate was reacted with 100% orthophosphoric acid at 75°C. The reproducibility (1 σ) based on replicate measurements of a laboratory internal carbonate standard (Solnhofen limestone) is +/- 0.07 $^{0}/_{00}$.

A second sample series was freeze-dried, ground in an agate mortar, and used for carbon and alkenone analyses. Organic carbon was determined on decalcified samples by combustion at 1050°C using a Heraeus CHN-O-Rapid elemental analyzer [*Müller et al.,* 1994]. The precision of the measurements was better than 3% on the basis of duplicates and a laboratory internal reference sediment (WS2).

The concentrations of C_{37} alkenones (long-chain unsaturated ketones, which are biosynthesized by coccolithophorids of the class *Haptophytes* [*Volkman et al.,* 1995]) were

determined in 2 g aliquots of freeze-dried sediment samples. The samples were extracted with a UP200H ultrasonication disruptor probe (S3 micropoint, amplitude 0.5, and pulse 0.5) and successively less polar solvent mixtures (MeOH, MeOH/CH_2Cl_2 (1:1), and CH_2Cl_2), each for 3 min. The extracts were combined, washed with demineralized water to remove sea salt and methanol, dried over Na_2SO_4, concentrated under N_2, and finally taken up in 25 µL of a 1:1 (volume) MeOH/CH_2Cl_2 mixture.

3 µL aliquots of the final extracts were analyzed by capillary gas chromatography using a HP 5890 Series II gas chromatograph (GC) equipped with a 50 m x 0.32 mm inner diameter (ID) HP Ultra 1 (cross-linked methyl silicone) fused silica column, a split injector (1:10), and a flame ionisation detector. Helium was used as carrier gas. The GC was programmed from 50° to 150°C at 30°C/min, 150° to 230°C at 8°C/min, and 230° to 320°C at 6°C/min, followed by an isothermal period of 45 min. Quantification of C_{37} alkenones was achieved by an internal standard method using octacosane acid methyl ester (OCSME) and the relative response factor of the C_{38} *n*-alkane as internal standards.

To avoid dilution effects caused by changes in the sedimentation rate due to varying input of terrigenous detritus and other major biogenic components (e.g., carbonate when considering the TOC and alkenone fluctuations), mass accumulation rates of TOC (TOC MAR) and C_{37} (C_{37} MAR) were calculated for all cores: The concentrations of TOC and C_{37} were multiplied with the dry bulk density of the sediments and the linear sedimentation rates between stratigraphic tie-points.

To correlate the last 300 kyr with a record from the EAS, core sampling of MD 900963 was extended to a depth of 1720 cm. For the extended part of MD 900963, TOC was determined using a NA 1500 (FISONS) elemental analyzer. Samples were treated using the method described by *Verardo et al.* [1990]. Sample preparation and technical details used at Centre Européen de Reserche et d'Enseignement en Géosciences de l'Environment (CEREGE) for extending the alkenone record of core MD 900963 are given elsewhere [*Sonzogni et al.,* 1997a,b]. Sample treatment and determination of TOC and alkenone data of ODP Site 723, provided by K.-C. Emeis, were previously described in detail by *Emeis* [1993].

The software program SPECTRUM developed by *Schulz and Stattegger* [1997] was used to identify the dominant frequencies in the records of $\delta^{18}O$, TOC, TOC MAR, C_{37}, and C_{37} MAR and to carry out cross-spectral analyses. Because of an internal algorithm this software does not need equidistant time series. To prove the statistical significance, a Fischer/Siegel test was employed in the subroutine „Harmonic". The same parameters were used in these calculation procedures (level of significance is 0.05, Oversampling Factor

(OFAC) is 4, and High Frequency Factor (HIFAC) is 1). For a more precise evaluation of temporal correspondence between boreal summer insolation and TOC time series, cross-spectral analyses were performed. This method does not only include an estimation of coherency, a linear correlation coefficient in the spectral domain, but also estimates the lead (+) or lag (-) reported as phase angles between +180° and -180°, respectively, between records sharing a similar variance at a given frequency [*Jenkins and Watts,* 1968; *Imbrie et al.,* 1989].

Three records of Northern Hemisphere summer insolation were generated for June 21 at 30°N after *Berger* [1978], with time resolutions of 2.5, 1.6, and 0.75 kyr in accordance with the mean time resolutions of the TOC records from ODP Site 723, MD 900963 and GeoB 3005, respectively. The calculation procedure of the cross-spectral analyses was also kept constant for all records (level of significance is 0.1, OFAC is 4, HIFAC is 1; window type is Welch, and 2 segments with 50% overlap; see *Schulz and Stattegger* [1997] for further details).

Stratigraphy

The $\delta^{18}O$ records of the planktonic foraminifera *N. dutertrei* of GeoB 3005-1 (gravity core), GeoB 3005-2 (piston core), and GeoB 3005-3 (multicorer core) were used to combine these three cores and to build a stratigraphic framework. The gravity and piston cores were brought together within an overlapping section from 938 to 1158 cm (original core depth) by peak to peak correlation. On the basis of both the isotopic and TOC records, GeoB 3005-3 was set on top of the stacked cores (Figure 2a). Zero age is assumed for the multicorer surface. Afterward, for the sake of homogeneity with a common timescale, the stable oxygen isotope record of *N. dutertrei* was correlated to the widely used marine oxygen isotope stages (MIS) of the SPECMAP $\delta^{18}O$ stack (Table 1) [*Imbrie et al.,* 1984] using the software program AnalySeries 1.0a7 [*Paillard et al.,* 1996].

According to our age model, the composite sediment record at site GeoB 3005 resolves the last 307 kyr, showing an average sedimentation rate of ~ 7 cm/kyr. The linear sedimentation rates were calculated between stratigraphic tie-points and range from 5 cm/kyr in MIS 7 up to 10 cm/kyr in MIS 2, as shown in Figure 2b. Thus the mean time resolution of samples taken at intervals of 5 cm lies between 500 and 1000 years.

Event	Time, kyr	Depth, cm
Sediment Surface	0	0.5
2	12	98
2.2	19	163
3.1	28	253
3.3	53	453
4.2	65	558
5.1	80	673
5.2	87	728
5.3	99	808
5.4	107	858
5.5	122	958
6.2	135	1033
6.4	151	1128
6.5	171	1238
6.6	183	1313
7.1	194	1383
7.2	205	1438
7.4	228	1563
7.5	238	1633
8.2	249	1718
8.4	269	1883
8.5	287	1998
8.6	299	2078
End of core	307	2138

Table 1: Isotopic events used as stratigraphic control points from correlation of the timescale of the Spectral Mapping Project (SPECMAP) with GeoB 3005. SPECMAP is from *Imbrie et al.* [1984], and GeoB 3005 is in centimeters.

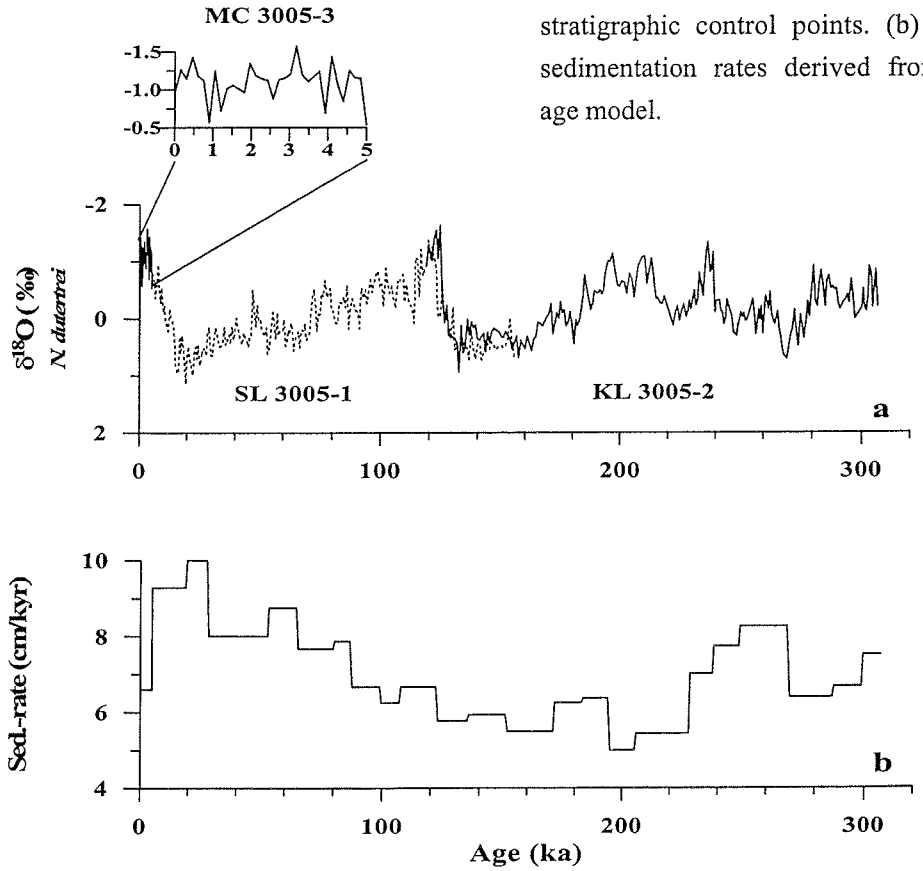

Figure 2: (a) Combination of GeoB cores 3005-1 and 3005-2 within an overlapping section (119 to 156 kyr). GeoB 3005-3 was set on top. Isotopic events (Table 1) were used as stratigraphic control points. (b) Linear sedimentation rates derived from this age model.

The $\delta^{18}O$ signals of the planktonic foraminiferal species *Pulleniatina obliquiloculata* and *Globigerinoides ruber* were used to establish the stratigraphic framework of ODP Site 723 [*Niitsuma et al.,* 1991; *Emeis,* 1993; *Emeis et al.,* 1995] and of core MD 900963 [*Bassinot et al.,* 1994], respectively.

Results

Western Arabian Sea, Open Ocean: GeoB 3005

The $\delta^{18}O$ signal of the planktonic foraminifera *N. dutertrei* (Figure 3) reflects the typical late Quaternary pattern of global glacial to interglacial climate changes. In contrast, the records of TOC and C_{37} (Figure 3), paralleling each other, reach maximum values every 20 to 25 kyr. Except for the high values during the Holocene, probably because of lacking diagenetic equilibrium, TOC ranges between 0.4 and 2.1%. The absolute concentration of C_{37} shows pronounced variations between 400 and 6900 ng/g dry sediment. During the Holocene the alkenone content remains relatively low.

TOC MAR and C_{37} MAR of GeoB 3005 show variations between 0.2 and 1.31 g/m^2 per year, and 14 and 356 $\mu g/m^2$ per year, respectively. The pronounced periodicity with minimum and maximum values occurring during glacial as well as interglacial stages every 20 to 25 kyr are still obvious in the TOC MAR and C_{37} MAR of GeoB 3005.

In the variance power spectrum the $\delta^{18}O$ signal (Figure 4) exhibits peaks at periods (1/frequency) of 112, 40, and 23 kyr in the eccentricity, obliquity, and precessional bands, respectively, with decreasing variance toward the higher frequencies. Periodicities > 100 kyr have to be interpreted with caution because of the relative shortness of the time series of GeoB 3005, but they clearly indicate that the $\delta^{18}O$ record reflects the global changes in sea water $\delta^{18}O$ due to the buildup and retreat of continental icemasses and changes in sea surface temperatures during the last 307 kyr.

A different distribution of variance is revealed in the time series of TOC and C_{37} (Figure 4). Dominant variance is concentrated within the precession band of both records. Only TOC reveals a significant peak in the obliquity band. Variance in the low-frequency domain of eccentricity is present in C_{37} but is of only secondary importance in the TOC record. The overall dominance of the 23 kyr periodicity in the TOC and C_{37} records indicates a precessionally related forcing rather than changes in the glacial boundary conditions. The results of the spectral analyses of TOC MAR and C_{37} MAR (Figure 4) are in accordance with

TOC and C_{37}, which indicates that changes in the sedimentation rate do not significantly influence these signals at this site.

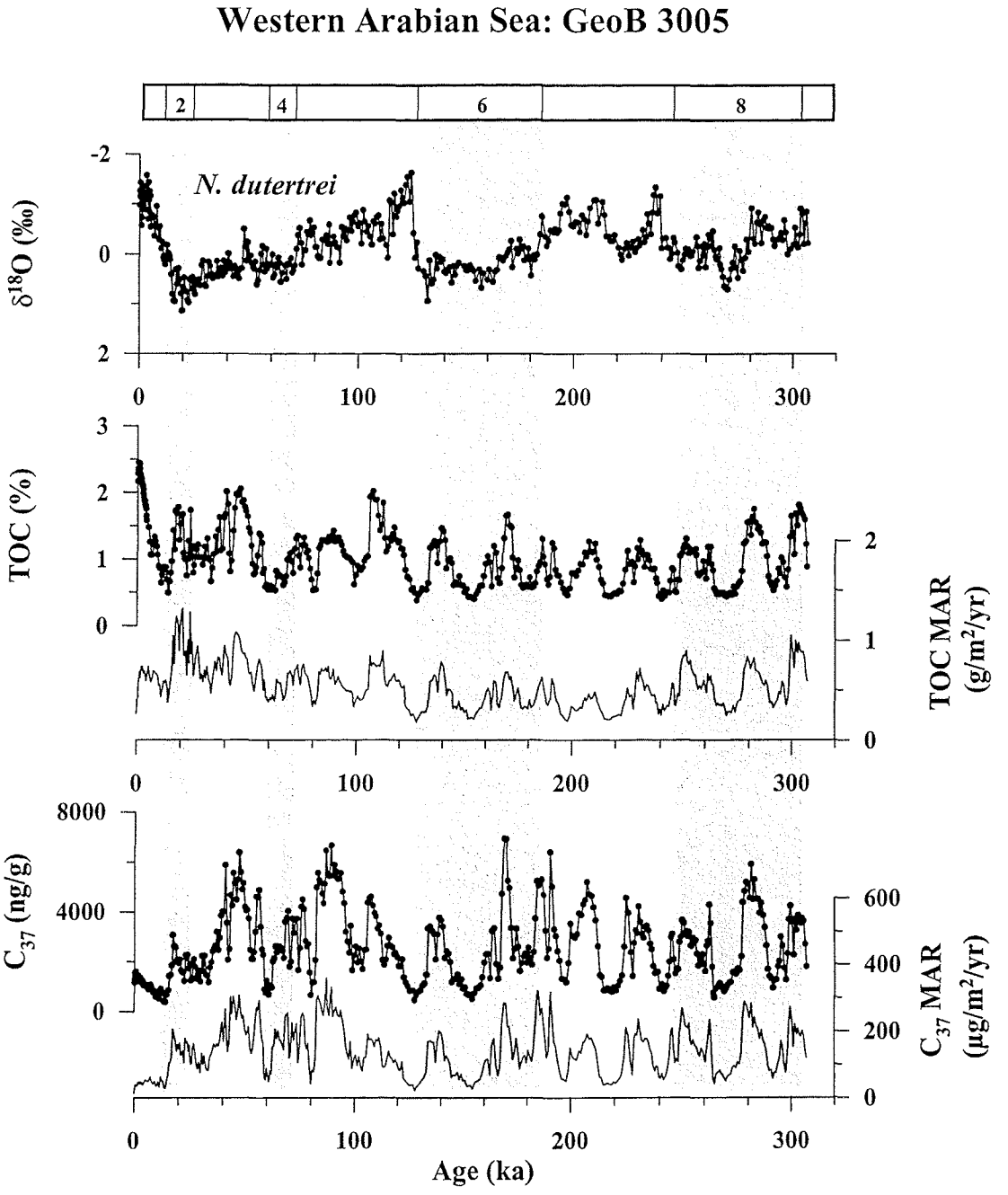

Figure 3: Time series of the $\delta^{18}O$ record of the planktonic foraminifera *Neogloboquadrina dutertrei*, total organic carbon (TOC) concentrations and mass accumulation rates (TOC MAR), and C_{37} alkenone concentrations (C_{37}) and mass accumulation rates (C_{37} MAR) for core GeoB 3005.

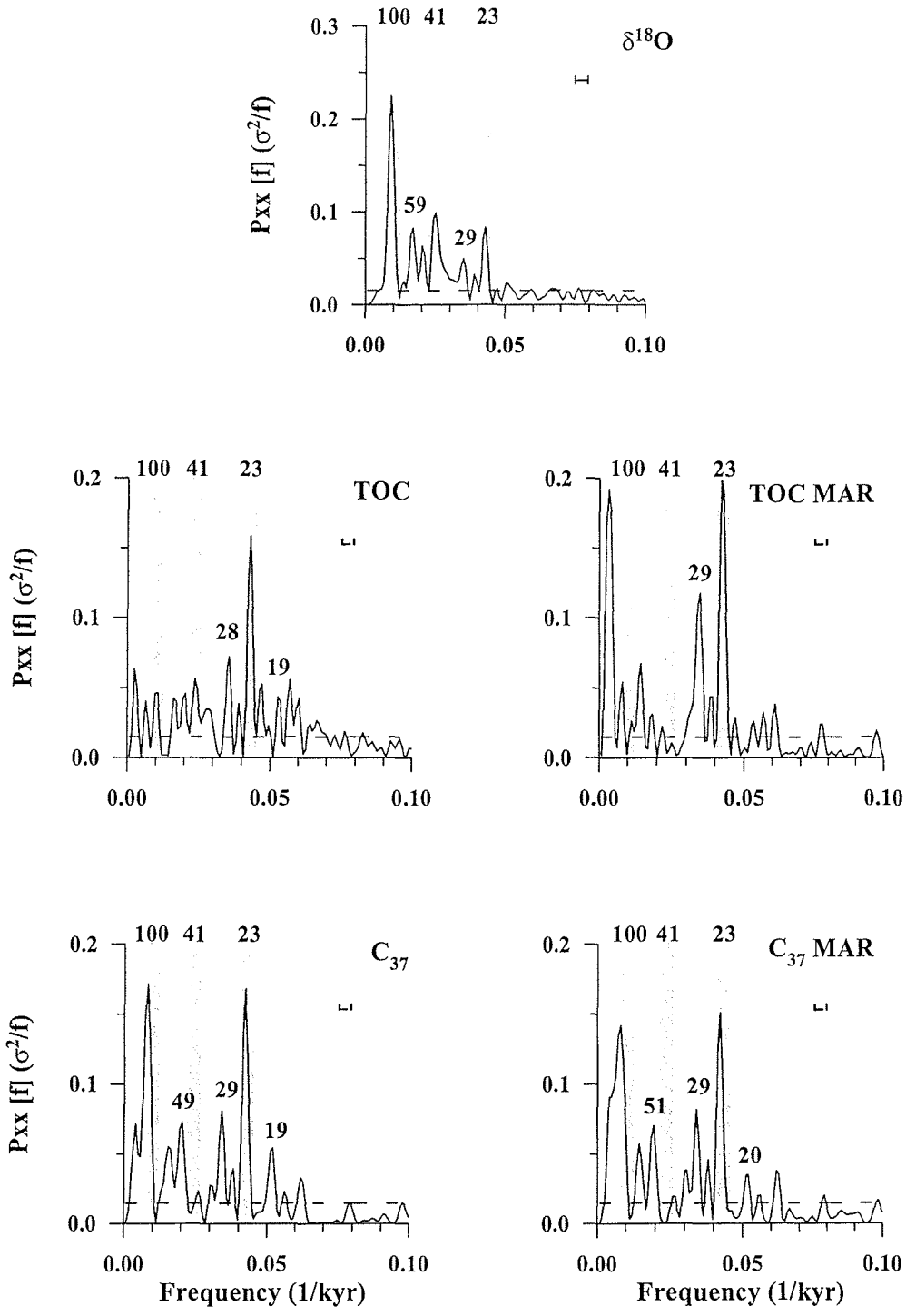

Figure 4: Results of harmonic analysis calculated on the $\delta^{18}O$, TOC, TOC MAR, C_{37} and C_{37} MAR records of GeoB 3005 using the software program SPECTRUM [*Schulz and Stattegger,* 1997]. A Fischer/Siegel test (dashed line) for compound periodicity was employed, and significant peaks outside the eccentricity (100), obliquity (41), and precession band (23) are labeled separately. Horizontal bar marks 6 dB bandwidth for each calculation.

Western Arabian Sea, Continental Slope off Oman: ODP Site 723

For comparison with a coastal upwelling site in the WAS we here reconsider results from ODP Site 723 [*Emeis,* 1993; *Emeis et al.,* 1995]. Variations of TOC (Figure 5) range between 0.5 and 7.5%. At ODP Site 723, TOC values are consistently higher during interglacial periods [*Emeis,* 1993; *Emeis et al.,* 1995] (Figure 5). Superimposed on these fluctuations in the low-frequency domain are variations which indicate, similar to GeoB 3005, periodic increases at time intervals of ~ 20 to 25 kyr. These are still evident within the TOC MAR (0.8 to 13 g/m^2 per year) (Figure 5), although ODP Site 723 exhibits intervals of very high TOC accumulation around 10 to 20 kyr, 60 to 80 kyr, and 130 to 150 kyr corresponding to the glacial maxima in MIS 2, 4, and 6, respectively [*Emeis et al.,* 1995]. The difference between glacial and interglacial sedimentation rates seems to be less pronounced in sediments older than MIS 6, when TOC and TOC MAR show a more parallel progress [*Emeis,* 1993; *Emeis et al.,* 1995].

At ODP Site 723 the concentrations of C_{37} (Figure 5) range between 47 and 4508 ng/g dry sediment, and thus are rather low compared to the other sites. In contrast, C_{37} MAR (Figure 5) (5 to 1158 $\mu g/m^2$ per year) is higher than in the WAS and EAS open ocean sites. Variations of C_{37} and C_{37} MAR are in good accordance with each other, while higher amounts of C_{37} are revealed in glacial stages 8 to 4, following more closely the pattern of TOC MAR.

The results of the spectral analyses of TOC (Figure 7) show the major peak in the eccentricity band and decreasing variance toward the higher frequencies, while TOC MAR is dominated by variance in the obliquity band. Although of minor importance at this site, variance in the precessional frequency band is still present. In contrast to ODP Site 723, the productivity records of GeoB 3005 have varied in tune with precessional forcing but have no clear 41 kyr cyclicity.

Eastern Arabian Sea, Open Ocean: MD 900963

At site MD 900963, TOC varies between 0.2 and 0.9 % during the last 330 kyr. Thus highest values are reached off Oman, and intermediate and lowest values are reached in the WAS and EAS, respectively. In the EAS, highest TOC (Figure 6) values are associated with glacial $\delta^{18}O$ maxima, and lower values are associated with interglacial minima every 20 to 25 kyr [*Rostek et al.,* 1994]. The TOC MAR (0.08 to 0.33 g/m^2 per year) follow the pattern of the TOC record, while the concentrations of C_{37} alkenones (243 to 6696 ng/g dry sediment)

and C_{37} MAR (6 to 242 $\mu g/m^2$ per year) (Figure 6) also parallel these variations [*Rostek et al.*, 1994].

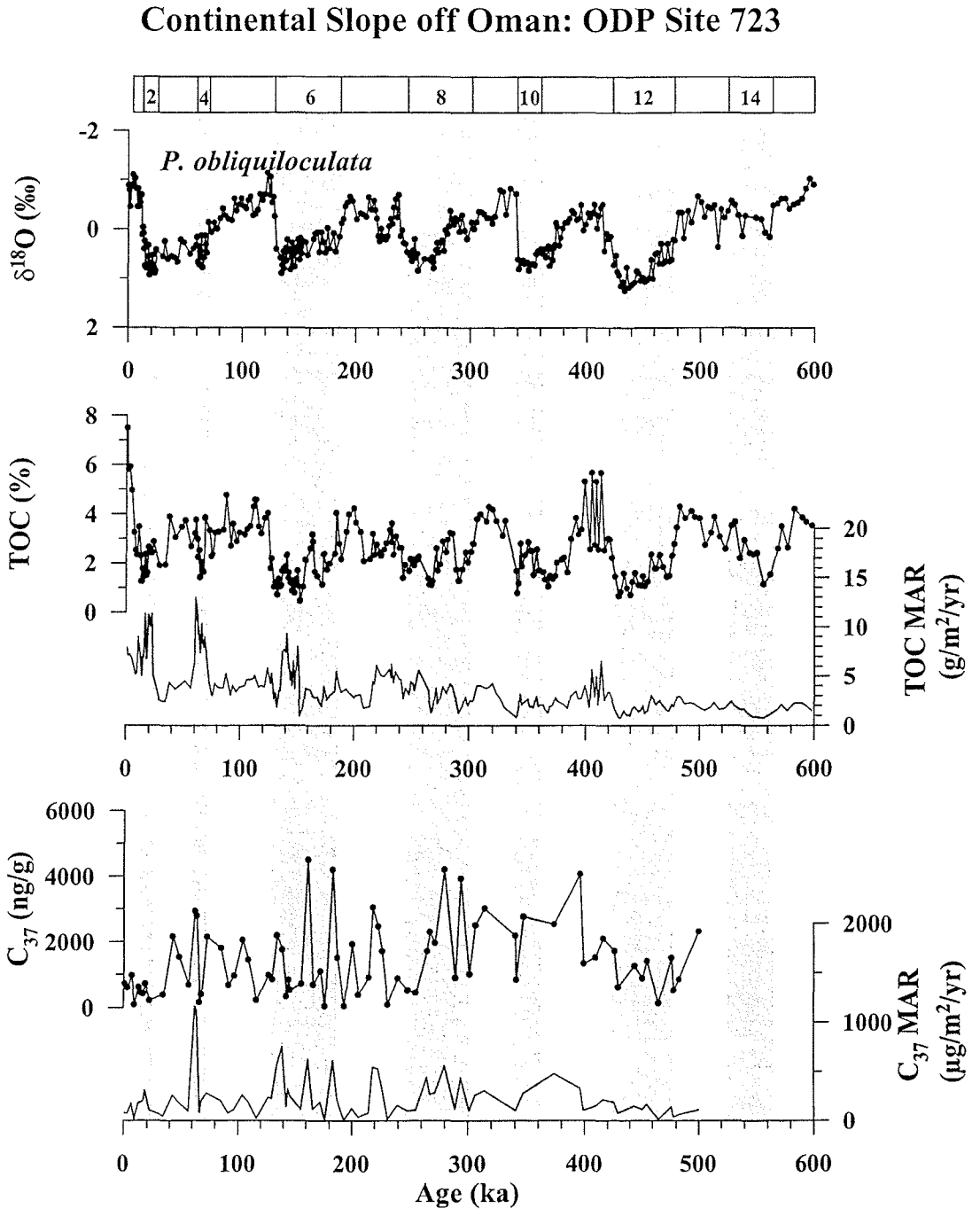

Figure 5: Time series of $\delta^{18}O$ of the planktonic foraminifera *Pulleniatina obliquiloculata*, TOC, TOC MAR, C_{37}, and C_{37} MAR for ODP Site 723 [*Niitsuma et al.*, 1991; *Emeis, 1993*; *Emeis et al.*, 1995]. Data was kindly provided by K.-C. Emeis.

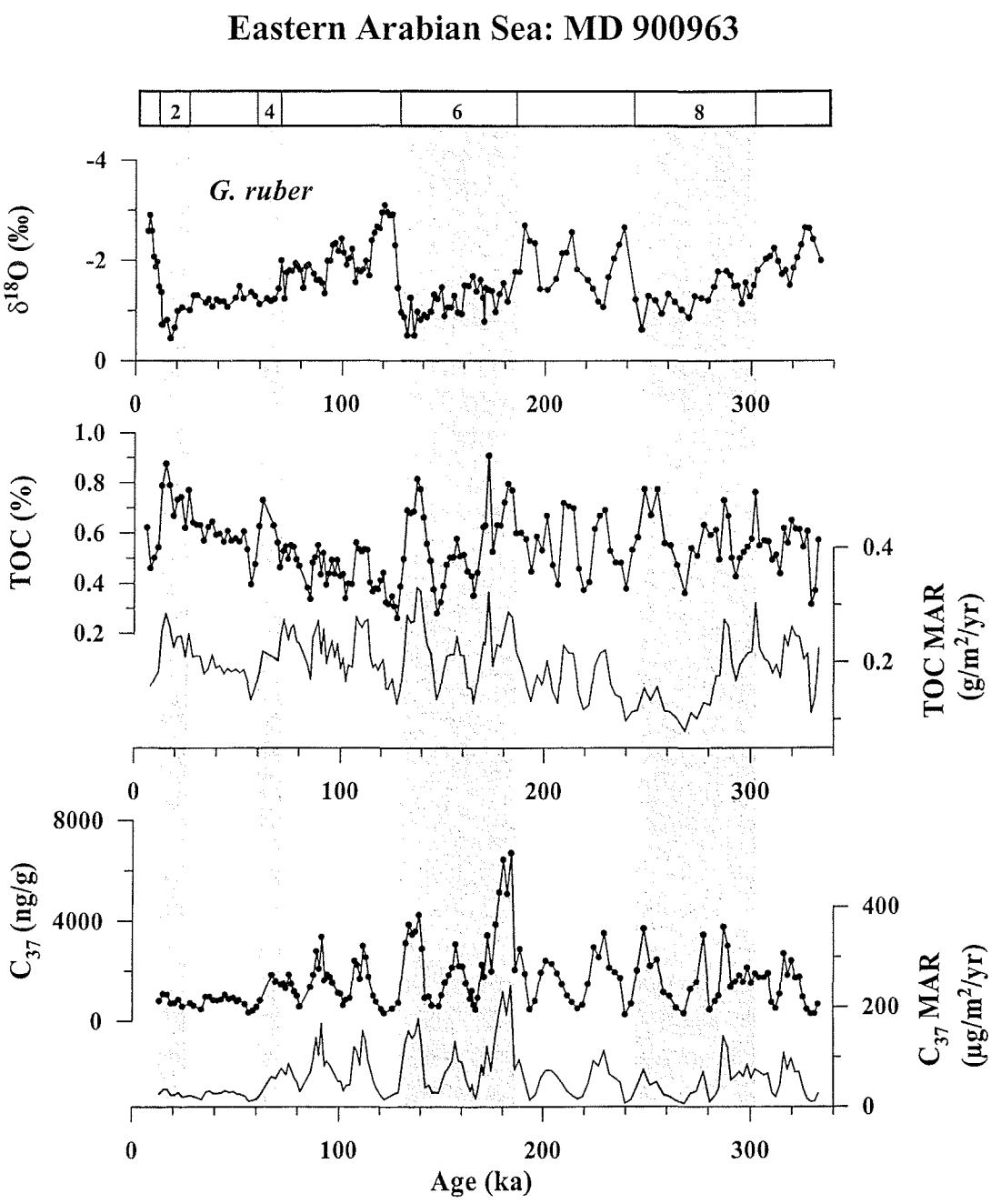

Figure 6: Time series of $\delta^{18}O$ of the planktonic foraminifera *Globigerinoides ruber*, TOC, TOC MAR, C_{37} and C_{37} MAR for MD 900963 [*Rostek et al.*, 1994, 1997].

The results of the spectral analyses on TOC and TOC MAR (Figure 7) are in good accordance to GeoB 3005. Again, dominant variance is concentrated at the 23 kyr period [*Rostek et al.*, 1997] in both records, while TOC MAR, additionally, reveals a peak in the frequency band of eccentricity. Thus the 23 kyr periodicity is revealed in the WAS and EAS

and at the continental margin off Oman, although with much lower importance at the coastal site.

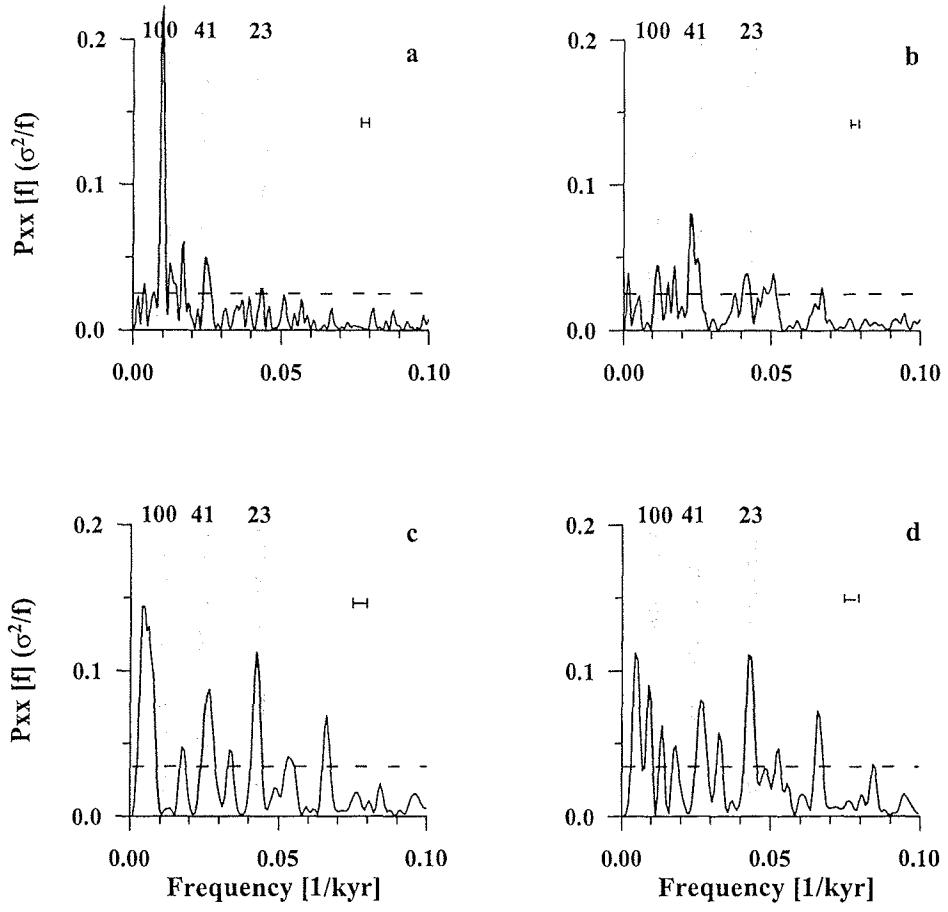

Figure 7: Results of harmonic analysis calculated on (a) TOC and (b) TOC MAR of ODP Site 723 [*Emeis,* 1993; *Emeis et al.,* 1995] and (c) TOC and (d) TOC MAR of core MD 900963 [*Rostek et al.,* 1994, 1997] using the software program SPECTRUM [*Schulz and Stattegger,* 1997]. A Fischer/Siegel test (dashed line) for compound periodicity was employed, and significant peaks outside the eccentricity (100), obliquity (41), and precession band (23) are labeled separately. Horizontal bar marks 6 dB bandwidth for each calculation.

Cross-Spectral Analysis

The results of the cross-spectral analyses (Figure 8) reveal differences in the frequency domain as well as in the phase relationship to boreal summer insolation for June 21 at 30°N of all three cores in the WAS (GeoB 3005), at the continental slope off Oman (ODP Site 723), and in the EAS off the Maldives (MD 900963).

The 23 kyr cyclicity of GeoB 3005 (Figure 8a) is coherent (k = 0.9931) with boreal summer insolation but reveals a phase relationship of +11.3 kyr (+177°) (Table 2). This opposite phasing between summer insolation and TOC in GeoB 3005 is shown more illustratively in Figure 9.

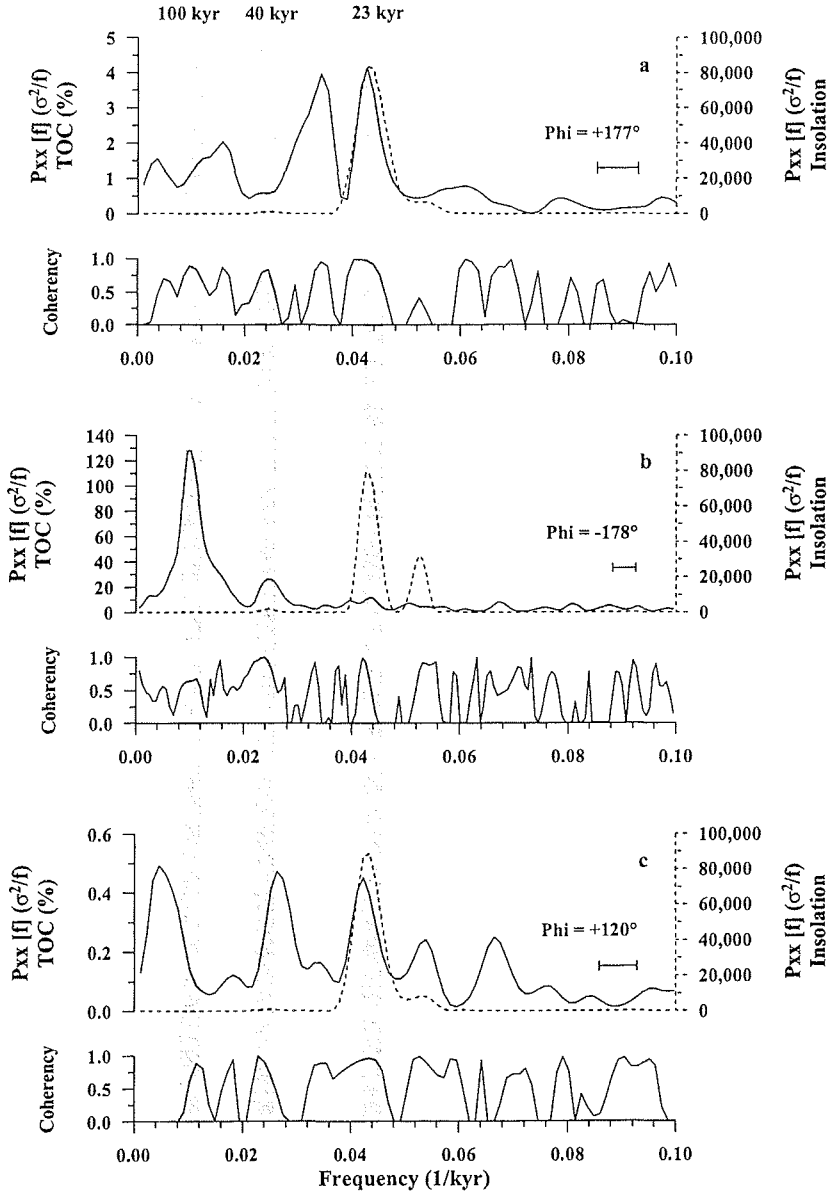

Figure 8: Results of the cross-spectral analyses between boreal summer insolation (June 21, 30°N) calculated after *Berger* [1978] using the AnalySeries software package [*Paillard et al.*, 1996] and TOC records of (a) GeoB 3005, (b) ODP Site 723 [*Emeis*, 1993; *Emeis et al.*, 1995], and (c) MD 900963 [*Rostek et al.*, 1994, 1997] applying the software program SPECTRUM [*Schulz and Stattegger*, 1997]. Horizontal bar marks 6 dB bandwidth for each calculation.

ODP Site 723 (Figure 8b) exhibits strong variances in the low-frequency domain, which links TOC variations mainly to the glacial-interglacial cycles dominated by the 100 kyr period. However, a strong coherency (k = 0.9906) is still evident between boreal summer insolation and TOC time series within the precession band. The phase relationship of -11.4 kyr (-178°) is similar to that calculated for GeoB 3005 (Figure 9, Table 2).

The coherence between TOC of MD 900963 and boreal summer insolation (Figure 8c) is strong (k = 0.9609) in the precession band, but phase relationship reveals a 7.7 kyr (+120°) lead of TOC.

Discussion

With the availability of longer proxy records the precessional component of the Earth's parameters became evident in productivity changes all over the Arabian Sea, although with varying intensity [e.g., *Prell,* 1984; *Clemens and Prell,* 1990, 1991; *Shimmield et al.,* 1990; *Murray and Prell,* 1992; *Anderson and Prell,* 1993; *Emeis,* 1993; *Bassinot et al.,* 1994; *Rostek et al.,* 1997; *Altabet et al.,* 1995; *Reichart et al.,* 1998; *Schubert et al.,* 1998]. On the basis of biological, biogeochemical, and lithogenic evidence, *Clemens et al.* [1991] concluded that the response of the summer monsoon winds over the Arabian Sea to insolation changes is of more importance to the timing and wind strength than the glacial-interglacial climate variability. Additionally, *Sirocko et al.* [1993] discussed variations in the records of marine oxygen isotopes and carbonate and aeolian dust supply, which originated from Arabia and Mesopotamia by northwesterly winds, in relation with insolation changes in the WAS.

Recent studies suggest a coupling between increased biogenic as well as lithogenic particle fluxes, higher SW monsoon wind speeds, and decreasing sea surface temperatures in the WAS and EAS [*Nair et al.,* 1989; *Ittekkot et al.,* 1992; *Haake et al.,* 1993]. Thus, if the SW monsoon wind strength responds directly to insolation changes, then biological, biogeochemical, and lithogenic proxies for paleoupwelling and wind intensity should be in phase with boreal summer insolation. However, numerous studies concerning the reconstruction of upwelling-related paleoproductivity in the Arabian Sea reveal a wide range of phase angles (-6.6 to +7.7 kyr) between the various proxies and boreal summer insolation [e.g., *Clemens and Prell,* 1990, 1991; *Shimmield et al.,* 1990; *Murray and Prell,* 1992; *Emeis,* 1993; *Altabet et al.,* 1995; *Beaufort et al.,* 1997; *Reichart et al.,* 1998]. This indicates that maxima in wind strength, paleoproductivity, and upwelling significantly deviate from maxima in boreal summer insolation at June 21. None of them even has a maximum within the half

cycle of enhanced insolation. On the basis of their phase angles these proxies used to reconstruct monsoonal climate can be divided into three groups (Table 2, Figure 9) reflecting (1) summer monsoon wind strength and related upwelling intensity in the WAS (Group 1: -6.4 to -9.6 kyr), (2) paleoproductivity in the WAS (-10.9 to +9.6 kyr), and (3) paleoproductivity in the EAS (+8.3 to +6.4 kyr).

Group 1: SW Monsoon Wind Strength and Upwelling Intensity in the Western Arabian Sea (-6.4 to -9.6 kyr)

Clemens and Prell [1990] and *Clemens et al.* [1991] used marine and terrestrial proxies, giving independent information on marine biological processes and the timing of maxima in summer monsoon wind intensity. The marine proxies, consisting of the concentration of the planktonic foraminifera *Globigerina bulloides*, barium, and biogenic opal fluxes, reveal a strong coherency with boreal summer insolation but show phase lags of -8.7 (-121°), -6.6 (-104°), and -7.2 kyr (-113°), respectively, in the precession band. A grain size record was used as terrestrial indicator for the SW monsoon intensity, revealing a phase lag of -9.5 kyr (-148°) [*Clemens et al.,* 1991]. Together these proxies forming group 1 reveal a time lag of roughly 6 to 9 kyr, which was attributed to variations in the cross-equatorial transport of latent heat originating from the southern Indian Ocean and its release over the Asian Plateau, which according to the model of *Clemens et al.* [1991], determines the strength of the SW monsoon.

Altabet et al. [1995] used the sedimentary $^{15}N/^{14}N$ ratios to reconstruct denitrification intensity, the process by which nitrate is reduced to gaseous nitrogen species, an important limiting factor for marine productivity [*Altabet and Curry,* 1989]. In the precessional frequency band the $\delta^{15}N$ record from the Owen Ridge is coherent and nearly in phase with *G. bulloides* (percent) suggesting a strong link between denitrification and upwelling. Similar to the other records described above, $\delta^{15}N$ lags boreal summer insolation by 9 kyr (Table 2) [*Altabet et al.,* 1995] and thus belongs to group 1.

Reichart et al. [1998] applied an age model independent of the SPECMAP timescale, which reduced the phase lag between monsoon proxies and summer insolation by 2 kyr. In spite of this alternative chronology tuned to the $\delta^{18}O$ timescale of MD 84641 [*Lourens et al.,* 1996] from the Mediterranean a time lag between the productivity proxies *G. bulloides* (percent) and TOC with respect to early summer insolation of 6 to 7.5 kyr (Table 2) is still evident. This was attributed by the authors to a prolonged upwelling season caused by an increased insolation during August and September, suggesting that the length of the summer

monsoon is more important to annual fluxes of *G. bulloides* and TOC than the wind strength at the time of early summer insolation maximum.

	Author (s)	Core	Time Series	Precession (June 21)	
				Phase, deg.	Lead/Lag, kyr
Group1	*Clemens et al.* [1991]	ODP Site 722	Opal MAR	-113 +/-21	7.2 +/-1.3
			Ba flux	- 04 +/-10	6.6 +/-0.6
		RC27-61	*G. bulloides* (%)	-121 +/-23	8.7 +/-1.3
			Lithogenic Grain Size	-148 +/-12	9.5 +/-0.6
Group1	*Altabet et al.* [1995]	RC27-61	d15N	-141 +/-20	9.0 +/-1.3
Group1	*Reichart et al.* [1998]	NIOP 464	*G. bulloides* (%)	-103 +/-31	6.6 +/-2.0
			TOC (%)	-116 +/-29	7.4 +/-1.9
Group 2	*Murray & Prell* [1992]	RC27-61	TOC (%)	+170 +/-25	10.9 +/-1.6
			TOC MAR	+155 +/-15	9.9 +/-1
			PP estimates [*Müller and Suess*, 1979]	+162 +/-28	10.4 +/-1.8
Group 2	*Emeis* [1993]	ODP Site 723	PP estimates [*Sarnthein et al.*, 1992]	+167 +/-27	10.7 +/-1.7
Group 2	this study	GeoB 3005	TOC (%)	+177 +/-4	11.3 +/-0.3
			TOC MAR	+173 +/-4	11.1 +/-0.3
			C_{37} (ng/g)	+172 +/-7	11 +/-0.4
			C_{37} MAR	+168 +/-6	10.7 +/-0.4
Group 2		ODP Site 723	TOC (%)	-178 +/-5	11.4 +/-0.3
			TOC MAR	+153 +/-6	9.8 +/-0.4
Group 3	*Beaufort et al.* [1997]	MD 900963	PP (*F. profunda*)	+118	7.5
Group 3	this study		TOC (%)	+120 +/-10	7.7 +/-0.6
			TOC MAR	+129 +/-8	8.2 +/-0.5
			C_{37} (ng/g)	+108 +/-2	6.9 +/-0.1
			C_{37} MAR	+110 +/-4	7 +/-0.3

Table 2: Summary of phase angles between time series of different cores and precessional insolation (June 21). Positive values indicate a lead with respect to insolation maximum, whereas negative values indicate a lag. A detailed description of the age models and cross-spectral analyses of MD 900963, NIOP 464, ODP Site 723, RC27-61, and ODP Site 722 are given by *Bassinot et al.* [1994] (age model) and *Beaufort et al.* [1997] (cross-spectral analysis), *Reichart et al.* [1998], *Emeis* [1993], and *Clemens and Prell* [1990] and [1991], respectively. The proxies were divided into three groups reflecting summer monsoon wind strength and related upwelling intensity in the western Arabian Sea (WAS) (-6.4 to -9.6 kyr) and paleoproductivity in the WAS (-10.9 to +9.6 kyr) and eastern Arabian Sea (+8.3 to +6.4 kyr).

Group 2: Paleoproductivity in the Western Arabian Sea (-10.9 to +9.6 kyr)

Group 2, consisting only of records of TOC and C_{37} alkenones, reveals opposite phasing between -10.9 and +9.6 kyr to boreal summer insolation maxima in the precessional frequency band (Table 2, Figure 9). *Murray and Prell* [1992] described similar opposite relationships of +10 kyr (+157°) (Table 2) between maxima of TOC, TOC MAR, and estimates of paleoproductivity, inferred from the sedimentary TOC content after *Müller and Suess* [1979], and maxima in Northern Hemisphere summer insolation. In their study the phase of TOC and productivity records lie directly between the phasing of indicators for summer monsoon strength at about -7.7 kyr (-120°) on average (group 1) and that of high sedimentation rates associated with lithogenic input at 5.8 kyr (+90°) in phase with maximum ice volume. From this they concluded that either the TOC signal reflects preservation changes due to enhanced sedimentation rates or the production of organic carbon is not directly linked to monsoonal upwelling.

Variations in TOC and the C_{37} alkenone concentrations may be attributed to changes in either productivity or preservation. Today, the Arabian Sea is characterized by a pronounced oxygen minimum zone (OMZ) between 150 and ~ 1500 m [*Wyrtki,* 1971], initiating a controversial discussion about its influence on proxies used to reconstruct paleoproductivity, especially sedimentary TOC. Higher sedimentary TOC contents may be the result of generally higher export production rates and a probably somewhat better preservation of organic matter settling through a stronger OMZ. *Paropkari et al.* [1992] compared the sedimentary TOC contents on the continental slopes of the Indian margin and the Arabian Peninsula. They inferred that bottom water anoxia plays an important role on the sedimentary TOC concentrations. In contrast, *Pedersen et al.* [1992] examined the 0 to 1 cm depth interval from 14 undisturbed box cores collected from the outer shelf-upper continental slope area off Oman from water depths < 1650 m. Their findings suggested that there is little relationship between the bottom water oxygen concentration and the sedimentary content of marine organic matter on the Oman margin.

Reichart et al. [1998] compared TOC patterns in cores from different water depths in the northern Arabian Sea. They found that TOC fluctuations in cores from within and below the OMZ can be correlated one by one with each other, although TOC contents are lower in the deep water cores, and concluded that variations in TOC are not caused by fluctuations in the OMZ but are primarily controlled by changes in surface water productivity. Additionally, *Schubert et al.* [1998] examined several organic biomarker compounds, such as alkenones in

relation with variations of TOC over the past 200 kyr. They confirmed the use of alkenones, TOC, and other organic biomarkers as qualitative indicators for paleoproductivity changes in Arabian Sea sediments.

While *Paropkari et al.* [1992] suggest that bottom water anoxia plays an important role on the sedimentary TOC concentrations, several other studies indicate that variable bottom water oxygen concentrations in the OMZ have only little or no effect on TOC variations in the Arabian Sea [e.g., *Pedersen et al.,* 1992; *Reichart et al.,* 1998; *Schubert et al.,* 1998]. *Rostek et al.* [1994, 1997] assumed that variations of organic matter are related to changes in marine productivity in the WAS and EAS. They used the distribution of the coccolithophorid species *F. profunda* as a proxy to estimate variations in surface productivity. High TOC contents and alkenone concentrations are accompanied by a low ratio of *F. profunda* to total coccoliths, indicating a shallow thermocline and enhanced surface water productivity. This is corroborated by transfer functions based on coccolithophorids [*Beaufort et al.,* 1997] and planktonic foraminifera [*Cayre et al.,* 1999] at site MD 900963. Additionally, different kinds of organic biomarker compounds [*Schulte et al.,* 1999] and redox-sensitive trace metals [*Pailler et al.,* 1998] revealed that the bottom waters remained oxygenated during the last 330 kyr at site MD 900963. Intense bioturbation throughout the whole core indicates oxygenated bottom water conditions at site GeoB 3005 [*Hemleben et al.,* 1996]. The good agreement between the TOC and TOC MAR, as well as between C_{37} and C_{37} MAR records in both GeoB 3005 and MD 900963 indicates that variations in these records reflect changes in surface water productivity rather than preservation changes due to varying sedimentation rates [*Müller and Suess,* 1979].

In contrast, dilution effects due to higher sedimentation rates of terrigenous lithogenic material and preservation as an additional controlling factor on TOC and C_{37} cannot be excluded at ODP Site 723. The higher TOC concentrations during interglacial times at ODP Site 723 are corroborated by a *G. bulloides* record [*Emeis et al.,* 1995] also indicating higher productivity levels during interglacial times. Thus, *Emeis et al.* [1995] suggested TOC to be a more suitable indicator of productivity than accumulation rates at this site.

The results of the cross-spectral analyses of GeoB 3005 and ODP Site 723 described in this study (Table 2, Figure 9) are in good agreement with *Emeis* [1993] and *Murray and Prell* [1992], who calculated the paleoproductivity rates after *Sarnthein et al.* [1992] or *Müller and Suess* [1979] using TOC MAR at ODP Site 723 and RC27-61, respectively. These calculations revealed a phase relationship to boreal summer insolation of about +10.5 kyr (+165°) (Table 2). We therefore assume that variations of TOC in the precessional frequency

domain in the WAS can be attributed to productivity rather than to preservation changes. To explain the opposite phasing, we propose that variations of paleoproductivity indicated by TOC, alkenones, and other organic biomarkers are not directly linked to maximum monsoonal upwelling intensity and wind strength in the WAS.

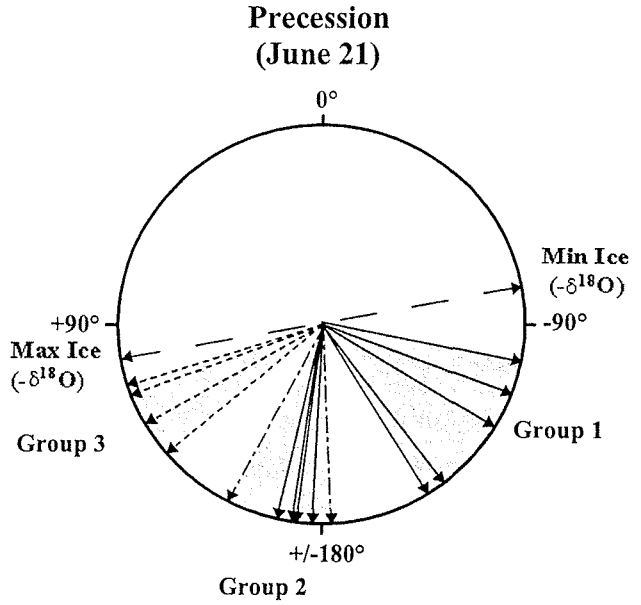

Figure 9: Precessional phase wheel summarizing proxies of group 1 (-6.4 to -9.6 kyr) used to reconstruct SW monsoon wind intensity and related upwelling in the WAS [*Clemens and Prell,* 1990; *Clemens et al.,* 1991; *Altabet et al.,* 1995] referenced to maximum insolation corresponding to June 21. Groups 2 (-10.9 to +9.6 kyr) and 3 (+8.3 to +6.4 kyr) indicate productivity proxies (TOC, TOC MAR, C_{37}, and C_{37} MAR) from cores GeoB 3005 (solid line) as well as from ODP Site 723 (long- and short-dashed line) and MD 900963 (dashed line) in the WAS and EAS, respectively, calculated in this study.

Group 3: Paleoproductivity in the Eastern Arabian Sea (+8.3 to +6.4 kyr)

Group 3 summarizes phase angles between +8.3 (+130°) and +6.4 kyr (+100°) (Figure 9) in phase with maximum precessional ice volume. The leading of productivity records of site MD 900963 of +7.7 kyr (+120°) on average (Table 2) is consistent with the previously published work of *Beaufort et al.* [1997]. They used the relative abundance of the coccolithophorid *F. profunda* as a marker for variations in primary productivity for the past 910 kyr at site MD 900963. *Beaufort et al.* [1997] suggested that productivity in the EAS is coherent and in phase with the early spring equatorial insolation and therefore is related to the wind intensity of the westerlies.

On the other hand, *Rostek et al.* [1994, 1997] inferred a link between precession-dominated paleoproductivity and deeper mixing due to stronger and predominating NE monsoons during glacial times in the EAS on the basis of higher TOC and C_{37} alkenone contents during glacial interstadials. Additionally, recent studies suggested that the

NE monsoon winds are responsible for deepening of the mixed layer, thereby injecting nutrient-rich subsurface waters into the photic zone [*Rao et al.,* 1989]. According to *Emeis et al.* [1995], an expanded and thickened snow cover over the Tibetan Plateau may have at least prolonged the NE monsoon season. Consequently, in the EAS, paleoproductivity seems to be predominantly linked to variations in the NE monsoon winds, which are probably related to maximum precessional ice volume.

Implications for the Sedimentary TOC and C_{37} Alkenone Signal in the Arabian Sea

Although *Clemens et al.* [1991] attributed the 6 to 9 kyr time lag between proxies belonging to group 1 and boreal summer insolation to variations in the cross-equatorial transport of latent heat, the TOC and C_{37} signals from the WAS and EAS indicate that the SW monsoon and related upwelling intensity alone cannot account for the different phasing of groups 1, 2, and 3. The explanations of group 1, cross-equatorial transport of latent heat [*Clemens et al.* 1991], and prolonged summer monsoon season [*Reichart et al.,* 1998] cannot be resolved here. The timing of groups 2 and 3 between maxima in the monsoon indices of group 1 and maximum ice cover leading insolation at June 21 by about +6.4 kyr (+100°) (Figure 9) implies a pronounced influence of the NE monsoon winds on TOC and C_{37} fluxes in the WAS and EAS. According to *Prell* [1984], a stronger snow cover over Asia delays the onset and shortens the summer monsoon season. Thus a prolonged NE monsoon due to minimum summer insolation and increased ice volume may have lead to a deepening of the mixed layer enhancing the primary productivity and particle fluxes in the WAS and EAS [*Nair et al.,* 1989; *Rao et al.,* 1989] rather than inducing stronger upwelling. A strengthening and prolongation of the NE monsoon season, increasing the vertical mixing during boreal winter at times opposite to maxima in precessional summer insolation, were previously proposed by *Van Campo et al.* [1982] and *Emeis et al.* [1995].

Additionally, recent studies of *Rixen et al.* [1996] suggest that during periods of strong SW monsoon winds, cold, nutrient-depleted, south equatorial water is transported to the north into the WAS, where these water masses reduce the amount of nutrients, thereby diminishing productivity related biogenic particle fluxes. Thus highest flux rates associated with upwelling occur during SW monsoons of minor to intermediate strength [*Rixen et al.,* 1996]. Consequently, variations in paleoproductivity in the WAS are probably linked to deeper mixing of surface waters through the action of stronger and prolonged NE monsoon winds [*Emeis et al.,* 1995] and to rather moderate SW monsoon intensity, as suggested by recent

studies of *Rixen et al.* [1996]. In the EAS the TOC and alkenone maxima are in phase with maximum ice volume, indicating an additional influence of stronger and prolonged NE monsoon winds associated with cold climates, as proposed by *Rostek et al.* [1994, 1997].

Conclusions

Variations in the sedimentary content of TOC and C_{37} at sites GeoB 3005 and MD 900963 reveal a dominating 23 kyr cyclicity, indicating a precession-related insolation forcing on paleoproductivity in the WAS and EAS. It is worth noting that while in the EAS variance in the frequency domain of eccentricity is present in TOC MAR associated with interstadials in glacial $\delta^{18}O$ maxima [*Rostek et al.,* 1994, 1997], the record from the western regions is exclusively characterized by the precession component. In contrast, ODP Site 723 exhibits strong variance in the eccentricity band [*Emeis,* 1993], showing higher TOC values during interglacial periods at the continental slope off Oman [*Emeis et al.,* 1995]. Superimposed on these fluctuations in the low-frequency domain are variations in the precession band at ODP Site 723.

According to their phasing related to precessional variations in boreal summer insolation, referenced to June 21, monsoonal indices as well as paleoproductivity proxies can be divided into three groups reflecting summer monsoon wind strength and related upwelling intensity in the WAS (group 1: -6.4 to -9.6 kyr) and paleoproductivity in the WAS (group 2: -10.9 to +9.6 kyr), and EAS (group 3: +8.3 to +6.4 kyr). Cross-spectral analyses reveal a coherent but opposite phase relationship of TOC records of GeoB 3005 and ODP Site 723 with respect to Northern Hemisphere summer insolation. These productivity-related proxy records lie directly between the indicators for SW monsoon wind strength and related upwelling intensity as described by *Clemens et al.* [1991] belonging to group 1, and maximum ice volume, which probably prolongs and strengthens the NE monsoon winds. TOC of MD 900963 leads summer insolation by +7.7 kyr (group 3) thus is very close to maximum ice volume in the precession band.

We interpret the maxima in TOC and C_{37} alkenone variations to be a combined signal of moderate SW monsoon wind strength, as suggested by *Rixen et al.* [1996], and additionally strengthened and prolonged NE monsoon winds enhancing primary productivity due to deeper mixing in the WAS, while paleoproductivity seemed to predominantly correspond to the NE monsoon winds in the EAS.

Acknowledgments

We thank Hella Buschhoff, Dietmar Grotheer, and Ralph Kreutz for technical assistance in the home laboratory; the officers, crew, and scientists aboard *R/V Meteor* for their help with coring and sampling operations; the Ocean Drilling Program (ODP) and Kai-Christian Emeis for providing data from ODP Site 723. This research was funded by the Deutsche Forschungsgemeinschaft and the Bundesminister für Bildung und Forschung (BMBF), Bonn. Paleoclimate work at CEREGE is supported by CNRS (PNEDC), the European Community (projects ENV4-CT97-0564, FMRX-CT96-0046, and ENV4-CT97-0659), and the IFCPAR (project 1809-1). Previous versions of this manuscript greatly benefited from reviews by M. Delaney, G.J. Reichart, and an anonymous reviewer. The data of GeoB 3005 presented in this paper will be archived in the Pangaea database (www.pangaea.de/Projects/SFB261/DBudziak_et_al_2000/).

4.2 Variations of alkenone-derived sea-surface temperatures and productivity patterns in the Arabian Sea during the Late Quaternary

(to be submitted to *Earth and Planetary Science Letters*)

Variations of alkenone-derived sea-surface temperatures and productivity patterns of C_{37} alkenones in the Arabian Sea during the Late Quaternary

Dörte Budziak[1], Ralph R. Schneider[1], Frauke Rostek[2], Peter J. Müller[1], Edouard Bard[2], and Gerold Wefer[1]

[1]Fachbereich Geowissenschaften, Universität Bremen, Postfach 330 440, 28334 Bremen, Germany

[2]Centre Européen de Reserche et d'Enseignement en Géosciences de l'Environment, Université d'Aix-Marseille III et CNRS-UMR-6635, Europôle de l'Arbois, BP80, 13545 Aix-en-Provence Cedex 4, France

Abstract

In order to compare variations of the surface ocean circulation in the western and eastern Arabian Sea, sea-surface temperatures (SSTs) were reconstructed on the basis of the unsaturation ratio of C_{37} alkenones. Alkenone determined SSTs reflect an annual mean temperature rather than explicitly the season of upwelling. This is evident from alkenone SSTs in a transect of surface sediments extending from the inner Gulf of Aden into the western Arabian Sea. SST records from the open-ocean and coastal upwelling areas of the western Arabian Sea as well as from the eastern Arabian Sea off the Maldives show similar periodic glacial to interglacial changes with highest SSTs during interglacial and lowest SSTs during glacial times. Marine oxygen isotope stage (MIS) 6 differs from this pattern, for it remained relatively warm. As indicated by spectral analyses these SST changes are in good agreement with the modulation of precessional insolation changes by eccentricity. However, they do not show a pronounced cyclicity in the precessional band like variations in the alkenone accumulation. This discrepancy between SST and productivity variations implies a strong eccentricity forcing on annual mean temperatures in the entire tropical Indian Ocean, whereas the tracer of paleoproductivity changes in C_{37} alkenone accumulation reveals the well known precession-dominated pattern of monsoonal variations characteristic for the Arabian Sea.

Introduction

The surface hydrography of the Arabian Sea is linked to the seasonal reversal of the atmospheric circulation associated with the Asian monsoon system. Due to the differential heating of the Asian continent in the north and the Indian Ocean in the south, strong and humid SW monsoon winds (Figure 1) emerge during boreal summer. While these winds drive the ocean circulation, surface water is transported away from the coasts of Somalia and Oman and replaced by colder, nutrient-rich subsurface water masses. This upwelling results in lowered SSTs and high primary productivity during the summer season, where strongest upwelling appears within a narrow band (100 km) along the coast off Oman. Farther offshore, an open ocean type upwelling develops in a broad region (400 km) due to the positive curl in the wind stress [*Wyrtki*, 1971; *Swallow,* 1984; *Luther et al.,* 1990; *Brock & McClain,* 1992].

In winter, moderate but cool NE monsoon winds (Figure 1), originating from the seasonally snow-covered Tibetan Plateau and blow across the Arabian Sea. These winds, too, lower the SSTs and produce a second productivity maximum due to deeper mixing of the sub-surface waters, thereby injecting nutrients into the photic zone [e.g. *Nair et al.,* 1989*; Brock & McClain,* 1992*; Haake et al.,* 1993].

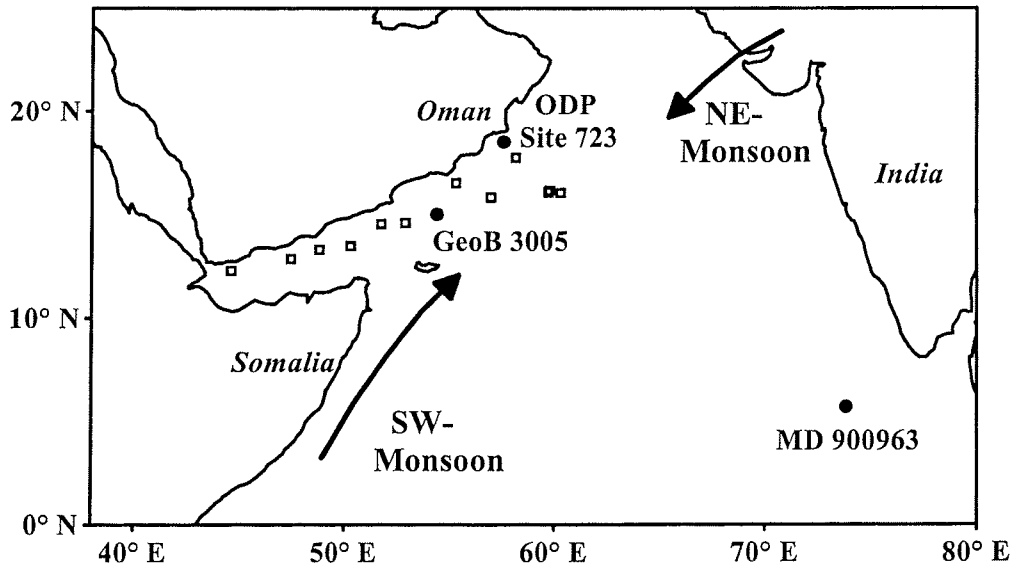

Figure 1: Map of the Indian Ocean north of the equator. Indicated are the locations of cores GeoB 3005, ODP Site 723, MD 900963 (full circles), and surface sediments (open squares). Arrows show major wind directions of the Indian monsoon system during summer (SW monsoon) and winter seasons (NE monsoon).

The history of monsoonal climate is preserved in the sediments of the Arabian Sea indicating substantial variations in upwelling intensity. Previous studies point to an intensification of the SW monsoon winds and enhanced upwelling with increased northern hemisphere summer insolation as primary forcing mechanism and, additionally, reduced glacial-age boundary conditions [e.g. *Prell & Kutzbach*, 1987; *Clemens et al.*, 1991; *Anderson et al.*, 1992]. Accordingly, *Anderson & Prell* [1993] suggested that during glacial times increased Asian snow cover may have weakened the SW monsoon by reducing the land-sea pressure gradient, which drives the monsoonal circulation.

The UK'37 unsaturation ratio of C_{37} alkenones is a widely used biomarker-based method for the reconstruction of past SSTs from marine sediments [see review in *Brassell*, 1993]. *Emeis* [1993], *Emeis et al.* [1995] and *Rostek et al.* [1994, 1997] described SST variations from the coastal upwelling cell off Oman and from the eastern Arabian Sea, respectively, which follow in general the pattern of eccentricity-related global climate change with highest SSTs during interglacial times. This pattern differs from the one expected, if only upwelling intensity would affect SSTs in the Arabian Sea raising three major questions. First, what temperature signal is reflected by the unsaturation ratio of C_{37} alkenones in the western Arabian Sea, where strong upwelling occurs? Second, why are alkenone-derived SST records seemingly dominated by eccentricity-related variations, whereas the tracers of paleoproductivity reveal a dominance of precession-related variation in the western, eastern and northern Arabian Sea surface hydrography [*e.g. Rostek et al.*, 1997; *Schubert et al.*, 1998; *Budziak et al.*, 2000]? Third, are the temperature variations in the western and eastern part of the Arabian Sea really that similar as it seems to be on first sight?

In order to answer these questions alkenone-derived SSTs from surface sediments (Figure 1), taken along a W-E transect from the Gulf of Aden into the upwelling area of the western Arabian Sea are compared with modern temperatures. For the investigation of Late Quaternary SST changes SST records are presented from core GeoB 3005 (Figure 1), an open ocean upwelling site, in relation to ODP Site 723 (Figure 1) from the coastal upwelling area off Oman [*Emeis*, 1993; *Emeis et al.*, 1995] and MD 900963 (Figure 1) from the equatorial eastern Arabian Sea [*Rostek et al.*, 1993, 1994, 1997].

Oceanographic Setting

Because of the influence of the monsoonal circulation, annual SST variations show two warming phases during the intermonsoon periods (February to May and September to mid-November), and two cooling phases lasting from May to August and from mid-November to January [*e.g. Colborn,* 1976; *Shetye,* 1986], the upwelling and winter cooling seasons, respectively. These variation patterns are more pronounced in the western than in the eastern Arabian Sea [*e.g. Haake et al.,* 1993].

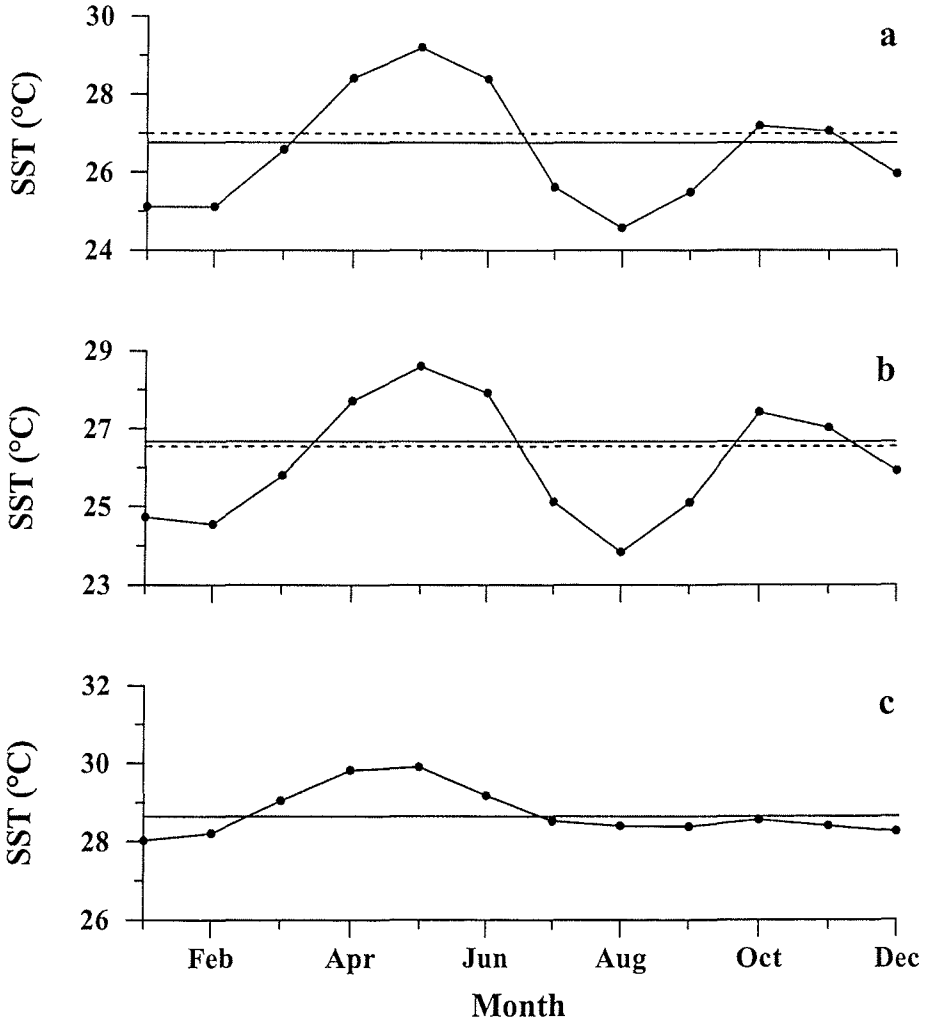

Figure 2: Monthly SST variations at the core locations of GeoB 3005 (a), ODP Site 723 (b) and MD 900963 (c) derived from the NOAA World Ocean Atlas 1994 [*Levitus & Boyer,* 1994]. Annual mean temperature derived from the NOAA World Ocean Atlas 1994 [*Levitus & Boyer,* 1994] and estimated alkenone temperature [*Müller et al.,* 1998] of the according core top samples are indicated by full and dashed lines, respectively.

Seasonal temperature variations at the sea surface were derived from the NOAA World Ocean Atlas 1994 [*Levitus & Boyer,* 1994, referred to as Levitus atlas in the following] for each core site (Figure 2). In the open ocean upwelling area at site GeoB 3005 the modern SSTs show an annual amplitude of 4.6 °C ranging from 24.6 °C in August to 29.2 °C in May. At ODP Site 723 within the coastal upwelling area off Oman the temperatures are on average by 1 °C lower than in the open ocean upwelling area. Here, the temperatures lie between 23.8 °C in August and 28.6 °C in May. The annual temperature amplitude in the coastal upwelling region is nearly equal to that of site GeoB 3005. Highest temperatures are revealed in the eastern Arabian Sea at site MD 900963. In contrast to the other sites lowest temperatures are reached in January with 28 °C, while the SST maximum of 29.9 °C, too, is reached in May. Thus, the resulting modern annual SST amplitude is smallest in the eastern Arabian Sea.

Material and Methods

Material

Core GeoB 3005 (Figure 1) was recovered during R/V *Meteor* cruise M31/3 from a station within the open-ocean upwelling area off the Arabian Peninsula (14°58.3'N, 54°22.2'E, water depth 2310; site 108 in *Hemleben et al.,* [1996]). The site was positioned on a submarine plateau, to minimize possible effects caused by lateral sediment transport. Samples were taken at 5 cm intervals with 10 ml syringes. In addition, surface sediment samples (0-1cm and 1-2cm) were obtained from multicorer core-tops along a W-E transect (Figure 1, Table 1) reaching from the inner Gulf of Aden into the western Arabian Sea. This was done in order to compare the modern seasonal SST range from out- and inside the upwelling area with the sedimentary alkenone signal.

Sites MD 900963 (05°04'N, 73°53'E; 2450 m) [*Rostek et al.*, 1993, 1994, 1997] and ODP Site 723 (18°03.079'N, 57°36.561'E; 816 m) [e.g. *Emeis*, 1993; *Emeis et al.*, 1995] are situated in the equatorial eastern Arabian Sea and within the coastal upwelling cell off Oman (Figure 1), respectively.

Multicorer	Lat. (°N)	Long. (°E)	Water depth (m)	SST (°C) 0-1cm	SST (°C) 1-2cm
GeoB 3002-1	12° 17.3	44° 38.2	752		27.8
GeoB 3003-5	13° 29.6	50° 17.7	2013	27.6	27.6
GeoB 3004-4	14° 36.3	52° 55.2	1801	27.5	27.5
GeoB 3005-3	14° 58.2	54° 22.2	2313	27.1	27.1
GeoB 3006-2	15° 49.7	56° 59.7	3521	27.1	27.1
GeoB 3007-3	16° 10.2	59° 46.2	1914	27.4	27.4
GeoB 3008-5	16° 05.4	59° 41.0	2223	27.1	27.1
GeoB 3009-2	16° 12.6	60° 16.8	4071	27.2	27.2
GeoB 3010-3	17° 45.0	58° 09.0	3165	27.7	27.5
GeoB 3011-3	16° 31.9	55° 19.9	2624	26.9	26.9
GeoB 3012-1	14° 32.4	51° 44.9	1538	27.8	27.5
GeoB 3013-2	13° 18.6	48° 47.0	1731	27.4	27.5
GeoB 3014-2	12° 51.7	47° 26.1	1626	26.7	26.7

Table 1: Positions, water depths and estimated alkenone SSTs calculated after *Müller et al.* [1998] for surface sediments used in this study. Sites are given in accordance to *Hemleben et al.* [1996].

Methods

Sample preparation and technical details for isotope and alkenone measurements of core GeoB 3005 are given in *Budziak et al.* [2000]. To remove fatty acid methyl esters, possibly interfering with the alkenone fraction, the extracts of the surface sediments were additionally saponified with 300 µl of a 0.1 M KOH in CH_3OH:H_2O (90:10) for 2 hours at 80 °C. The neutral fraction containing the alkenones was obtained by partitioning into hexane, concentrated, and finally taken up in 25 µl of a 1:1 (vol.) MeOH/CH_2Cl_2 mixture. 3µl aliquots of the fresh extracts were analysed by capillary gas chromatography using a HP 5890 Series II gas chromatograph (GC) equipped with a 50 m x 0.32 mm i.d. HP Ultra 1 (cross-linked methyl silicone) fused-silica column, a split injector (1:10), and a flame ionisation detector as described in *Budziak et al.* [2000] using helium as carrier gas. The GC was programmed from 50 to 150 °C at 30 °C/min, 150 to 230 °C at 8 °C/min, 230 to 320 °C at 6 °C/min, followed by an isothermal period of 45 min.

The ketone unsaturation index UK'37 was calculated from the concentrations of di- and tri-unsaturated C_{37} alkenones using the expression UK'37 = [37:2] / [37:3 + 37:2] [*Prahl & Wakeham,* 1987] and converted to temperature values applying the global core-top calibration of *Müller et al.* [1998: UK'37 = 0.033 T + 0.044]. This calibration is virtually identical with the widely used *Emiliania huxleyi* culture calibration of *Prahl & Wakeham* [1987:

UK'37 = 0.033 T + 0.043]. The precision of the measurements was better than 0.02 UK'37 units (+/-0.6 °C) based on replicate extractions of lab-internal reference sediments. Temperature estimates of the surface sediments 0-1 cm and 1-2 cm along the W-E transect were averaged for each station and the single SSTs for each sample are given in Table 1.

Alkenone measurements carried out on samples of core MD 900963 are described by *Müller et al.* [1994]. Core sampling of MD 900963 was extended to a depth of 1,720 cm. Details of sample preparation and techniques used at CEREGE for extending the alkenone record are given in *Sonzogni et al.* [1997a, b]. Sample treatment and determination of alkenone data of ODP Site 723 provided by K.-C. Emeis, were previously described in detail by *Emeis* [1993]. The UK'37 index of core MD 900963 and ODP Site 723, too, was converted to temperature values using the global core top calibration of *Müller et al.* [1998].

Mass accumulation rates of C_{37} alkenones were calculated for all cores by multiplying the concentration of C_{37} alkenones with the dry bulk density of the sediments and the linearly interpolated sedimentation rates between stratigraphic tie-points. This was done in order to avoid dilution effects caused by varying input of terrigenous detritus and other major biogenic components.

To identify the dominant frequencies in the records of $\delta^{18}O$, SST and C_{37} alkenones, the software program SPECTRUM developed by *Schulz & Stattegger* [1997] was used. To prove the statistical significance, a Fischer/Siegel-test was employed in the sub-routine 'Harmonic'. The calculation procedure was kept constant for all records (level of significance = 0.05; oversampling factor (OFAC) = 4; high frequency factor (HIFAC) = 1; see *Schulz & Stattegger* [1997] for further details). For a more precise evaluation of temporal correspondence between changes in eccentricity, obliquity and precessional insolation (21^{st} of June, northern hemisphere), calculated after *Berger* [1978] using the AnalySeries 1.0a7 software package of *Paillard et al.* [1996] and referred to as ETP [*Imbrie et al.,* 1989] in the following, and the SST records from the western and eastern Arabian Sea, cross-spectral analyses were performed. This method does not only include an estimation of coherency, a linear correlation coefficient in the spectral domain, but also estimates the lead (+) or lag (-) reported as phase angles between +180° and -180°, respectively, between records sharing a similar variance at a given frequency [*Jenkins & Watts,* 1968*; Imbrie et al.,* 1989]. The calculation procedure of the cross-spectral analyses, too, was kept constant for all records (level of significance = 0.1; OFAC = 4; HIFAC = 1; window type = Welch; 2 segments with 50% overlap; see *Schulz & Stattegger* [1997] for further details). Coherencies are significant above the critical level of 0.9.

For the direct comparison of GeoB 3005 with MD 900963 the SST records of both cores were converted to 2 kyr time intervals by linear interpolation using the AnalySeries 1.0a7 software package of *Paillard et al.* [1996].

Stratigraphy

The $\delta^{18}O$ records of the planktonic foraminifera *Neogloboquadrina dutertrei* (d'Orbigny) of GeoB 3005-1 (gravity core), 3005-2 (piston core) and 3005-3 (multicorer core) were used to combine these three cores and to build a stratigraphic framework. The age model of the composite core GeoB 3005 was derived from graphic correlation of the $\delta^{18}O$ record of *N. dutertrei* with the marine oxygen isotope stages (MIS) of the SPECMAP $\delta^{18}O$ stack [*Imbrie et al.*, 1984] using the software program AnalySeries 1.0a7 of *Paillard et al.* [1996]. Further details are given in *Budziak et al.* [2000]. According to this age model the core covers the last 307 kyr with a mean time resolution of about 700 years.

The chronologies of MD 900963 and ODP Site 723 are based on the $\delta^{18}O$ signals of the planktonic foraminiferal species *Globigerinoides ruber* [*Bassinot et al.*, 1994] and *Pulleniatina obliquiloculata* [*Niitsuma et al.*, 1991; *Emeis*, 1993; *Emeis et al.*, 1995], respectively.

Results & Discussion

Surface Sediments

In order to assess the alkenone signal in relation to modern SST conditions sediment surface samples were taken along a W-E transect from the inner Gulf of Aden into the western Arabian Sea (Figure 1, Table 1) and compared with Levitus atlas data [*Levitus & Boyer*, 1994]. During August, the time of most intense upwelling and highest productivity [*Brock et al.*, 1994], modern SSTs show a temperature decrease of about 5 °C along this transect [*Levitus & Boyer*, 1994]. In contrast, the alkenone-derived temperature signal of the surface sediments only slightly decreases by about 1 °C from west to the east (Figure 3), following closely the gradient of annual mean temperatures. This indicates that the alkenone signal rather reflects an integrated temperature signal of all seasons, than preferentially the season of highest productivity and most intense upwelling in the western Arabian Sea. Additionally, the core top samples of ODP Site 723 and MD 900963, too, show alkenone-derived SSTs very

similar to the modern annual mean SSTs (Figure 2), even though upwelling and related productivity is most intense in the coastal area off Oman [e.g. *Brock & McClain*, 1992].

Using sediment trap samples from a one-year experiment in the central Arabian Sea (15°59'N, 61°30'E) *Prahl et al.* [2000] described distinct maxima in C_{37-39} alkenone fluxes at the start and stop of the SW as well as NE monsoon seasons. This alkenone time series suggests that alkenone production is not limited to the season of highest biogenic particle fluxes during the SW monsoon.

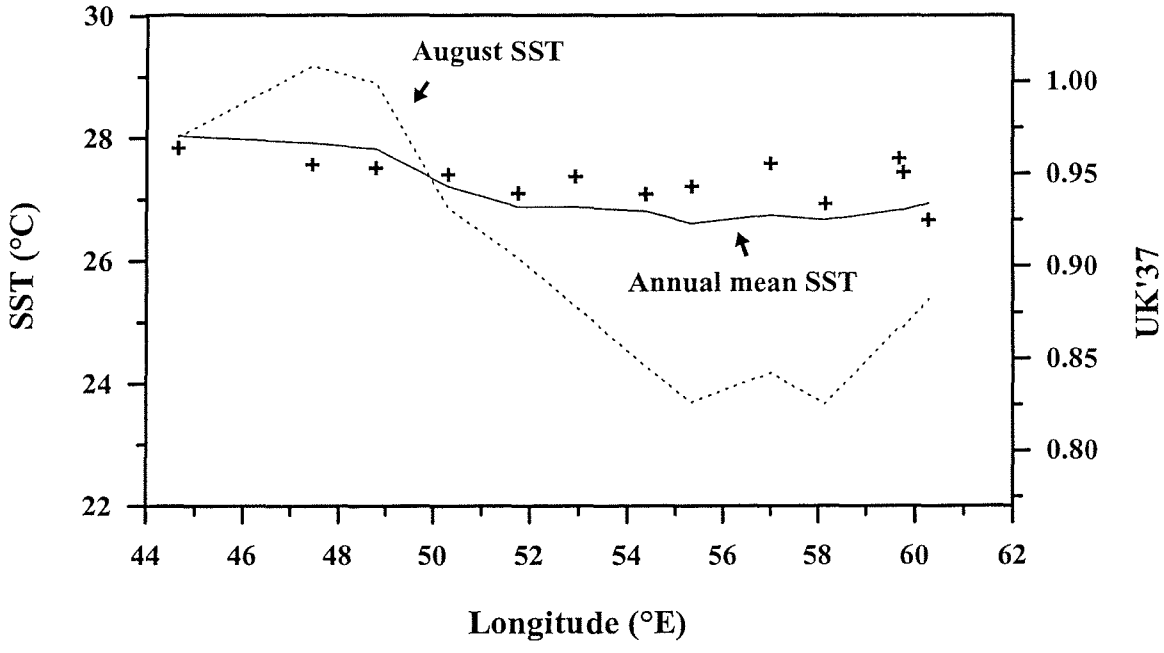

Figure 3: Alkenone-derived SSTs of surface sediments (0-1 cm and 1-2 cm) calculated using the equation of *Müller et al.* [1998] along a W-E transect from the Gulf of Aden into the Western Arabian Sea in comparison with modern annual mean and August temperatures obtained from the NOAA World Ocean Atlas 1994 [*Levitus & Boyer*, 1994] for 0 m water depth. Graphs concerning SSTs have double y-axis in °C and UK'37 here, and in the following figures.

Based on earlier studies it was assumed that alkenone SST reconstruction is related to seasonal productivity patterns [*Conte et al.*, 1992; *Conte & Eglinton*, 1993], and thus in the Arabian Sea may provide a SST record of the monsoon seasons when highest productivity occurred [e.g. *Nair et al.*, 1989; *Haake et al*, 1993]. Instead, a core-top calibration from the Indian Ocean [*Sonzogni et al.*, 1997a, b] showed that productivity-weighted alkenone-derived temperatures are generally very similar to annual mean temperatures. For productivity

weighted SST estimates monthly primary production rates were considered by *Sonzogni et al,* [1997a, b]. These were derived by *Antoine et al.* [1996] from Coastal Zone Color Scanner (CZCS) chlorophyll data, describing a productivity maximum during the SW monsoon from June to September in the Arabian Sea, particularly within the upwelling areas off Somalia, Oman and south-west India. Using a similar approach, it was confirmed by *Müller et al.* [1998] for the eastern South Atlantic that the UK'37 signal in sediments is only slightly affected by seasonal changes in surface water productivity assuming that coccolithophorid production follows the same seasonal productivity patterns.

Consequently, alkenone-derived SSTs in the tropical ocean are likely to reflect the annual mean temperature variations, and not preferentially those of the upwelling seasons in the Arabian Sea. This is in contrast to the fluxes of alkenones, which reveal strong seasonality together with other biogenic and terrigenous components [*e.g. Nair et al.,* 1989; *Ittekkot et al.,* 1992; *Haake et al.,* 1993; *Prahl et al.,* 2000].

Late Quaternary SST Variations in the Arabian Sea

Western Arabian Sea

The alkenone SST variations at site GeoB 3005 (Figure 4) follow in general the $\delta^{18}O$ record of *N. dutertrei* (Figure 4), with absolute temperatures ranging between 22.9 and 28.3 °C. SSTs are highest during interglacial MIS 7 and 5, and in the Holocene. Lowest glacial SSTs are observed in MIS 8, 4 and 3. Interestingly, MIS 6 remains relatively warm with glacial temperatures decreasing by only about 2 °C.

SST variation patterns of ODP Site 723 [*Emeis,* 1993*; Emeis et al.,* 1995] (Figure 5) are similar to the one described for GeoB 3005, although ODP Site 723 is situated within the coastal upwelling cell. Here, alkenone derived SSTs range between 22.8 and 28.0 °C. Both cores show a sharp drop in SSTs of about 1 to 2 °C within MIS 8 at 280 kyr.

Another core from the open ocean upwelling area off the Arabian Peninsula (TY93-929: 13°42'N, 53°15'E; 2490 m water depth) was previously investigated for its alkenone-derived SST variations by *Rostek et al.* [1997]. In this study seasonal variations of phytoplankton, deduced from the sediment trap WAST, were taken into account to calculate a flux-weighted annual mean SST. This flux-weighted SST is slightly colder than the simple annual mean, but still very close to the mean Holocene SST derived from alkenones [*Rostek et al.,*1997]. During the last 240 kyr the SST variations in core TY93-929 match those described for GeoB 3005 and ODP Site 723.

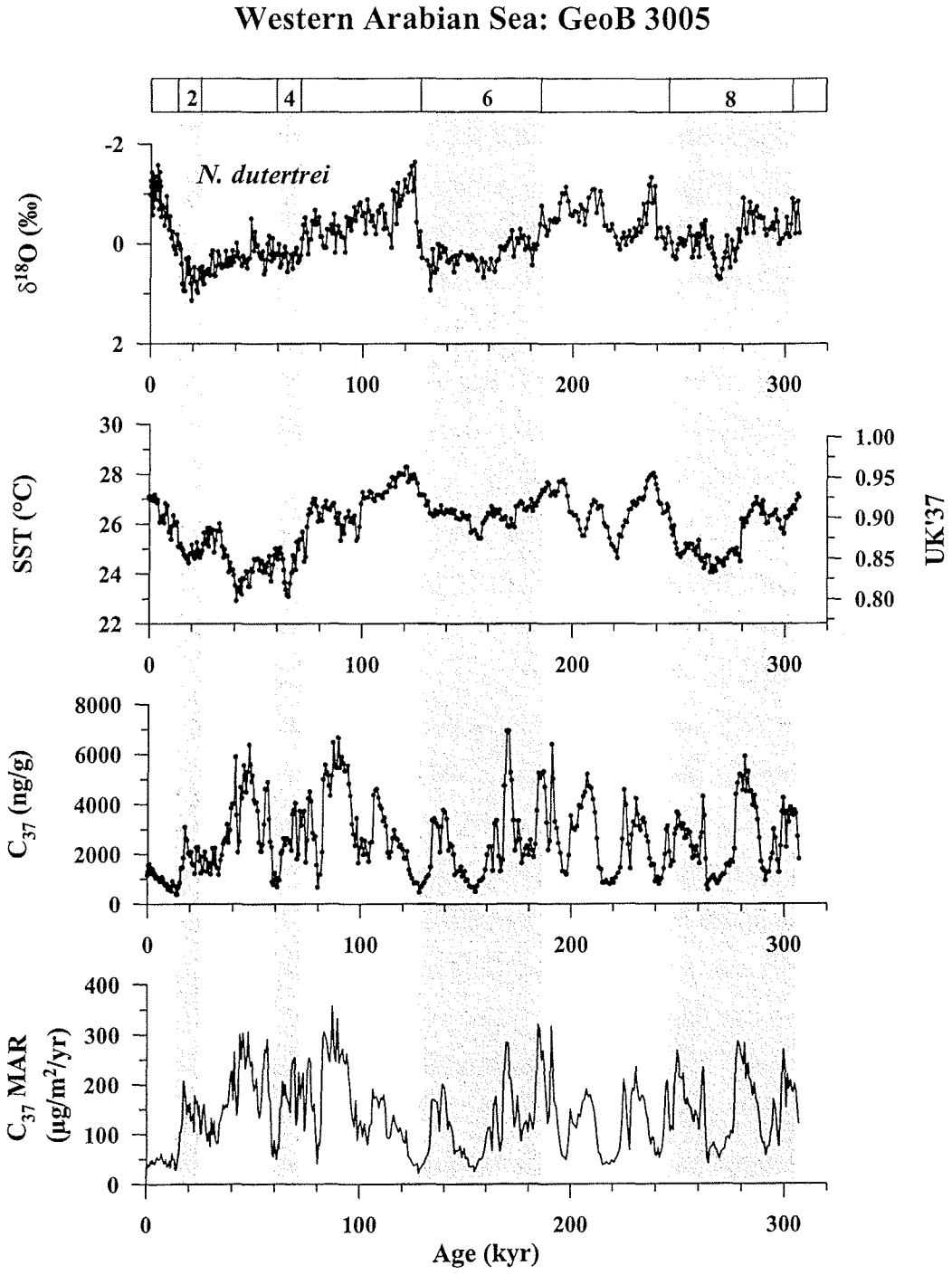

Figure 4: Time series of the $\delta^{18}O$ record of the planktonic foraminifera *Neogloboquadrina dutertrei*, alkenone-derived SSTs (calculated after *Müller et al.*, [1998]), C_{37} alkenones and C_{37} MAR for core GeoB 3005.

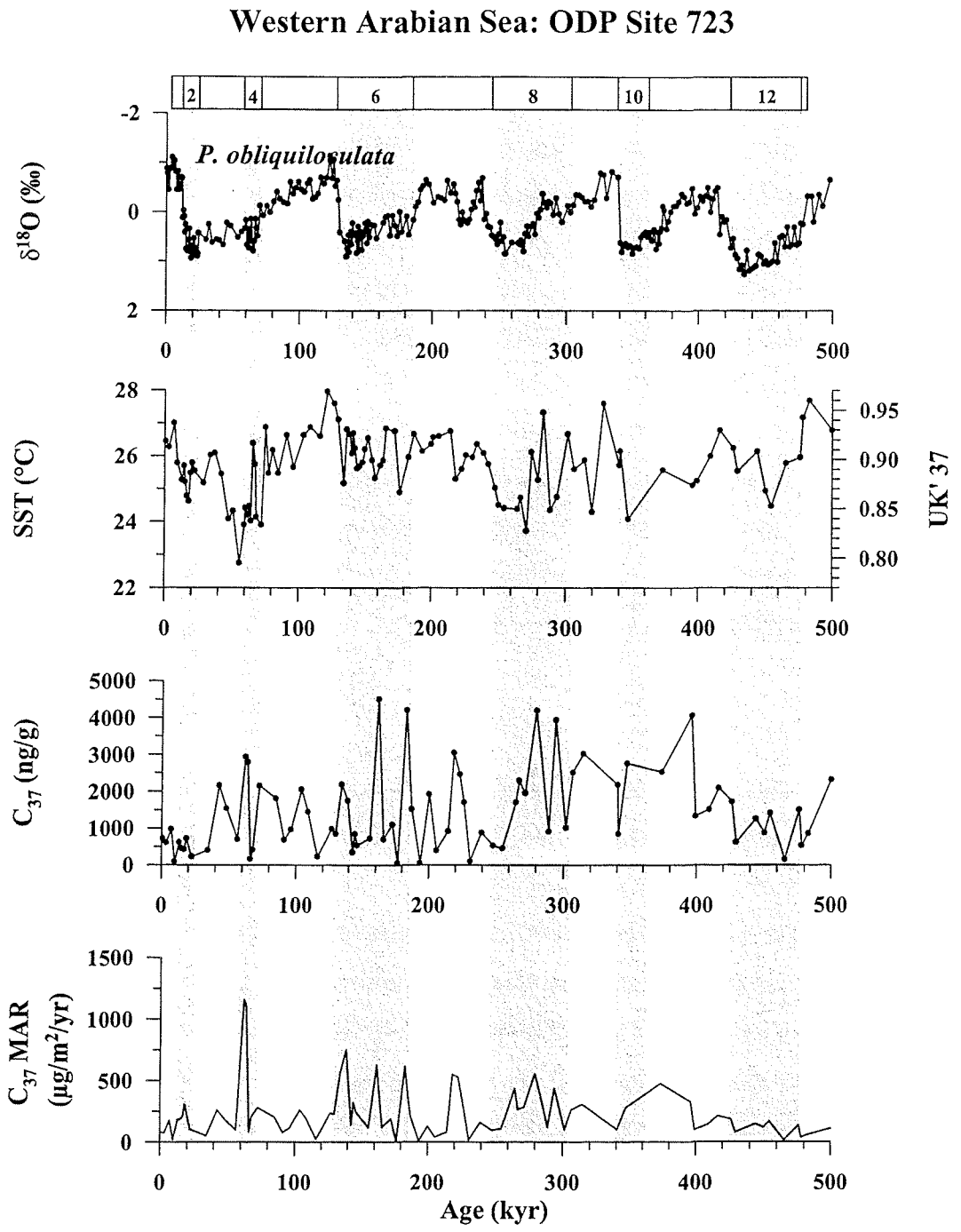

Figure 5: Time series of $\delta^{18}O$ of the planktonic foraminifera *Pulleniatina obliquiloculata* [*Niitsuma et al.*, 1991], alkenone-derived SSTs (calculated after *Müller et al.* [1998]), C_{37} alkenones and C_{37} MAR for ODP Site 723 [*Emeis*, 1993; *Emeis et al.*, 1995]. Data was kindly provided by K.-C. Emeis.

Eastern Arabian Sea

In the eastern Arabian Sea at site MD 900963 the entire Late Quaternary SST range (Figure 6) is by 1 °C smaller than at site GeoB 3005 and past temperatures vary between 25.7 and 28.8 °C [*Rostek et al.,* 1993]. Thus, SST estimates are systematically higher than in the western Arabian Sea. During the last deglaciation the alkenone-derived SST signal indicates a warming of about 2.5 °C. This is corroborated by a SST reconstruction based on foraminiferal transfer functions calculated for the glacial MIS 2 and the Holocene of core MD 900963 [*Cayre & Bard,* 1999] confirming the credibility of the alkenone estimates.

The alkenone SST signal in core MD 900963 shows a relative warm MIS 6 as is observed in GeoB 3005 and ODP Site 723. *Rostek et al.* [1994] previously compared the alkenone-derived temperature record of MD 900963 with the SST time series of core RC17-98 from the tropical Indian Ocean (13°S, 65°37'E, 3409 m) based on foraminifer transfer functions [*Clemens et al.*, 1991]. Because of the good agreement between these two SST records *Rostek et al.* [1994] suggested that a warm stage 6 is a genuine phenomenon rather than a local anomaly in the Arabian Sea.

Periodic Variations of SSTs in the Arabian Sea

Various studies documented a strong link between precessionally driven insolation changes and monsoon intensity [*e.g. Prell & Kutzbach,* 1987*; Clemens & Prell,* 1990 *and* 1991*; Murray & Prell,* 1992*; Beaufort et al.,* 1997*; Reichart et al.,* 1998]. If the alkenone temperature signal would reflect upwelling intensity in the western Arabian Sea, then the SST records should reveal a strong variance in the precession band. Instead, the results of time series analyses applied on the alkenone-derived SST record from site GeoB 3005 (Figure 7) exhibit peaks at periods (1/frequency) of 112, 40, and 23 kyr, near the eccentricity, obliquity, and precessional bands, respectively, with decreasing variance towards the higher frequencies of precessional insolation. This variance pattern is very similar to that of the $\delta^{18}O$ record of the planktonic foraminifera *N. dutertrei* (Figure 7). These results are consistent with the frequency analyses applied on ODP Site 723 by *Emeis* [1993]. Additional significant peaks are revealed at periods of 59 and 29 kyr in the $\delta^{18}O$ and SST records of GeoB 3005. A 52 and 29 kyr periodicity have already been found in other records of the western and eastern Arabian Sea [*Clemens & Prell,* 1991*; Bassinot et al.,* 1994*; Rostek et al.,* 1997]. *Clemens & Prell* [1991] interpreted them as non-linear interactions between external insolation forcing and internal climatic feedback mechanisms due to the interdependence of snow cover on the Asian

Plateau (variations in albedo and sensible heating) and variations in cross-equatorial latent heat transport and tropospheric heating.

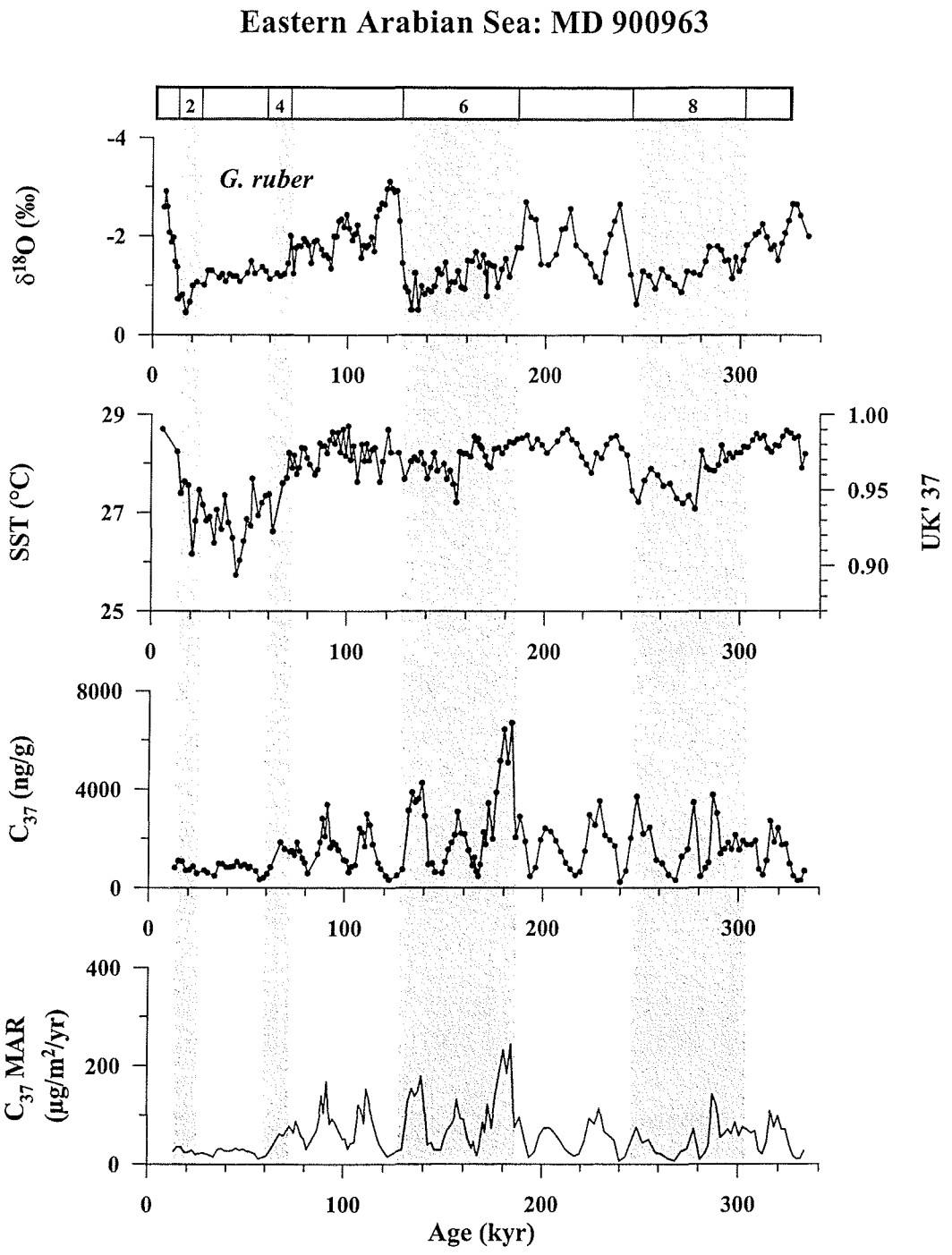

Figure 6: Time series of $\delta^{18}O$ of the planktonic foraminifera *Globigerinoides ruber*, alkenone-derived SSTs (calculated after *Müller et al.* [1998]), C_{37} alkenones and C_{37} MAR for MD 900963 [*Rostek et al.*, 1994, 1997].

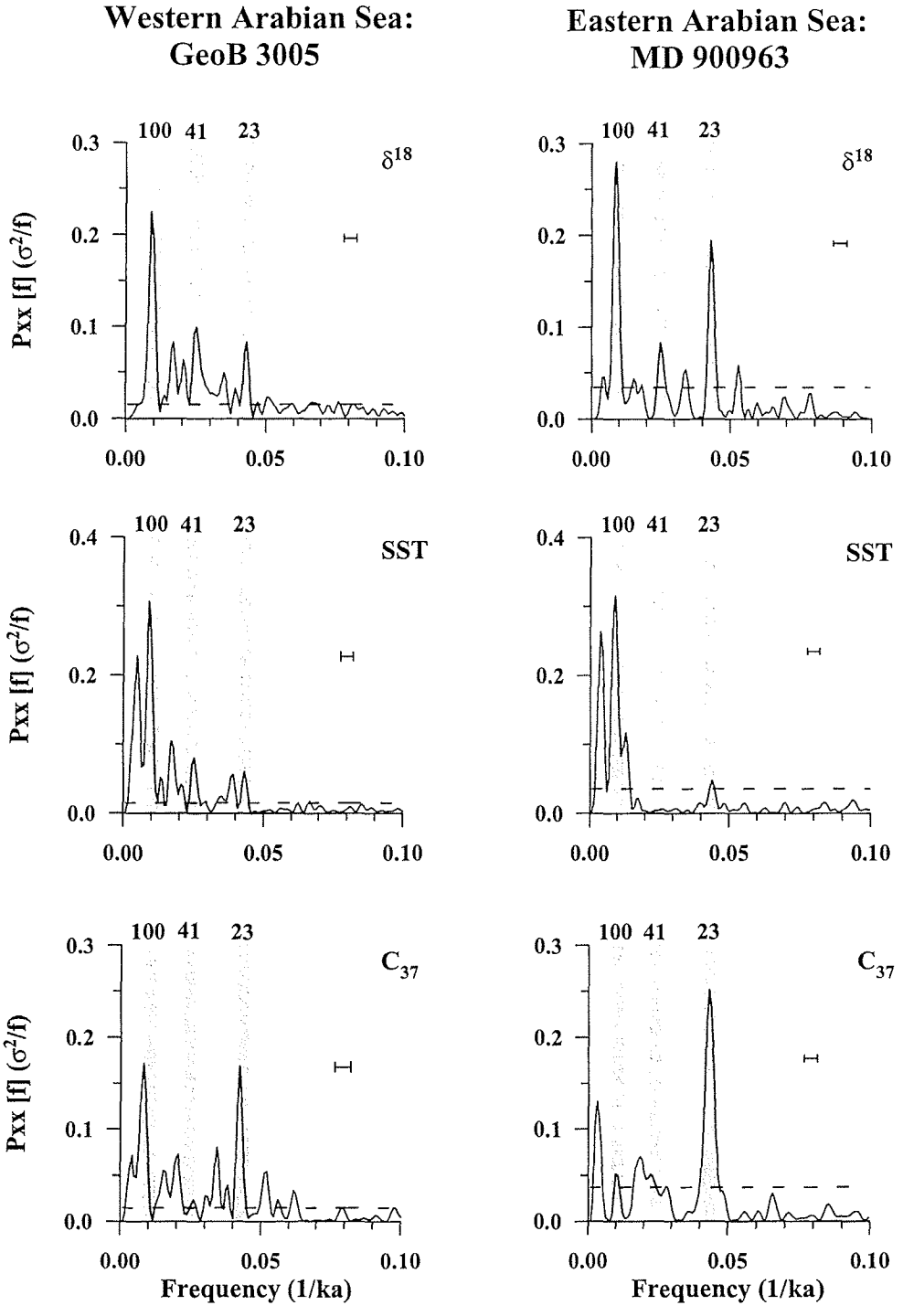

Figure 7: Results of harmonic analyses calculated on the $\delta^{18}O$-, SST- and C_{37} alkenone records of GeoB 3005 and MD 900963 using the software programme SPECTRUM [*Schulz & Stattegger,* 1997]. A Fischer/Siegel test (dashed line) for compound periodicity was employed and significant peaks outside the eccentricity (100), obliquity (41) and precession band (23) are labelled separately. Horizontal bar marks 6 dB bandwidth for each calculation.

The $\delta^{18}O$ and SST records of MD 900963 (Figure 7), too, are dominated by variations in the eccentricity band. Additionally, minor variance is present in the frequency band of precession. Power associated with obliquity is characteristic for the $\delta^{18}O$ but not for the SST record. SST records varying predominantly at the 100 kyr and 23 kyr periodicities were previously described for the east equatorial Atlantic by *Schneider et al.* [1995; 1996]. Although periodicities greater than 100 kyr have to be interpreted with caution, because of the relative shortness of the time series of GeoB 3005 and MD 900963, they indicate that the SST records reflect rather the low frequencies of eccentricity and related glacial-interglacial variability than precessional insolation changes.

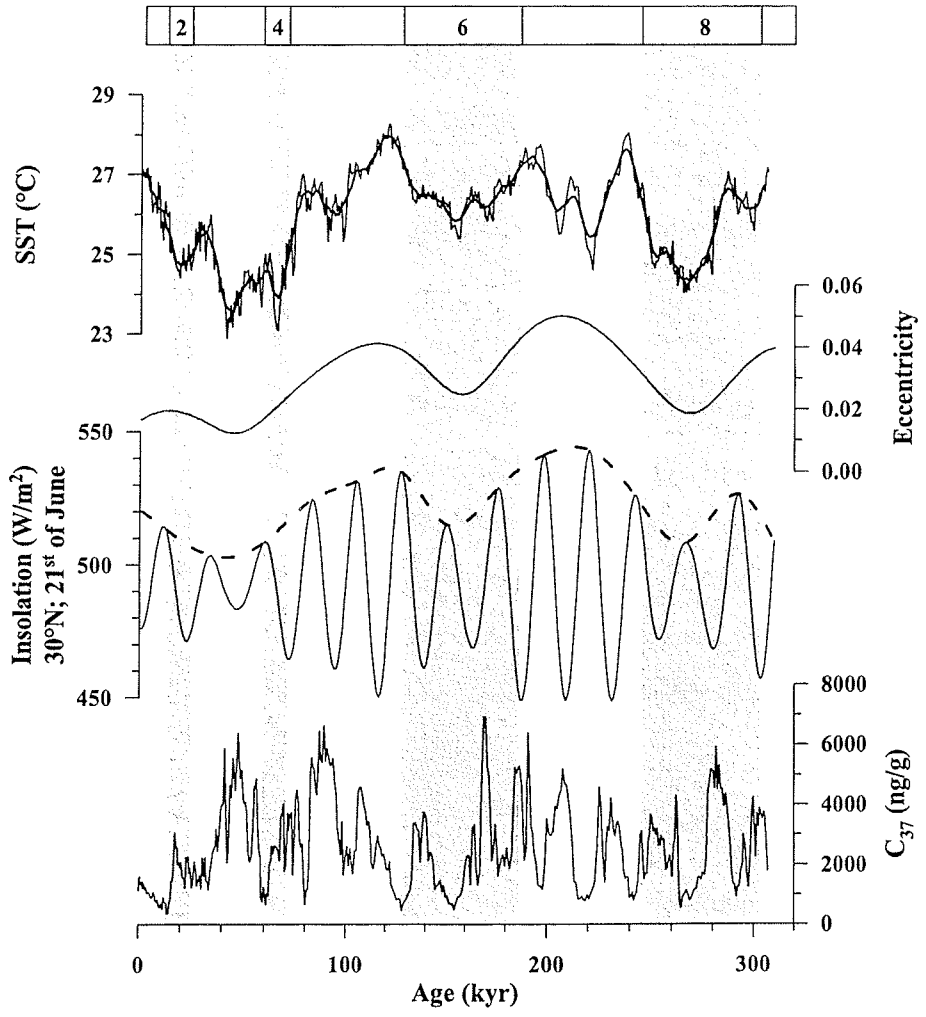

Figure 8: Alkenone-derived SSTs (calculated after *Müller et al.* [1998]) and C_{37} records of core GeoB 3005 in comparison with boreal summer insolation for June 21 at 30° N and eccentricity calculated with the AnalySeries software package [*Paillard et al.*, 1996] following the equations after *Berger et al.* [1978].

On the other hand, SST fluctuations are very similar to tropical insolation, when the amplitude variations of insolation changes, which are modulated by the Earth's eccentricity curves, are considered and not the precession related changes itself (Figure 8) [*Schneider et al.*, 1996; 1999]. As to the long-term trend, lowest alkenone-derived SSTs correspond to minimum amplitudes in precessional insolation during MIS 8 and 4 to 2. Although MIS 6 shows reduced insolation amplitudes, compared to changes in the interglacials, the amplitude reduction is less than in MIS 8 and 4 to 2, providing a possible explanation for the relatively warm SSTs in MIS 6. *Schneider et al.* [1999] suggested that the climatic response in the tropical surface ocean to glacial-interglacial variations is directly related to the 100 kyr and 400 kyr modulations of low-latitude insolation changes, which causes variations in tropical insolation for all seasons. This signal superimposes the variation pattern of global ice volume changes as reflected by the foraminiferal $\delta^{18}O$ records. A possible reason why this 100 kyr and 400 kyr amplitude modulation of low-latitude insolation is so clearly seen in the alkenone SST records, even in those from the upwelling areas, is that alkenone-derived SSTs do reflect rather annual mean temperatures and not the temperature variance of one particular season [*Schneider et al.*, 1999].

Differences between the western and eastern Arabian Sea

A previous comparison between the western Arabian Sea (TY93-929/P; 13°42'N, 53°15'E) and the eastern Arabian Sea (MD 900963) already revealed resembling SST changes in both regions [*Rostek et al.*, 1997]. Although similar patterns of temperature variations are observed in all records from the Arabian Sea, a more detailed visual comparison between the western and the eastern SSTs (Figure 9) reveals larger temperature differences during cold

dSSTmin (°C)	MIS	Time (kyr)
0.7	3.1	32
1.2	5.1	82
-0.1	5.4	118
(1.5)	(6.4)	(162)
0.6	7.1	194
0.5	7.5	238
1.1	8.5	286

Table 2: ΔSST minima (°C) with corresponding marine isotope sub-stages and ages.

events than during warmer periods. A ΔSST (°C) record, established by subtracting the interpolated temperature signals (Δt = 2 kyr) of GeoB 3005 from MD 900963, confirms temperature differences of more than 3 °C in MIS 8.4, 8.3, 7.3, 5.2, 4.2, and 3.2. Smallest differences of less than 1 °C are observed in MIS 8.5, 7.5, 7.1, 5.4, 5.1 and 3.1. In the time interval between 115 kyr and 125 kyr both records display nearly identical temperature values. As can be derived from Table 2, minima in ΔSST occur about every 40 kyr except within MIS 6. Here, the changes in ΔSST are of intermediate amplitude ranging between about 1.0 and 2.5 °C.

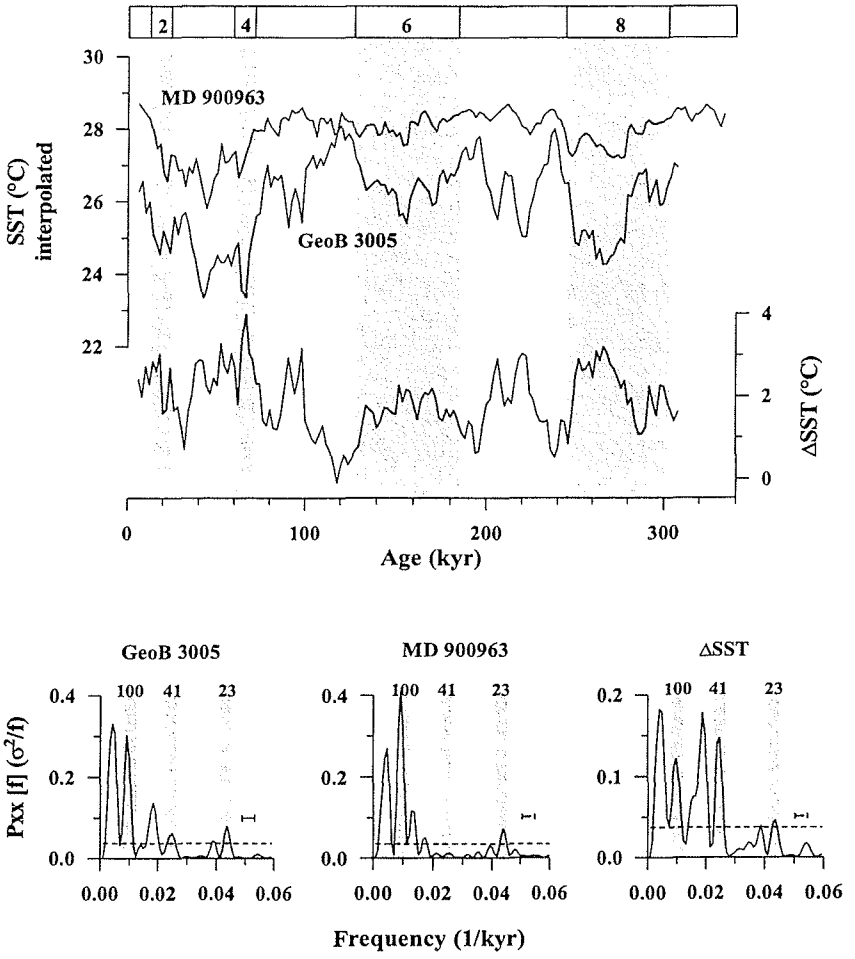

Figure 9: Interpolated SST records (Δt = 2 kyr) of GeoB 3005, MD 900963 (calculated using the AnalySeries software package [*Paillard et al.*, 1996]) and ΔSST. Results of harmonic analyses calculated on GeoB 3005, MD 900963 and ΔSST using the software programme SPECTRUM [*Schulz & Stattegger*, 1997]. A Fischer/Siegel test (dashed line) for compound periodicity was employed. The eccentricity (100), obliquity (41) and precession bands (23) are labelled. Horizontal bar marks 6 dB bandwidth for each calculation.

The results of the time series analyses confirms that, within the primary orbital parameters, variance in the ΔSST record is most pronounced in the frequency band of obliquity (Figure 9). Although the Indian monsoon system was previously described as being mainly forced by precessional insolation [*e.g. Clemens et al.,* 1991*; Prell & Kutzbach,* 1987, 1992] and additionally by changes in glacial boundary conditions in tune with eccentricity [*Niitsuma et al.,* 1991; *Anderson & Prell,* 1993; *Emeis*, 1993], variations associated with obliquity were found in several proxy records from the western Arabian Sea [e.g. *Clemens & Prell*, 1990; *Clemens et al.,* 1991; *DeMenocal et al.*, 1991]. Based on the results of cross-spectral analyses between ETP (variations in past patterns of eccentricity, obliquity and precessional parameters as summarised by a normalised and summed time series) and SW monsoon indicators from the Owen Ridge (such as the planktonic foraminifera *Globigerina bulloides*, lithogenic grain size as well as opal and barium fluxes) *Clemens et al.* [1991] suggested that over the obliquity frequency band strong monsoons occur simultaneously with maxima in Northern Hemisphere insolation. To calculate the phase relationship between ETP and large-scale variations in continental ice volume *Clemens et al.* [1991] used the $\delta^{18}O$ SPECMAP stack of *Imbrie et al.* [1984]. Their estimates indicate that ice volume minima lag the primary orbital parameters by -11° (~3 kyr), -78° (~9 kyr) and -82° (~5 kyr) for eccentricity, obliquity and precessional insolation, respectively. At the same time, they ruled out glacial-interglacial ice volume changes as primary forcing mechanism on SW monsoon intensity, because of the low coherence with the monsoon indicators and because ice volume minima occur ~8 kyr after monsoon maxima in the frequency band of obliquity.

In contrast, the 41 kyr periodicity found in the record of the lithogenic mass accumulation rates by *Clemens and Prell* [1990] and *DeMenocal et al.* [1991] at the Owen Ridge is coherent and in phase with maximum ice volume leading insolation maxima by ~11 kyr. This phase relationship is assumed to indicate increased source area aridity related to maximum Northern Hemisphere ice cover [*DeMenocal et al.,* 1991].

In order to distinguish whether the 41 kyr periodicity found in the SST record of GeoB 3005 and the ΔSST record is related to insolation changes associated with obliquity or rather correspond to variations in the global ice volume, cross-spectral analyses were carried out on ETP and the interpolated SST records of sites GeoB 3005 and MD 900963 as well as on the ΔSST record (Table 3). Significant coherencies were found within the frequency bands of obliquity (0.9784) and precession (0.9359) at site GeoB 3005 (Table 3). The coherency in the low frequency band of eccentricity is high but does not reach the significance level of 0.9. The phase relationship indicates that SST maxima lag obliquity by -117° (~13 kyr) and

precessional insolation referenced to June 21 by -106° (~7 kyr). The SST record of MD 900963 is coherent with ETP in the frequency bands of eccentricity (0.9576) and precessional insolation (0.9671), while it lacks coherency associated with obliquity. The phasing indicates a lag of -16° (~4 kyr) and -125° (~8 kyr) with respect to eccentricity and precessional insolation, respectively. The ΔSST is coherent with ETP only in the frequency band of obliquity (0.9838) with maximum SST differences between the western and eastern Arabian Sea leading obliquity by +58° (~7 kyr).

Core	Eccentricity		Obliquity		Precession (June 21)	
	Coherency	Phase (°)	Coherency	Phase (°)	Coherency	Phase (°)
GeoB 3005	(0.7341)	(+3 +/-24)	0.9784	-117 +/-6	0.9359	-106 +/-10
MD 900963	0.9576	-16 +/-8	-	-	0.9671	-125 +/-7
dSST	-	-	0.9838	+58 +/-5	(0.804)	(+103+/-20)
min ice volume SPECMAP stack	0.986	-11 +/-5	0.946	-78 +/-11	0.971	-82 +/-8

Table 3: Results of the cross-spectral analyses between variations in past patterns of eccentricity, obliquity and precessional parameters (referenced to June 21) as summarised by a normalised and summed time series referred to as ETP, and SST records of GeoB 3005, MD 900963 as well as ΔSST. Positive values indicate a lead and negative values indicate a lag with respect to ETP. Coherencies and phase estimates of the $\delta^{18}O$ SPECMAP stack with respect to ETP [*Clemens et al.*, 1991] are given for comparison.

Taking into account the phasing of ice volume changes estimated by *Clemens et al.* [1991] it is indicated that maximum SSTs in the western Arabian Sea and maximum SST differences between the western and eastern Arabian Sea lag minimum ice volume and maximum ice volume, respectively, by about -40° (~4 kyr) in the frequency band of obliquity. Still, the phasing of the SST variations is close to that of ice volume changes, which implies a link between low-latitude temperature variability of the western Arabian Sea and climate changes in the high latitudes of the Northern Hemisphere. A relationship between monsoonal climate and rapid temperature fluctuations of the high northern latitudes as revealed by the Greenland ice records was previously described by *Schulz et al.* [1998] in sediment cores from the northeastern Arabian Sea. They observed laminated, organic carbon-rich bands, reflecting strong monsoon induced productivity that correlate with the mild interstadial climate events in the northern North Atlantic, while bioturbated, organic carbon-poor bands, indicating periods

of lowered SW monsoon intensity, were associated with intervals of high-latitude atmospheric cooling.

Emeis et al. [1995] suggested that on the basis of a glacially expanded snow cover over central Asia the NE monsoon season lasted longer and cool adiabatic winds kept especially the SSTs in the northern part of the Arabian Sea low into spring and early summer. A prolonged NE monsoon season and cooler NE monsoon winds were probably more effective in lowering the annual mean SSTs in the western than in the eastern Arabian Sea contributing to the obliquity signal in the western Arabian Sea SST record.

SST Variations and the Productivity Record of C_{37} Alkenones in the Arabian Sea

In contrast to the SST variations the records of C_{37} alkenones and C_{37} mass accumulation rates reveal maximum values at higher frequencies (Figures 4, 5 and 6). This is most clearly visible at the open ocean sites of GeoB 3005 and MD 900963 (Figures 4 and 6) showing periodic increases at time intervals of about 20 to 25 kyr during glacial as well as interglacial times.

To identify periodic variations spectral analyses has been carried out on the records of C_{37} alkenones of sites GeoB 3005 and MD 900963 from the western and eastern Arabian Sea, respectively (Figure 7). In contrast to the SST record the C_{37} alkenones of GeoB 3005 reveals strong variance near the eccentricity and within the precession band but only minor variance within the obliquity band. Variance in the frequencies of eccentricity and obliquity is of only minor importance in the C_{37} record of site MD 900963, which is clearly dominated by the higher frequencies of precessional insolation. Periods of more than 100 kyr are not taken into account, because of the relative shortness of the time series. The distinct 23 kyr periodicity of these records indicates a precessionally related forcing rather than changes caused by the waxing and waning of the continental ice-sheets. This is in accordance with the observations made by *Schubert et al.* [1998], who described spectral peaks within the precession band for TOC and several marine biomarker compounds, while the $\delta^{18}O$ record of the planktonic foraminifera *G. ruber* shows a dominant 100 kyr periodicity.

This difference between SST and C_{37} alkenone variations is illustrated in Figure 8, which compares the alkenone-derived SST signal and the absolute C_{37} alkenone concentrations of GeoB 3005 with the eccentricity and summer insolation for June 21 at 30° North calculated after *Berger* [1978]. While SST changes follow the pattern of eccentricity, modulating the amplitude variations of tropical insolation, a good correlation is obvious between higher

contents of C_{37} alkenones and insolation minima. *Budziak et al.* [2000] interpreted this antiphase relationship between indicators of surface water productivity and Northern Hemisphere summer insolation to be the result of a combined signal of only moderate SW monsoon wind strength and of additionally strengthened and prolonged NE monsoon winds enhancing primary productivity due to deeper mixing in times of increased snow-cover over the Tibetan Plateau.

Conclusions

The reconstruction of alkenone-derived SSTs obtained from sediment surface samples along a W-E transect from the Gulf of Aden into the western Arabian Sea does not reflect a seasonal upwelling signal, but annually integrated temperatures. This indicates that in the Arabian Sea the sedimentary unsaturation ratio of C_{37} alkenones is not affected by seasonal productivity patterns.

The alkenone-derived SST variations observed in core GeoB 3005 from the open ocean upwelling region are in good agreement with ODP Site 723 from the Oman margin and MD 900963 from the eastern Arabian Sea. They roughly follow the $\delta^{18}O$ record with highest SSTs in MIS 7 and 5. Only moderate cooling is observed in MIS 6. These SST changes are very similar to the amplitude of precessional insolation modulated by eccentricity. As indicated by frequency analyses SST records from the western and eastern Arabian Sea show a pronounced cyclicity in the frequency band of eccentricity, while variance in the precessional frequency band is of only minor importance. In contrast, variations in C_{37} alkenone accumulation are dominated by the higher frequencies of precessional insolation.

The ΔSST record of GeoB 3005 and MD 900963 shows larger temperature differences between the western and eastern Arabian Sea sites during cold intervals than during periods of warm SSTs. In contrast to the SST record of core MD 900963, SSTs of GeoB 3005 and especially ΔSST reveal strong variance in the obliquity band. This suggests that a prolonged NE monsoon season and cooler NE monsoon winds on the basis of increased snow-cover over the Tibetan Plateau during times of expanded Northern Hemisphere ice-sheets were probably more effective in lowering the annual mean SSTs in the western than in the eastern Arabian Sea contributing to the obliquity signal in the western Arabian Sea SST record.

Acknowledgements

We thank Hella Buschhoff, Dietmar Grotheer and Ralph Kreutz for technical assistance in the home laboratory, the officers, crew and scientists aboard R/V *Meteor* for their help with coring and sampling operations, and Kai-Christian Emeis for providing data from ODP Site 723. This research was funded by the Deutsche Forschungsgemeinschaft (Mu 788/2-2) and the Bundesminister für Bildung und Forschung (BMBF), Bonn. Paleoclimater work at CEREGE is supported by CNRS (PNEDC), the European Community (projects ENV4-CT97-0564, FMRX-CT96-0046, and ENV4-CT97-0659), and the IFCPAR (project 1809-1).

The data of GeoB 3005 and MD 900963 presented in this paper will be archived in the Pangaea database (www.pangaea.de).

4.3 Late Quaternary productivity variations in the Arabian Sea induced by meridional movements in Findlater Jet position

(to be submitted to *Palaeogeography, Palaeoclimatology, Palaeoecology*)

Late Quaternary productivity variations in the Arabian Sea induced by meridional movements in Findlater Jet position

Dörte Budziak, Christopher Moos, Ralph R. Schneider, Peter J. Müller, and Gerold Wefer

Fachbereich Geowissenschaften, Universität Bremen, Postfach 330 440, 28334 Bremen, Germany

Abstract

Past productivity variations were reconstructed for the Owen Ridge (GeoB 3007) and for the open ocean upwelling region near the Gulf of Aden (GeoB 3005) using the sedimentary amount of C_{37} alkenones and total organic carbon (TOC). These records indicate productivity maxima during glacial substages 8.2, 6.2 and 2.2 at the Owen Ridge, whereas precession-related changes are of only minor importance at this location. In contrast, highest productivity occurred every 20 to 25 kyr in the open ocean upwelling region near the Gulf of Aden. The results of frequency analyses confirm that productivity at site GeoB 3007 responds predominantly to glacial-interglacial climate changes, while site GeoB 3005 is dominated by precessional insolation. The productivity pattern at the Owen Ridge is attributed to periodic NW-SE displacements of the Findlater Jet axis and related line of zero wind stress curl in tune with glacial-interglacial changes. This axis separates the region of open ocean upwelling to the northwest from downwelling to the southeast of the jet.

Alkenone-derived sea-surface temperature (SST) records from the Owen Ridge and from the open ocean upwelling region near the Gulf of Aden follow in general the glacial-interglacial variations of the $\delta^{18}O$ signal of planktonic foraminifera. The $\delta^{18}O$ and SST records do not exhibit pronounced differences between both sites, except for the on average slightly higher alkenone-derived temperatures at site GeoB 3007.

Our results imply a major control of paleoproductivity by open ocean upwelling at the Owen Ridge during glacial times, when the mean position of the Findlater Jet axis prevailed south of its modern position. Site GeoB 3005 lies well within the open ocean upwelling region and, therefore, is insensitive to changes in the position of the Findlater Jet axis. Here, the productivity pattern is interpreted to be a combined signal of moderate SW monsoon winds and of strengthened and prolonged NE monsoon winds.

Introduction

The surface circulation of the Arabian Sea is controlled by the Indian monsoon system, which originates in the differential heating of the Indian Ocean and the southern part of the Asian continent. The seasonally reversing pressure gradient drives the SW and NE monsoon winds (Figure 1) in boreal summer and winter, respectively. The SW monsoon winds are focused into a low-level jet, the so called Somali or Findlater Jet, situated in the lowest 3 km of the atmosphere [*Findlater,* 1969; *Findlater,* 1977]. This jet originates in the southeast trade winds over the southern Indian Ocean during boreal summer. Heading north across the flat arid lands of eastern Kenia, Ethiopia and Somalia, it finally crosses the Arabian Sea [*Findlater,* 1977]. As the SW monsoon winds increase in speed between April and July the jet axis moves towards the Northwest closer to the coast of Oman [*Findlater*, 1971], crossing the Owen Ridge today [*Luther & O'Brien*, 1985] (Figure 1).

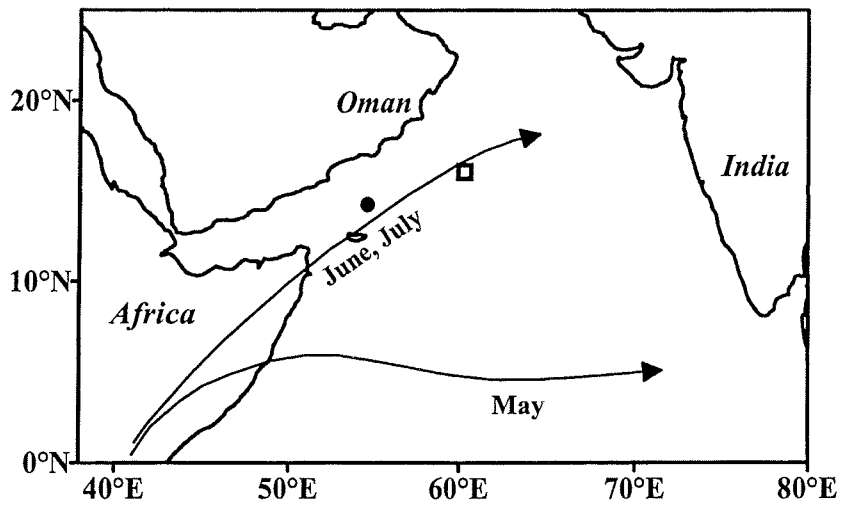

Figure 1: Map of the Indian Ocean north of the equator. Indicated are the locations of cores GeoB 3007 (open square) and GeoB 3005 (full circle). Arrows show the mean May and June-July position of the Findlater Jet redrawn from *Brown et al.* [1998].

Beside these seasonal variations, the Arabian Sea is also subject to considerable spatial variability producing strong gradients in oceanographic and related biogeochemical processes. To the NW of the Findlater Jet axis, the wind stress curl is positive and creates a divergence of surface water-masses driving open ocean upwelling through Ekman pumping. To the SE of the jet, the wind stress curl is negative and creates a convergence resulting in a deepening of

the mixed layer by downward transport of surface waters. Thus, the jet axis marks the line of zero wind stress curl [*Brock et al.,* 1992; *Brock & McClain,* 1992].

While coastal upwelling off Oman seems to respond linearly to stronger wind stress [*Prell & Streeter*, 1982; *Anderson et al.*, 1992] little correlation has been found between wind stress and the resultant wind stress curl near the Owen Ridge [*Anderson & Prell*, 1992]. Instead, a 4 year observation (1979-1982) of interannual variations in the SW monsoon winds indicated that upwelling over the Owen Ridge is sensitive to NW-SE displacements of the jet axis, which separates the upwelling from the downwelling region. During the year with highest wind-speeds the jet axis lay closer to the Owen Ridge, while during the years with lower wind-speeds the jet axis was situated farther to the SE maintaining its NE orientation. Thus, the movement of the Findlater Jet axis has large influence on upwelling over the Owen Ridge [*Anderson & Prell,* 1992].

To asses how the monsoon winds and the seasonal circulation might have been affected by glacial-interglacial and related insolation changes *Luther et al.* [1990] and *Anderson & Prell* [1992] compared model simulations over a wide range of modified summer insolation forcing. Both model studies show a NW displacement of the Findlater Jet axis and an increase in the positive as well as negative wind stress curl with increasing insolation. *Anderson & Prell* [1992] concluded that higher insolation forcing produces increased upwelling up to a point where spatial changes in the position of the jet become important. Additionally, strongest upwelling over the Owen Ridge occurs at intermediate wind strength, when the region of maximum wind stress curl moves closer to the Owen Ridge at times of reduced summer insolation.

To test this conclusion of *Anderson & Prell* [1992], sea-surface temperature (SST) as well as productivity records of a core from the Owen Ridge (GeoB 3007) were compared with a sediment core from the open ocean upwelling area near the Gulf of Aden (GeoB 3005) (Figure 1). Time series of the $\delta^{18}O$ signal of *Neogloboquadrina dutertrei*, alkenone-derived SSTs, and the C_{37} alkenone and total organic carbon (TOC) records were studied by means of frequency as well as cross-spectral analyses in relation with the orbital parameters of eccentricity, obliquity and precession. Alkenone-derived SSTs, which have the potential to show overall decreases of annual mean SST caused by generally more intense upwelling, as well as C_{37} alkenone and TOC values, indicative of precession-related productivity variations, should reflect a different pattern at the Owen Ridge compared to the open ocean upwelling site near the Gulf of Aden.

Modern Setting

The monsoonal coupling between atmosphere and ocean produces a complete semi-annual reversal of surface currents in the Arabian Sea basin. This causes drastic changes in oceanic surface processes and related effects on modern SSTs and particle fluxes through the water-column. During the SW monsoon upwelling of cold and nutrient-rich subsurface water masses due to Ekman transport occurs along the southern coastline of the Arabian Peninsula giving rise to high rates of primary productivity. Farther offshore, an open ocean type upwelling develops in a broad region because of the positive curl in the wind stress to the NW of the Findlater Jet axis, while to the SE of the jet axis downwelling emerges [*Swallow*, 1984; *Brock & McClain*, 1992]. Additionally, the NE monsoon winds cause a deeper mixing of the surface layers thereby injecting nutrients into the photic zone during the winter season. Consequently, the Arabian Sea is one of the most productive regions of the modern world's oceans [e.g. *Nair et al.*, 1989; *Brock et al.*, 1992; *Brock & McClain*, 1992; *Ittekkot et al.*, 1992; *Haake et al.*, 1993]. Today, wind-speed, SSTs, mixed layer depths and primary productivity show similar variation patterns at both sites (Figure 2) during most of the year.

Wind-Speed

Wind-speed derived from the Comprehensive Ocean-Atmosphere Data Set (COADS: http://ferret.wrc.noaa.gov/fbin/climate_server) ranges between 3 and 4 m/s at both sites during the intermonsoon and reaches highest values of up to 15 m/s at site GeoB 3007 and 10 m/s at site GeoB 3005 during the SW monsoon season. The wind-speed during the NE monsoon barely exceeds values of 5 m/s at the Owen Ridge as well as in the open ocean upwelling region near the Gulf of Aden (Figure 2a). Except for the stronger SW monsoon winds at the Owen Ridge, the monthly succession is very similar at both sites.

Sea-Surface Temperatures

Monthly SSTs derived from the World Ocean Atlas 1994 (http://ferret.wrc.noaa.gov/fbin/climate_server) for sites GeoB 3007 and GeoB 3005 (Figure 2b) reveal temperature variations of similar magnitude and range at the Owen Ridge and in the open ocean upwelling region, respectively. Most of the year, SSTs are slightly higher at the Owen Ridge than at the open ocean upwelling site. The largest difference between both locations occurs during the summer months, when upwelling seems to be more effective in cooling SSTs at site GeoB 3005

although the wind-speed is not as high as at site GeoB 3007. The annual mean temperatures at sites GeoB 3007 and GeoB 3005 are nearly identical with values of 27.0 °C and 26.8 °C, respectively.

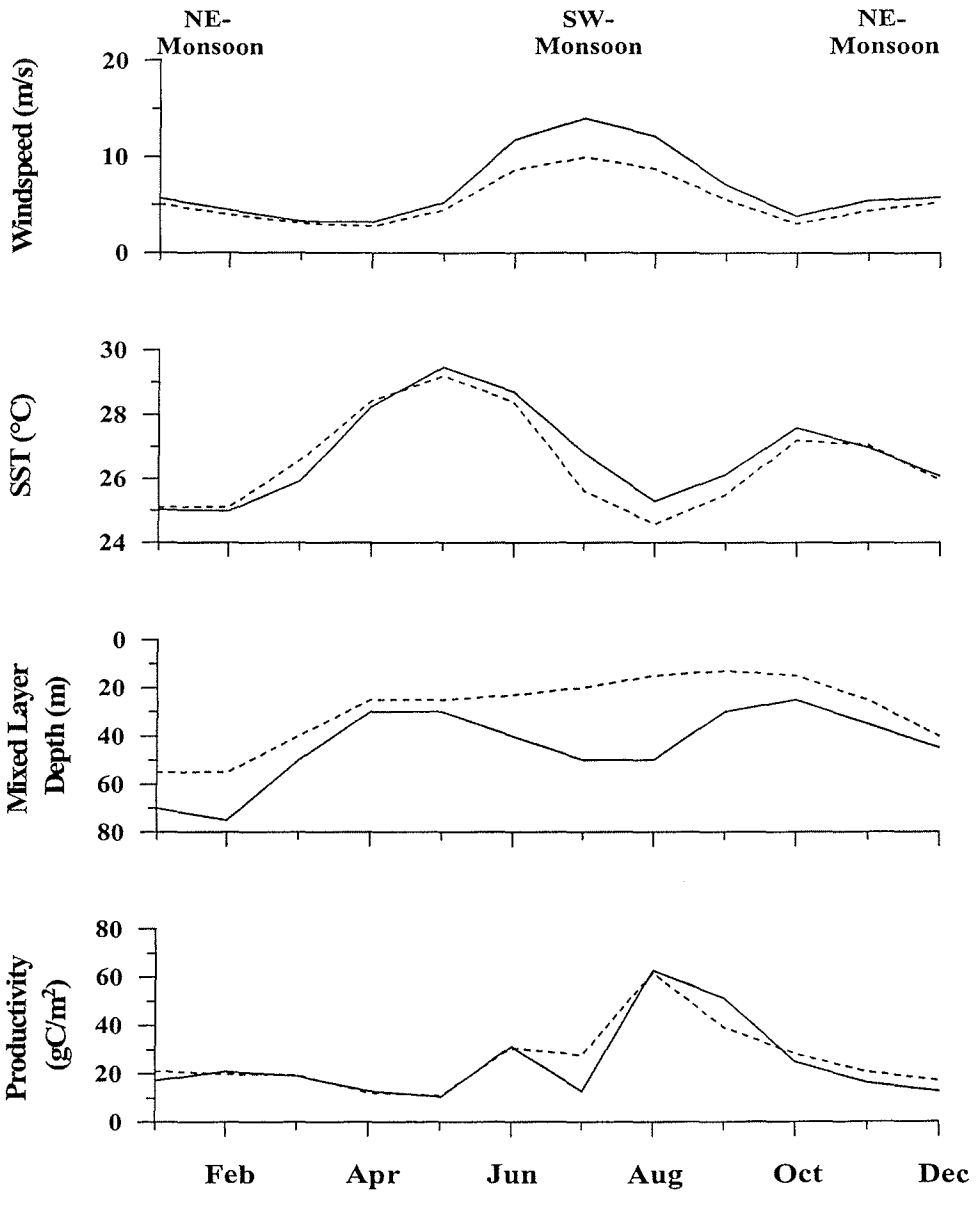

Figure 2: Modern wind-speed derived from the COADS Data Set, sea-surface temperatures and mixed layer depths obtained from the NOAA World Ocean Atlas 1994 (http//:ferret.wrc.noaa.gov/fbin/climate_server) as well as primary productivity [*Antoine et al.*, 1996] for the core locations of GeoB 3007 (full line) and GeoB 3005 (dashed line).

Mixed Layer Depth

The mixed layer depth (Figure 2c) was characterised after *Hastenrath & Merle* [1987] as the depth at which the temperature is 1 °C lower than at the sea-surface (World Ocean Atlas 1994: http://ferret.wrc.noaa.gov/fbin/climate_server). At the Owen Ridge the mixed layer depth shows two distinct minima of about 30 m during the intermonsoon and two maxima of depths around 50 m and nearly 80 m during the SW and NE monsoon, respectively. This indicates a modern downwelling during the SW monsoon season at the position of GeoB 3007.

In contrast, the mixed layer depth at site GeoB 3005 in the open ocean upwelling region near the Gulf of Aden reveals only one maximum of about 50 m during the NE monsoon indicating a deeper mixing. During the SW monsoon season the upwelling of sub-surface water masses pushes the top of the thermocline upwards to depths of only 20 m as was previously reported by *Brock & McClain* [1992].

This spatial pattern of mixed layer depths is in accordance to *Burkill* [1999], who introduced an Upwelling/Downwelling Index (UDI) calculated for a 1590 km long transect of stations reaching orthogonal from the southern Oman coast into the Arabian Sea. This UDI is based on the wind-driven mixed layer depths measured at each station during the SW monsoon and intermonsoon cruises in 1994 of the UK ARABESQUE program. The UDI values along this transect clearly separate the downwelling from the upwelling region where upwelling is most pronounced at the near-shore station and decreases in SE direction until downwelling is apparent at 17°30 N and 60°30 E.

Productivity

Antoine & Morel [1996] and *Antoine et al.* [1996] presented monthly maps of primary productivity based on coastal zone colour scanner (CZCS) pigment imagery. They combined satellite productivity estimates from CZCS with various ecological and physiological parameters. Today, the annual course of primary production is nearly identical for both sites (Figure 2d) with productivity maxima reaching peak values of 60 gC/m^2 in August. During the NE monsoon a second but less pronounced maximum occurs showing estimated values of about 20 gC/m^2 at the Owen Ridge and in the open ocean upwelling region.

Summarising the modern setting at sites GeoB 3007 from the Owen Ridge and GeoB 3005 from the open ocean upwelling region near the Gulf of Aden, the mixed-layer depth reveals the most important differences between both sites. The productivity pattern at

site GeoB 3007 is in contrast to the one expected regarding the mixed layer depth as indicator for upwelling/downwelling process during the SW monsoon season. A possible explanation for this discrepancy is the lateral transport of chlorophyll at the sea-surface from the open ocean upwelling into the downwelling region.

Material and Methods

Material

The sediment cores presented in this study were recovered during R/V *Meteor* cruise M31/3 from the Owen Ridge (GeoB 3007: 16°10.2'N, 59°45.3'E, water depth 1920 m, site 111-1 in *Hemleben et al.*, [1996]) and from the open ocean upwelling region near the Gulf of Aden (GeoB 3005: 14°58.3'N, 54°22.2'E, water depth 2310 m, site 108 in *Hemleben et al.*, [1996]). Both cores consist of foraminifera-bearing carbonate ooze with clay [*Hemleben et al.*, 1996]. They are intensely bioturbated, which indicate oxygenated conditions of the oceanic bottom waters overlying the sediment surface. No indications for sediment disturbances (hiatus, slumps, etc.) have been detected, except for two sandy foraminiferal layers in core GeoB 3007, which might indicate some winnowing of the fine fraction [*Hemleben et al.*, 1996].

Oxygen Isotopes and Stratigraphy

GeoB 3007 and GeoB 3005 were sampled at 5 cm intervals with 10 ml syringes and the samples were stored at 4 °C until further preparation. One sample series was wet sieved to obtain the coarse fraction (> 63 μm) which was used to pick the planktonic foraminiferal species *Neogloboquadrina dutertrei* (d'Orbigny). This was used for stable oxygen isotope ($\delta^{18}O$) measurements on GeoB 3007 and GeoB 3005. A Finnigan MAT 251 micromass-spectrometer coupled with a Finnigan automated carbonate device was used to analyse the samples. The carbonate was reacted with 100% orthophosphoric acid at 75 °C. The reproducibility (1 σ) based on replicate measurements of a lab-internal carbonate standard (Solnhofen limestone) is +/- 0.07 $^{0}/_{00}$. GeoB 3005 was previously investigated for its stable isotope geochemistry, fluxes of sedimentary biogenic components and alkenone SST reconstruction [*Budziak et al.*, 2000 and in prep].

The age model of GeoB 3007 is based on the correlation of the $\delta^{18}O$ record of the planktonic foraminifera *N. dutertrei* with the $\delta^{18}O$ timescale of the same foraminiferal species

in GeoB 3005 using the software package AnalySerie 1.0a7 of *Paillard et al.* [1996]. The stratigraphic framework of GeoB 3005 was derived from graphic correlation with the SPECMAP $\delta^{18}O$ stack (Figure 3a) of *Imbrie et al.* [1984]. Further details on that chronology are given in *Budziak et al.* [2000]. Sedimentation rates were calculated on the basis of the depth-age model between stratigraphic tie-points (Table 1).

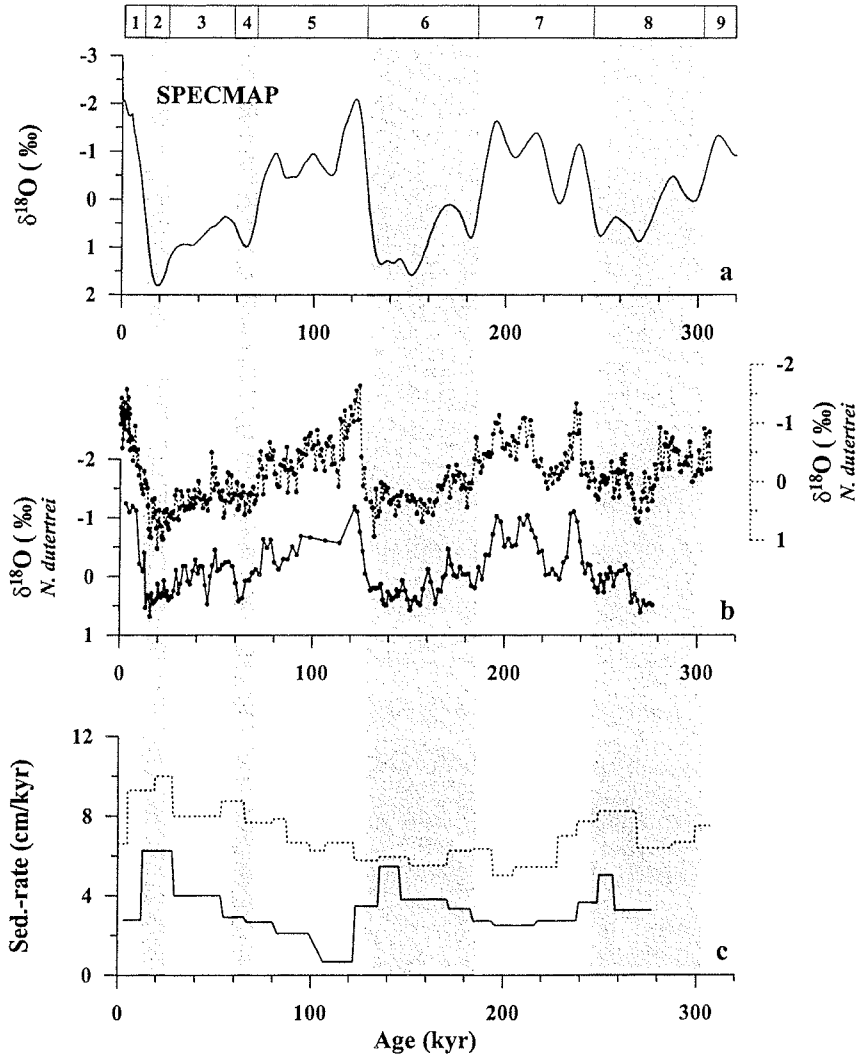

Figure 3: Correlation of the SPECMAP stack [*Imbrie et al.*, 1984] (a) with the $\delta^{18}O$ signals of *Neogloboquadrina. dutertrei* of GeoB 3007 (full line) and GeoB 3005 (dashed line; note that y scale is shifted) (b). Isotopic events were used as stratigraphic control points (Table 1) and linear sedimentation rates were derived from these agemodels (c).

Event	Time, kyr	Depth, cm
core top	3	3
2	12	28
3.1	28	128
3.3	53	228
4.2	65	263
5.1	80	303
5.3	99	343
5.5	122	358
6.2	135	403
6.3	146	463
6.5	171	558
6.6	183	598
7.1	194	628
7.3	216	683
7.5	238	743
8.2	249	783
8.3	257	823
end of core	277	888

Table 1: Isotopic events used as stratigraphic control points from correlation of the $\delta^{18}O$-timescale of core GeoB 3005 (kyr) [*Budziak et al.*, 2000] with the $\delta^{18}O$ signal of GeoB 3007 (cm).

According to our age model the sediment record at site GeoB 3007 resolves the time between 3 and 277 kyr (Figure 3b) showing an average sedimentation rate of about 4 cm/kyr. The linear sedimentation rates range from 0.7 cm/kyr in MIS 5.4 and 5.3 up to 6.3 cm/kyr between isotopic sub-stages 3.1 to 2.2 as shown in Figure 3c. Thus, the mean time resolution of samples taken at intervals of 5 cm is 1.5 kyr. GeoB 3005 resolves the last 307 kyr (Figure 3b) with an average sedimentation rate of 7 cm/kyr. The linear sedimentation rates are generally higher than at site GeoB 3007 and vary from 5 cm/kyr in MIS 7 up to 10 cm/kyr in MIS 2 (Figure 3c). Consequently, the mean time resolution of samples taken at intervals of 5 cm is about 700 years.

Organic Carbon and C_{37} Alkenones

A second sample series was freeze dried, ground in an agate mortar and used for carbon and alkenone analyses. Organic carbon was determined on decalcified samples by combustion at 1050 °C using a Heraeus CHN-O-Rapid elemental analyser [*Müller et al.*, 1994]. The precision of the measurements was better than 3 % based on duplicates and a lab-internal reference sediment (WS2).

To reconstruct past SSTs the concentrations of long-chain unsaturated ketones (alkenones) were determined in 5 g and 2g aliquots of freeze dried samples of GeoB 3007 and GeoB 3005, respectively [*Müller et al.*, 1994 and 1998]. The extraction procedure was kept similar for both cores, except for cleaning of every sample of GeoB 3007 by alkaline hydrolysis (saponification) before being analysed by gas chromatography [*Budziak et al.*, 2000] in order to remove possibly interfering fatty methyl esters.

The ketone unsaturation index UK'37 was calculated from the concentrations of di- and tri-unsaturated C_{37} alkenones according to *Prahl & Wakeham* [1987: UK'37 = (37:2) / (37:2 + 37:3)] and converted to temperature values using the global core top calibration of *Müller et al.* [1998: UK'37 = 0.033 T + 0.044]. This calibration is virtually identical with the widely used *Emiliania huxleyi* culture calibration of *Prahl & Wakeham* [1987: UK'37 = 0.033 T + 0.043]. The precision of the measurements was better than 0.02 UK'37 units (+/- 0.6 °C), based on replicate extractions of lab-internal reference sediments.

Mass accumulation rates were calculated by multiplying the sedimentary concentrations of C_{37} alkenones and TOC with the dry bulk density of the sediments and the linear sedimentation rates between stratigraphic tie points. This was done to quantify the fluxes of C_{37} alkenones (C_{37} MAR) and TOC (TOC MAR) into the sediment and to circumvent dilution effects caused by changes in terrigenous detritus or biogenic components when considering relative percentages.

Time Series Analyses

To identify the dominant frequencies in the time series of $\delta^{18}O$, SST and TOC/alkenone MAR and to carry out cross-spectral analyses the software program SPECTRUM developed by *Schulz & Stattegger* [1997] was used. To proof the statistical significance a Fischer/Siegel test was employed in the sub-routine 'Harmonic'. The same parameters were used during time series analyses (level of significance = 0.05; oversampling factor (OFAC) = 4; high frequency factor (HIFAC) = 1). The calculation procedure of the cross-spectral analyses, too, was kept constant for all records (level of significance = 0.2; OFAC = 4; HIFAC = 1; window type = Welch; 2 segments with 50% overlap; see *Schulz & Stattegger* [1997] for further details). This method does not only include an estimation of coherency, a linear correlation coefficient in the spectral domain, but also estimates the lead or lag reported as positive or negative phase angles, respectively, between records sharing a similar variance at a given frequency [*Jenkins & Watts*, 1968; *Imbrie et al.*, 1989]. Changes in eccentricity, obliquity and precession index

(21st of June, northern hemisphere, SPECMAP convention) were calculated after *Berger* [1978] using the AnalySeries 1.0a7 software package of *Paillard et al.* [1996], normalised and summed in an orbital record referred to as ETP [*Imbrie et al.,* 1989].

In order to compare both sites on similar sampling intervals, the time-series were linearly interpolated using the AnalySerie 1.0a7 software package of *Paillard et al.* [1996]. The time-resolution of the resulting equidistant records is 1.5 kyr. The number of the original data-points is 178 and 450, while the number of the interpolated data-points is 182 and 206 for GeoB 3007 and GeoB 3005, respectively.

Results and Discussion

Oxygen Isotopes and Alkenone-Derived Sea-Surface Temperatures

At the Owen Ridge and in the open ocean upwelling area near the Gulf of Aden the $\delta^{18}O$ records of the planktonic foraminifera *N. dutertrei* (Figure 3) reflect the typical Late Quaternary pattern due to the build up and retreat of the continental ice sheets and glacial-interglacial changes in surface water temperature. Except for minor differences in the age models the time series are in very good agreement with each other. The $\delta^{18}O$ signal of GeoB 3007 ranges between -1.24 ‰ and 0.69 ‰, while at site GeoB 3005 the values vary from -1.63 ‰ to 1.14 ‰ [*Budziak et al.,* 2000]. Thus, at the Owen Ridge the total amplitude of $\delta^{18}O$ values is by 0.84 ‰ smaller.

The alkenone temperature variations at the Owen Ridge (Figure 4) show generally lower SSTs during glacial compared to interglacial periods. The alkenone-derived SSTs vary between 23.9 and 28.6 °C with highest temperatures during MIS 7 and 5, and the Holocene. Lowest SSTs are observed in MIS 8, 4 and 3. An exception from strong glacial cooling occurred during MIS 6, which remained relatively warm with a decrease to glacial temperatures by only 2 °C on average.

The SST record at site GeoB 3005 reveals a similar temperature pattern in the open ocean upwelling region. Here, the absolute temperatures range between 22.9 and 28.3 °C [*Budziak et al.*, in prep]. Thus, the SST record at site GeoB 3005 (Figure 4) has generally slightly lower temperature values than site GeoB 3007. Again, MIS 6 remained relatively warm. At the Owen Ridge the absolute amplitude of SST variations is by nearly 1 °C smaller, which is in good correspondence with the smaller range in the $\delta^{18}O$ signal of *N. dutertrei.* This may, at

least partly, be an artefact caused by the on average two times lower sedimentation rates at site GeoB 3007 (Figure 3).

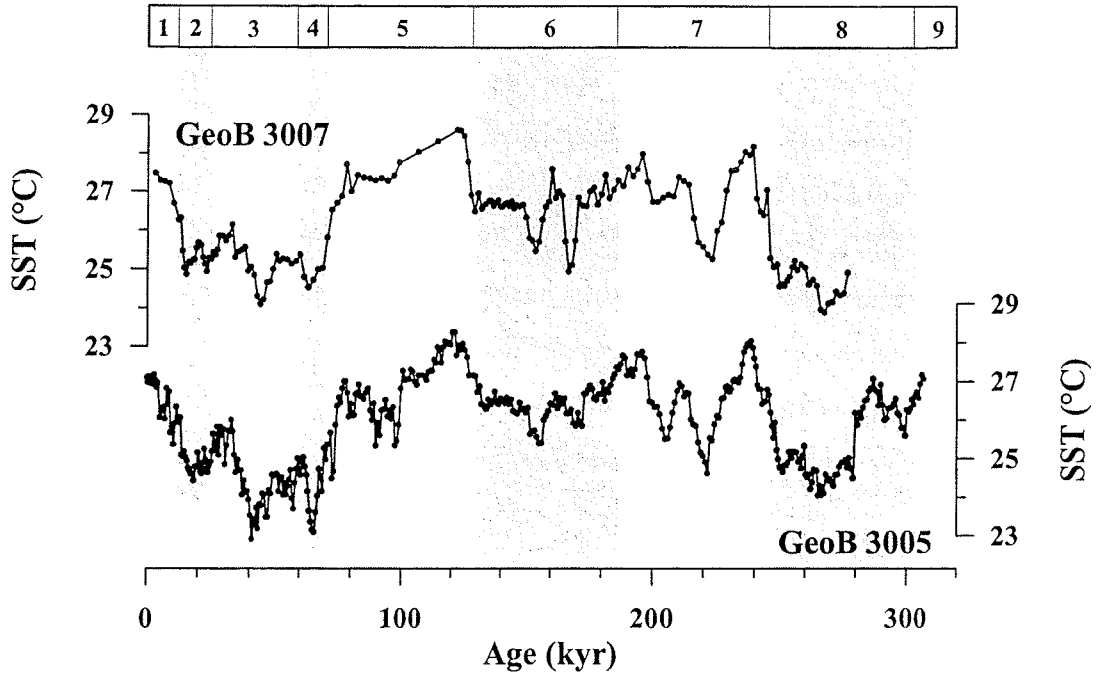

Figure 4: Time series of the alkenone-derived SSTs (calculated after *Müller et al.* [1998]) for sites GeoB 3007 and GeoB 3005.

The overall temperature changes at both sites are in good agreement with previous studies from the coastal upwelling cell off Oman [*Emeis*, 1993; *Emeis et al.*, 1995], and from the western and eastern Arabian Sea [*Rostek et al.*, 1993, 1994 and 1997]. A warm stage 6 in records of alkenone-derived SSTs was previously described for the equatorial Atlantic [*Schneider et al.*, 1996, 1999] and Indian Oceans [*Rostek et al.*, 1994 and 1997; *Emeis et al.*, 1995; *Budziak et al.*, in prep]. This and a SST record derived from foraminiferal transfer functions from the tropical Indian Ocean [*Clemens et al.*, 1991] suggest that a warm stage 6 is a genuine phenomenon rather than a local anomaly in the western Arabian Sea.

Although it was assumed that alkenone temperature estimates may be biased by seasonal productivity changes [*Conte et al.*, 1992; *Conte & Eglinton*, 1993; *Weaver et al.*, 1999], core-top calibrations from the Indian Ocean [*Sonzogni et al.*, 1997a,b] and from the eastern South Atlantic [*Müller et al.*, 1998] suggest that productivity weighted alkenone-derived SSTs are generally very similar to production-weighted mean temperatures. Additionally, *Budziak et al.* [in prep] have shown for the Gulf of Aden and the western Arabian Sea that the core-top

alkenone signal reflects a modern annual mean temperature rather than explicitly the season of upwelling in the study area.

The $\delta^{18}O$ and SST time series of GeoB 3007 and GeoB 3005 reveal glacial-interglacial temperature variations of similar magnitude, which is in good accordance with the modern situation at both sites. As expected, regarding the seasonal succession of modern SSTs (Figure 2), no pronounced differences exist between the $\delta^{18}O$ and SST records from the Owen Ridge and the open ocean upwelling region near the Gulf of Aden, except for the on average slightly higher SSTs at site GeoB 3007. Thus, SSTs are assumed to reflect the general trends in western Arabian Sea cooling or warming, whereby it is not possible to differentiate between the potential mechanism which may have lead to cooling of surface waters, e.g. stronger SW monsoon upwelling, enhanced mixing and adiabatic cooling associated with stronger NE monsoons, or movements in the axis of the Findlater Jet.

C_{37} Alkenones and Total Organic Carbon: The Productivity Record

At the Owen Ridge the absolute concentrations of C_{37} alkenones (Figure 5) range between 180 and 3220 ng/g dry sediment with a distinct maximum in MIS 6.2. The mean sedimentary alkenone content is generally higher during glacial compared to interglacial periods. Superimposed on this pattern are changes with minima and maxima every 20 to 25 kyr. With only minor exceptions the TOC record of GeoB 3007 (Figure 5) correlates well with the overall pattern described for the C_{37} alkenones showing values between 0.3 and 1.4 %. The TOC record, too, reveals higher concentrations during glacial times with pronounced maxima during MIS 8.2, 6.2, 3.3 and 2.2.

The C_{37} MAR (Figure 5) follow in general the concentration record of the C_{37} alkenones revealing higher accumulation rates during glacial times. Peak values of about 70, 170 and 95 $\mu g/m^2/yr$ are reached in MIS 2.2, 6.2., and 8.2, respectively, while the sedimentation rates reveal corresponding peaks (Figure 3c) with maximum values of 6.3 cm/kyr in MIS 2.2, and more intermediate values of 5.5 and 5.0 cm/kyr in MIS 6.2 and 8.2, respectively. Thus, better preservation on the basis of enhanced sedimentation rates [*Müller & Suess*, 1979] alone are unlikely to account for the maximum C_{37} MAR in MIS 6.2. The superimposed changes every 20 to 25 kyr are less defined in the mass accumulation rates. A similar pattern is revealed by the TOC MAR, which vary between 0.04 and 0.8 $g/m^2/yr$ with highest values in MIS 2.2, 6.2 and 8.2 (Figure 5). These peak values in the mass accumulation rates of C_{37} alkenones and

TOC indicate periods of higher productivity at the Owen Ridge corresponding to glacial maxima.

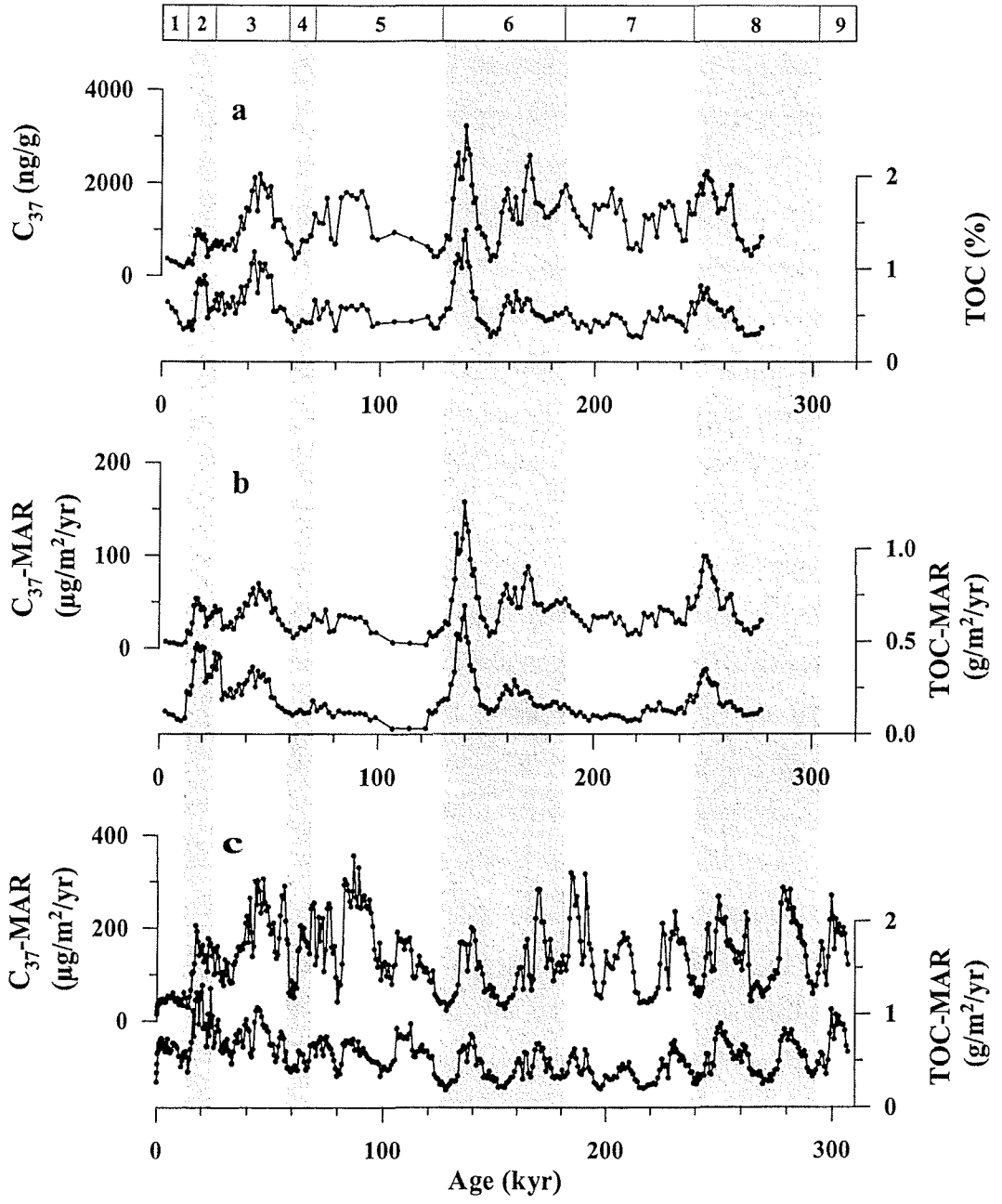

Figure 5: Time series of C_{37} alkenones and TOC (a) as well as C_{37} MAR and TOC MAR (b) for site GeoB 3007, and C_{37} MAR and TOC MAR for site GeoB 3005 (c).

In contrast to site GeoB 3007, the records of TOC/C_{37} alkenone MAR in the open ocean upwelling region near the Gulf of Aden reflect a pronounced periodicity with minimum and maximum values occurring during glacial as well as interglacial stages every 20 to 25 kyr. At

site GeoB 3005 the C_{37} MAR and TOC MAR records (Figure 5) range from 10 to 360 $\mu g/m^2/yr$, and 0.2 to 1.3 $g/m^2/yr$, respectively [*Budziak et al.*, 2000] and, thus, are generally higher than at the Owen Ridge site.

Intuitively, relationships between C_{37} alkenones as well as TOC records and the magnitude of past productivity should exist. Unfortunately, details such as ecology of the plankton community contributing to the signal of sedimentary organic matter or processes taking place during the transport into greater depths and burial into the sediment are still mostly unknown for the past. Thus, variations in the sedimentary content of organic matter can be accounted to changes in either productivity or preservation. Today, parts of the Arabian Sea are characterised by a pronounced oxygen minimum zone (OMZ) in midwater depths between 150 and 1250 m [*Wyrtki et al.*, 1973]. High productivity, which increases oxygen consumption during organic matter decomposition of the sinking particles, and moderate ventilation at intermediate depths could generate and maintain this low-oxygen layer [*Swallow*, 1984].

Although possible preservation artefacts caused by oxygen deficiency on the productivity signal have been subject of considerable debate [e.g. *Pedersen et al.*, 1992; *Paropkari et al.*, 1992 and 1993], more recent studies provided significant evidence that sedimentary variations in C_{37} alkenones and TOC reflect changes in past productivity in the Arabian Sea [e.g. *Reichart et al.*, 1998; *Schubert et al.*, 1998]. In the northern Arabian Sea *Reichart et al.* [1998] compared TOC patterns in cores from different water depths and observed that TOC fluctuations in cores from within and below the OMZ can be correlated with each other. Although, the concentrations of TOC are generally higher within the OMZ sediments, they concluded that TOC variations are not caused by changes in the intensity of the OMZ but are primarily controlled by surface water productivity. Additionally, *Schubert et al.* [1998] confirmed the use of organic biomarkers, such as C_{37} alkenones, as qualitative tracers for paleoproductivity changes in Arabian Sea sediments.

Orbital forcing on periodic productivity variations

Harmonic Variations

The results of the harmonic analyses, applied on the productivity records of GeoB 3007 and GeoB 3005, indicate significant differences between the Owen Ridge and the open ocean upwelling region near the Gulf of Aden. Exemplary, the variance patterns of the individual TOC MAR are given in Figures 6a and 6b. At the Owen Ridge (Figure 6b) the productivity

records are dominated by the low frequency band of eccentricity. Additionally, significant variance is present in the obliquity and precessional frequency bands as well as at periods of 55 kyr and 29 kyr. In contrast, in the open ocean upwelling region (Figure 6a) productivity variations are dominated by the high frequencies of precessional insolation. Here, no significant variance is present in the eccentricity and obliquity frequency bands but, additionally, at the 29 kyr period.

A 29 kyr and 52 kyr periodicity have already been found in other records of the western Arabian Sea and the equatorial Indian Ocean [*Clemens & Prell*, 1991; *Bassinot et al.*, 1994; *Rostek et al.*, 1997]. *Clemens & Prell* [1991] interpreted them as non-linear interactions between external insolation forcing and internal climatic feedback mechanisms due to the interdependence of snow cover on the Asian Plateau (variations in albedo and sensible heating) and variations in latent heat and tropospheric heating.

The long periods of 100 kyr have to be interpreted with caution, because of the relative shortness of both time series. Still, they indicate a more pronounced influence of global glacial-interglacial climate change than of precessional insolation changes on the productivity variations at site GeoB 3007.

Cross-Spectral Analyses

In order to evaluate the statistical and temporal correspondence of the above described time-series in relation to orbital parameters, cross-spectral analyses were performed. The productivity records from the open ocean upwelling region near the Gulf of Aden are coherent only with the precessional frequency band referenced to June 21, which was discussed before in detail by *Budziak et al.* [2000]. Therefore, only the results of the cross-spectral analyses between ETP and the productivity records from the Owen Ridge are summarised in Table 2 for obliquity and eccentricity as well.

The phase relationship between the productivity records and precessional insolation referenced to June 21 is virtually the same at both sites taking into account the uncertainty of the estimate. The average phasing of +172° (11 kyr) is opposite to variations in boreal summer insolation as illustrated in Figure 6d. Particularly, in the open ocean upwelling region near the Gulf of Aden, maxima in TOC and TOC MAR occur at the same time as minima in boreal summer insolation calculated for June 21. This phase relationship is in good agreement with results from *Emeis* [1993] and *Murray & Prell* [1992], who calculated the paleoproductivity

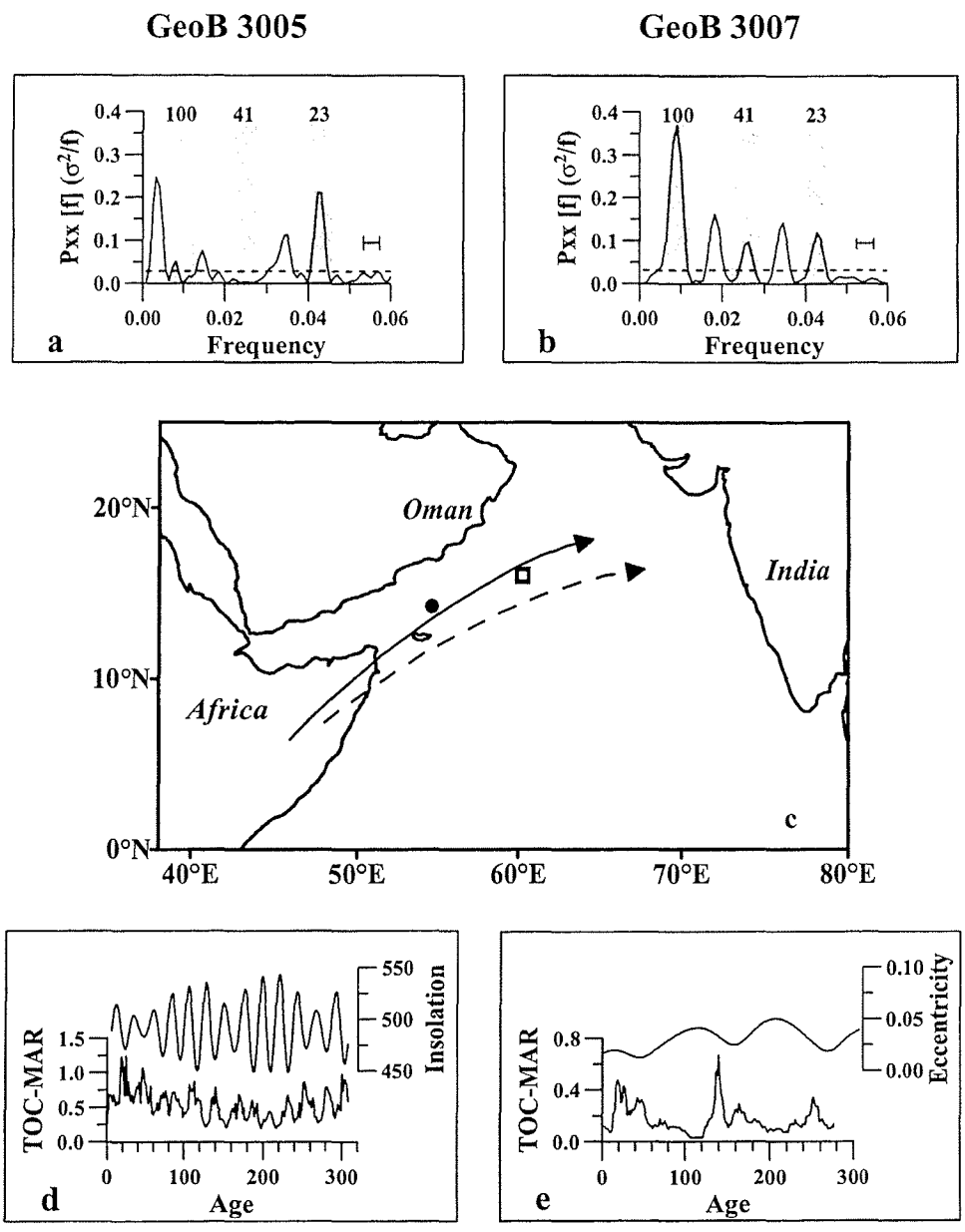

Figure 6: Results of the harmonic analyses on TOC accumulation rates of sites GeoB 3005 and GeoB 3007 using the software programme SPECTRUM [*Schulz & Stattegger*, 1997] are given in (a) and (b), respectively. A Fischer/Siegel test (dashed line) for compound periodicity was employed. Horizontal bar marks 6 dB bandwidth for each calculation. (c) Core locations (full circle = GeoB 3005; open square = GeoB 3007) with respect to the conceptual positions of the Findlater Jet axis: full line indicate mean modern position [*Brown et al.*, 1998], while dashed line suggest the mean position of the jet axis during glacial maxima. TOC MAR records of cores GeoB 3005 (d) and GeoB 3007 (e) in comparison with boreal summer insolation for the 21st of June at 30° N and eccentricity, respectively, calculated with the AnalySeries software package [*Paillard et al.*, 1996] following the equations after *Berger et al.* [1978].

rates after *Sarnthein et al.* [1992] or *Müller and Suess* [1979] using TOC MAR at ODP Site 723 off Oman and RC 27-61 from the Owen Ridge, respectively. To explain the opposite phasing, *Budziak et al.* [2000] suggested that variations of paleoproductivity indicated by C_{37} alkenones and TOC are not directly linked to maximum monsoonal upwelling intensity and wind strength in the western Arabian Sea. They interpreted the maxima in C_{37} alkenone and TOC variations to be a combined signal of moderate SW monsoon wind strength, as suggested by *Rixen et al.* [1996] and additionally strengthened and prolonged NE monsoon winds enhancing primary productivity due to deeper mixing in the western Arabian Sea.

In contrast to the open ocean upwelling region near the Gulf of Aden, the productivity records from the Owen Ridge show high coherencies with ETP in the frequency band of obliquity (Table 2), suggesting a link to high latitude climate changes. The phase relationships indicate that the productivity records lead maximum summer insolation in the obliquity band by +25° on average, whereas maximum ice-volume, which is reflected by the $\delta^{18}O$ record of the planktonic foraminifera *N. dutertrei*, leads obliquity by +97°. Thus, productivity lags ice volume changes by -72°. Taking into account only the mass accumulation rates of C_{37} alkenones and TOC with +36° and +43° (Table 2), respectively, the phase lag with respect to maximum ice-volume decreases to about -38°.

Clemens et al. [1991] used the relative abundance of the planktonic foraminifera *Globigerina bulloides*, lithogenic grain size as well as opal and barium fluxes as indicators for monsoonal upwelling strength. They observed a near-zero phase relationship between these monsoon proxies and insolation over the obliquity frequency band and suggested that strong monsoons occur simultaneously with maxima in Northern Hemisphere summer insolation. On the other hand, the phase relationship between lithogenic mass accumulation rates at the Owen Ridge and obliquity are in tune with changes in ice volume [*DeMenocal et al.*, 1991]. This was taken by *DeMenocal et al.* [1991] as evidence for increased aridity in dust source areas due to the expansion of the Northern Hemisphere's ice sheets.

The high coherency levels and the phase relationship between the productivity records of site GeoB 3007 with respect to ETP in the frequency bands of eccentricity and obliquity (Table 2) confirm higher productivity levels during glacial periods and only subdued sensitivity to precession-related changes in monsoon induced upwelling. In contrast, the lack of coherency between the records of GeoB 3005 and eccentricity suggests that 100 kyr glacial-interglacial variability is of only secondary importance to the open ocean upwelling

Precession (June 21)

Core	Time Series	k	Phase (°)	kyr
GeoB 3007	C37	0.9728	+163 +/-7	+10.4 +/-0.4
	MAR-C37	0.9879	+171 +/-4	+10.9 +/-0.3
	TOC	0.9735	+161 +/-7	+10.3 +/-0.4
	MAR-TOC	0.9706	+166 +/-7	+10.6 +/-0.4
GeoB 3005	C37	0.952	+171 +/-9	+10.9 +/-0.6
	C37 MAR	0.9549	+166 +/-9	+10.6 +/-0.6
	TOC	0.9477	+175 +/-9	+11.2 +/-0.6
	TOC MAR	0.955	+171 +/-9	+10.9 +/-0.6

Obliquity

Core	Time Series	k	Phase (°)	kyr
GeoB 3007	C37	0.9127	+12 +/-12	+1.4 +/-1.4
	MAR-C37	0.9745	+36 +/-6	+4.1 +/-0.7
	TOC	0.9092	+10 +/-13	+1.1 +/-1.5
	MAR-TOC	0.998	+43 +/-2	+4.9 +/-0.2

Eccentricity

Core	Time Series	k	Phase (°)	kyr
GeoB 3007	C37	0.9946	-141 +/-3	-39.2 +/-0.8
	MAR-C37	0.9729	+175 +/-7	+48.6 +/-1.9
	TOC	0.9542	+148 +/-9	+41.1 +/-2.5
	MAR-TOC	0.9416	+153 +/-10	+42.5 +/-2.8

Table 2: Results of cross spectral analyses on the interpolated (Δt=1.5 kyr) records of C_{37} alkenones, C_{37} MAR, TOC and TOC MAR with respect to changes in precession (referenced to June 21) for cores GeoB 3007 and GeoB 3005, obliquity and eccentricity for core GeoB 3007. ETP was calculated after *Berger* [1978] using the AnalySeries 1.0a7 software package of *Paillard et al.* [1996], normalised and summed in an orbital record referred to as ETP [*Imbrie et al.*, 1989]. Phase angles can be converted to time by dividing values in degrees by 360° and multiplying by orbital period in kyr. Coherencies are significant above the critical level of 0.9 [*Schulz & Stattegger*, 1997], k = coherency

region near the Gulf of Aden. Here, precession-related changes in upwelling and deeper mixing have mainly controlled variations in paleoproductivity at site GeoB 3005. These results suggest a stronger glacial-interglacial high latitude climate signal at the Owen Ridge (Figure 6e), whereas the open ocean upwelling region responds predominantly to changes in precessional low latitude insolation (Figure 6d). This difference in the pattern of TOC and alkenone time series is not revealed by the SST records from both sites.

As described for modern conditions (Figure 2) there exists fundamental difference in the mixed-layer depth between both sites during the SW monsoon season due to the separation of the upwelling from the downwelling region caused by the Findlater Jet. Therefore, the difference in paleoproductivity at the Owen Ridge is attributed to changes in the position of the monsoonal winds due to a possible southward shift of the Findlater Jet axis as indicated in Figure 6c. *Anderson and Prell* [1992] suggested that changes in the relative strength of the monsoon winds are not the primary mechanism in controlling the open ocean productivity, but movements in the position of the low-level jet, when the region of maximum wind stress curl moves closer to the Owen Ridge.

Additionally, *Sirocko* [1991] observed increased glacial flux rates of eolian dust transported by northwesterly winds. These winds overlay the SW monsoon winds during summer in such a way that the northernmost extent of the SW monsoon marks the southernmost extent of the northwesterlies. From dust fluxes recorded in Arabian Sea sediments he inferred a southward shift of the SW monsoon winds for about a few hundred kilometres during glacial times. Accordingly, results from atmospheric general circulation model experiments indicate a progressively northward shift of the jet-axis and decreased wind stress curl accompanied by stronger winds with increased insolation making the Owen Ridge a sensitive location for movements of the jet axis [*Anderson & Prell*, 1992].

We therefore assume that precessional variations of monsoon intensity can be only recorded at sites to the west of the Findlater Jet axis. On the other hand, if the jet axis moved to the southeast, the Owen Ridge is affected by upwelling instead of downwelling, as is the case for site GeoB 3005.

Conclusions

The alkenone temperature variations follow in general the oxygen isotope chemistry revealed by the $\delta^{18}O$ records of the planktonic foraminifera *N. dutertrei* with highest temperatures in MIS 7 and 5 at both sites. No pronounced temperature differences exist between the Owen Ridge and the open ocean upwelling region near the Gulf of Aden except for the on average slightly higher alkenone-derived temperatures at site GeoB 3007.

In contrast to the $\delta^{18}O$ and SST records, the sedimentary content of C_{37} alkenones and TOC shows pronounced differences between both sites. While highest productivity occurred during glacial substages 8.2, 6.2 and 2.2 at the Owen Ridge, maxima in productivity are revealed every 20 to 25 kyr in the open ocean upwelling region. The variance pattern obtained

from harmonic frequency analyses confirms a dominant influence of eccentricity on the productivity records at the Owen Ridge, while productivity in the open ocean upwelling region varies in tune with the frequency band of precession. This is in agreement with the results of the cross-spectral analyses between C_{37} alkenones, C_{37} MAR, TOC as well as TOC MAR and the orbital ETP record. The high coherencies between the productivity records from the Owen Ridge with precession, obliquity as well as eccentricity suggest a stronger glacial-interglacial variability at site GeoB 3007, whereas site GeoB 3005 responds predominantly to precessional low-latitude insolation changes.

The productivity pattern in tune with glacial-interglacial variability at site GeoB 3007 is attributed to changes in the mean position of the Findlater Jet axis and related line of zero wind stress curl. During glacial times the region of positive wind stress curl moves closer to the Owen Ridge. This results in a more effective transport of nutrients into the photic zone during periods of minima in glacial summer insolation at the Owen Ridge. This is in accordance with results from atmospheric general circulation models indicating a progressively northward shift of the monsoon axis and decreased wind stress curl at the Owen Ridge, accompanied by stronger winds with increased insolation [*Anderson & Prell*, 1992].

Acknowledgements

We thank Hella Buschhoff, Dietmar Grotheer and Ralph Kreutz for technical assistance in the home laboratory, the officers, crew and scientists aboard R/V *Meteor* for their help with coring and sampling operations. This research was funded by the Deutsche Forschungsgemeinschaft (Mu 788/2-2).

The data of GeoB 3005 and GeoB 3007 presented in this paper will be archieved in the Pangaea database (www.pangaea.de).

4.4 Carbon isotopes of planktic foraminifera recording nutrient and productivity variations in the northwestern Arabian Sea during the past 300,000 yr

(to be submitted to *Geology*)

Carbon isotopes of planktic foraminifera recording nutrient and productivity variations in the northwestern Arabian Sea during the past 300,000 yr

Christopher A. Moos, Dörte Budziak, Ralph R. Schneider and Gerold Wefer

Fachbereich Geowissenschaften, Universität Bremen, Postfach 330 440, 28334 Bremen, Germany

Abstract

Carbon isotopes of planktic foraminifera display nutrient related $\delta^{13}C$ variations of dissolved inorganic carbon ($\delta^{13}C_{\Sigma CO2}$) in the coastal upwelling area of the NW-Arabian Sea and identify nutrients as a major control mechanism of productivity variations during the past 307,000 yr. The carbon isotope composition of *Globigerinoides ruber* (w) and *Neogloboquadrina dutertrei* from site GeoB 3005 was compared with changes in global deep ocean $\delta^{13}C_{\Sigma CO2}$. The $\delta^{13}C$ record of *G. ruber* (w), revealing nutrient depleted surface water, is coherent and in phase with the global $\delta^{13}C_{\Sigma CO2}$ signal at the primary orbital periods. Additionally, the *G. ruber* (w) $\delta^{13}C$ signal contains variability at higher frequencies. The $\delta^{13}C$ of *N. dutertrei*, living deeper in the water column than *G. ruber* (w), shows stronger deviations relative to the global $\delta^{13}C_{\Sigma CO2}$. The difference between the carbon isotope records of *G. ruber* (w) and *N. dutertrei* ($\Delta\delta^{13}C_{r\text{-}d}$) of core GeoB 3005 displays nutrient variations in the coastal upwelling area. Frequency analyses of the $\Delta\delta^{13}C_{r\text{-}d}$ time series suggests cyclic changes in nutrient availability in tune with Earth's orbital parameters of eccentricity and precession, as well as at periods of 12,500 yr and 7,700 yr. To unravel the dependencies of upwelling related productivity on nutrient availability of subsurface water masses and SW monsoon wind strength during the late Pleistocene, the abundance of *G. bulloides* (ODP Site 723B) was compared with $\Delta\delta^{13}C_{r\text{-}d}$ (GeoB 3005) and lithogenic grain size records (RC27-61). The results of cross-spectral analyses indicate that productivity depends mainly on nutrient availability, while upwelling intensity seems to be of lower importance during the past 307,000 yr.

Introduction

Enhanced productivity during the summer season is a major characteristic of monsoon related upwelling in the northwestern Arabian Sea. Today, about 70% of the total annual productivity takes place during the upwelling season from June to August [*Smith et al.*, 1998]. Various tracers were used to study Arabian Sea upwelling history with respect to productivity e.g.: the relative abundance of the planktic foraminifera *Globigerina bulloides* [*Anderson and Prell*, 1991; 1993; *Prell*, 1984a], the stable isotope composition of planktic and benthic foraminifera [*Niitsuma et al.*, 1991; *Steens et al.*, 1992], organic carbon [*Budziak et al.*, 2000; *Emeis et al.*, 1995] and opal fluxes [*Murray and Prell*, 1992]. Nevertheless, productivity variations are not only controlled by upwelling intensity but are additionally dependent on the nutrient concentrations of the subsurface water masses, which are to be transported into the photic zone by upwelling. While modern nutrient concentrations in intermediate water masses of the northwestern Arabian Sea were nearly constant over the past decades [*Moos et al.*, in press] cadmium contents and carbon isotopes of benthic foraminifera imply nutrient-depleted conditions in intermediate waters during glacial times in the Indian Ocean [*Boyle*, 1992; *Kallel et al.*, 1988].

In this study $\delta^{13}C$ records of planktic foraminifera were used to investigate $\delta^{13}C$ variations of dissolved inorganic carbon ($\delta^{13}C_{\Sigma CO2}$) and nutrient concentrations in surface waters of the northwestern Arabian Sea during the past 307,000 yr. To interpret the carbon isotope time series of planktic foraminifera in terms of nutrient concentrations it is necessary to define a $\delta^{13}C$ reference reflecting constant nutrient levels. Therefore, the carbon isotope values of *G. ruber* (w) and *N. dutertrei* were corrected for their specific offsets relative to ΣCO_2 based on calibrations of *Moos et al.* [submitted] and *Mulitza et al.* [1999]. Today, the offset corrected carbon isotopes of *G. ruber* (w) display surface water $\delta^{13}C_{\Sigma CO2}$ stripped virtually free of nutrients, while *N. dutertrei* prefers high nutrient levels associated with low $\delta^{13}C_{\Sigma CO2}$ [*Moos et al.*, submitted]. Based on the recent calibration of *Moos et al.* [submitted] the carbon isotope difference between *G. ruber* (w) and *N. dutertrei* ($\Delta\delta^{13}C_{r\text{-}d}$) is interpreted with respect to nutrient gradients within Arabian Sea surface water masses.

To assess the contribution of global and regional effects to the carbon isotope signals of *G. ruber* (w) and *N. dutertrei* both records were compared with the global deep ocean $\delta^{13}C_{\Sigma CO2}$ signal estimated from the benthic foraminifera *Universa senticosa* of the core V19-30 located in the equatorial Pacific Ocean [*Shackleton et al.*, 1983].

Additionally, the relationships between nutrient availability, productivity, and the intensity of monsoonal upwelling during the late Pleistocene were investigated. Productivity in the northwestern Arabian Sea is mainly controlled by the combined influence of nutrient availability in the photic zone and upwelling intensity. Variations in nutrient concentrations depend on changes in ocean circulation, while upwelling intensity is mainly controlled by the strength of the SW monsoon winds.

Clemens and Prell [1990] and *Clemens et al.* [1991] established lithogenic grain size records of Arabian Sea sediments as a measure of SW monsoon wind strength, responsible for coastal upwelling off Oman. Coastal upwelling and the associated enhanced productivity are major features of SW monsoon hydrography in the northern Indian Ocean. Productivity variations are indicated by the relative abundance of the planktic foraminiferal species *G. bulloides*, which is widely used to trace changes in upwelling intensity [*Anderson and Prell*, 1991; 1993; *Prell*, 1984a]. Although the upwelling related productivity (% *G. bulloides*) and the eolian dust deposits (lithogenic grain size) seem to be related to the SW monsoon circulation, differences were found between the time series of the associated monsoon tracers [*Clemens et al.* 1996; *Anderson and Prell*, 1991]. Hence, additional mechanisms causing environmental variations have to be taken into consideration.

To study the coupling between the fertility of Arabian Sea water masses, upwelling related productivity as well as SW monsoon wind strength, we compared $\Delta\delta^{13}C_{r\text{-}d}$ record of core GeoB 3005 with the % *G. bulloides* of the coastal ODP Site 723B [*Anderson and Prell*, 1991] and the lithogenic grain size of core RC27-61 located on the Owen Ridge [*Clemens et al.*, 1991; *Clemens and Prell*, 1990).

Oceanography of the Study Area

The northern Arabian Sea is strongly affected by the Indian monsoon system. During northern hemisphere summer strong SW monsoon winds blow parallel to the coasts of Africa and the Arabian Peninsula driving the ocean surface circulation (Figure 1). This wind field induces Ekman drift causing an offshore transport of surface water. Upwelling of cold and nutrient-rich subsurface water-masses into the photic zone is the result [*Wyrtki*, 1971]. Due to the high fertility conditions numerous planktic forminifera are most abundant during the upwelling season [*Curry et al.*, 1992; *Peeters et al.*, 1999]. Additionally, the high nutrient concentrations of freshly upwelled water are documented by low $\delta^{13}C_{\Sigma CO2}$ values. The $\delta^{13}C_{\Sigma CO2}$ difference between winter and summer season ranges from 0.7 ‰ at the sea surface

to 1.3 ‰ between 30 m and 80 m, with mixed layer values about 1.4 ‰ during the NE monsoon season [*Moos et al.*, submitted].

From previous paleoceanographic studies it became evident that SW monsoon winds and related upwelling intensity have varied mainly with a major periodicity of orbital precession [*Prell*, 1984b; *Prell and Van Campo*, 1986]. Additionally, tracers of productivity indicate higher fertility during interglacial periods and lower during glacial times [*Clemens et al.*, 1991]. Carbon isotopes of benthic foraminifera suggest that the hydrographic conditions of intermediate and deep water have been different from the present situation [*Kallel et al.*, 1988]. The hydrography of intermediate water masses changes with sea level variations, because of a reduced contribution of Red Sea Water and Persian Gulf Water during times of low sea levels. In contrast, there might be an increased through-flow of pacific water masses into the Indian Ocean and a higher influence of Antarctic Intermediate Water during glacial times as revealed by carbon isotope records of planktic foraminifera [*Duplessy et al.*, 1989]. These suggest that hydrographic variations affect the transport of nutrients into the northwestern Arabian Sea.

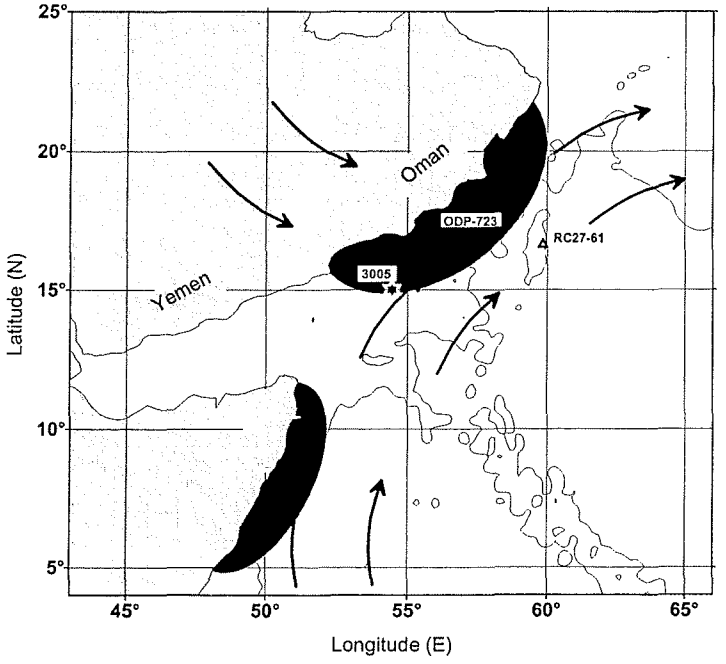

Figure 1: Map of the northwestern Arabian Sea including site locations of core GeoB 3005, RC27-61, and ODP Site 723B. The crosshatched areas indicate the upwelling cells off Somalia and Oman. Arrows show Shamal and SW monsoon winds causing coastal upwelling during summer season.

Materials and Methods

We studied core GeoB 3005 which was recovered off the Arabian coast during R/V *Meteor* cruise M31/3 in 1995 (14°58,3'N, 54°22,2'E; 2318 m) (Figure 1), for the isotope composition of planktic foraminifera.

Isotope analyses on the planktic foraminifera *G. ruber* (w) and *N. dutertrei* were carried out using a FINNIGAN/MAT-252 mass-spectrometer equipped with an automatic carbonate preparation device. Precision based on replicates of an internal limestone standard was better than 0.07 ‰ for $\delta^{18}O$ and 0.05 ‰ for $\delta^{13}C$. From each sediment sample 8 to 12 specimens of *G. ruber* (w) (250-315 mm) and *N. dutertrei* (>315 mm) were picked out for isotope analysis.

The stratigraphic framework of GeoB 3005 was derived from graphic correlation of the $\delta^{18}O$ record of *N. dutertrei* with the SPECMAP $\delta^{18}O$ reference stack [*Imbrie et al.* 1984]. Further details on that chronology are given in *Budziak et al.* [2000]. According to this age model the core resolves the last 307,000 yr showing an average sedimentation rate of about 7/1000 cm yr-1 and a mean time resolution of about 700 years at sample intervals of 5 cm.

To identify the dominant periodicities in each time series and to estimate the correlation between the single records cross-spectral analyses were carried out. All analyses were calculated by the Cross-Blackman-Tukey method [*Jenkins and Watts*, 1968] using the software package 'AnalySeries 1.0a7' developed by *Paillard et al.* [1996]. For the comparison of the $\delta^{13}C$ records of GeoB 3005 with the deep water $\delta^{13}C$ signal of *Universa senticosa* of east Pacific core V19-30, which can be considered as a global signal for $\delta^{13}C$ change [*Shackleton et al.*, 1983]. The original time series were converted to 750 yr time intervals by linear interpolation. Due to the time resolution of the *G. bulloides* and the grain size records all time series were linearly interpolated at intervals of 2000 yr for the purpose of cross-spectral analysis between the $\Delta\delta^{13}C_{r\text{-}d}$ record of core GeoB 3005 and tracers of monsoon wind strength (lithogenic grain size, RC27-61) and productivity (% *G. bulloides*, ODP Site 723B). With respect to this rather coarse resolution we only report cyclical changes of the primary orbital periods.

Results and Discussion

$\delta^{13}C$ of Planktic Foraminiferal Time Series (GeoB 3005)

Globigerinoides ruber (w)

The $\delta^{13}C$ data of *G. ruber* (w) of core GeoB 3005 range from 2.5 ‰ during the Holocene to 0.5 ‰ during isotope stage 6 (Figure 2a). The long-term variations show a good agreement with the benthic $\delta^{13}C$ record of *Universa senticosa* of core V19-30. Compared to the global variations the $\delta^{13}C$ record of *G. ruber* (w) reveals by about 0.9 ‰ higher $\delta^{13}C$ values during

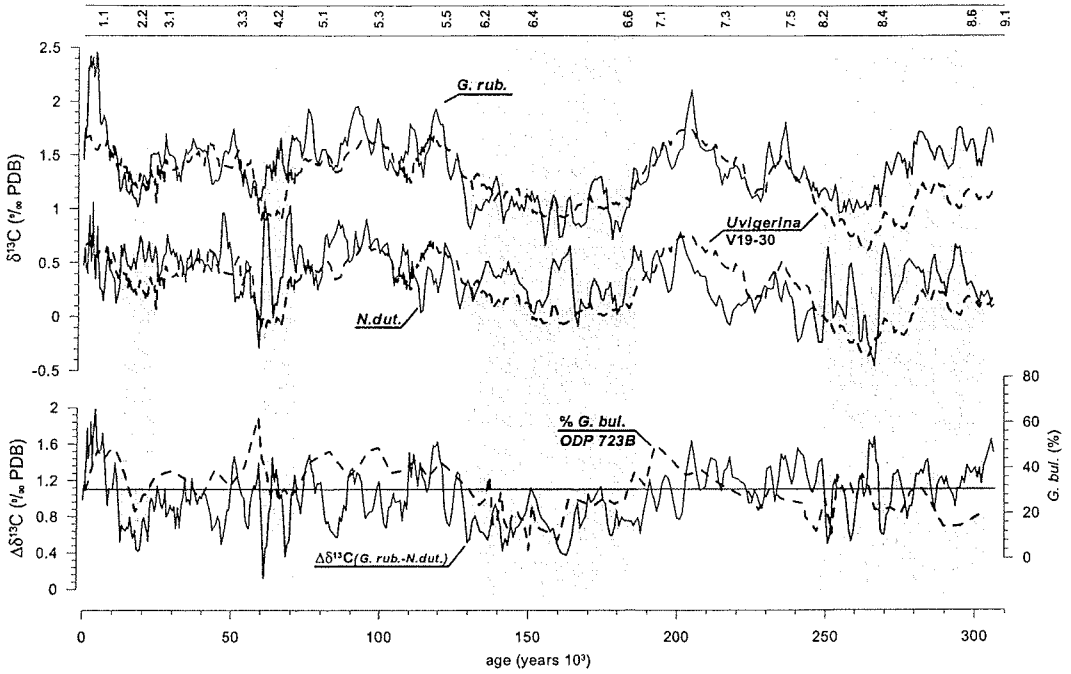

Figure 2: Carbon isotope records of core GeoB 3005. a) comparison of *G. ruber* (w) and *N. dutertrei* (straight lines) with the $\delta^{13}C$ time series of the benthic foraminifera *Universa senticosa* of the pacific core V19-30 (fat dashed line). Time series of *G. ruber* (w) and *N. dutertrei* are corrected for their specific offsets to $\delta^{13}C_{\Sigma CO2}$ given by *Moos et al.* [submitted] and *Mulitza et al.* [1999]. The record of *Universa senticosa* was shifted for the best fit relative to *G. ruber* (w) and *N. dutertrei*. b) straight lines indicate offset corrected carbon isotope difference between *G. ruber* (w) and *N. dutertrei* ($\Delta\delta^{13}C_{r\text{-}d}$). This approach only shifts the $\Delta\delta^{13}C$ curve to more positive values. Values above the horizontal line indicate $\delta^{13}C_{\Sigma CO2}$ values and nutrient concentrations higher as observed in surface sediments. Dashed line - relative abundance of *G. bulloides* of ODP Site 723B.

the Holocene. Deviations to higher $\delta^{13}C$ values occurred also during isotope stage 8. The results of the frequency analyses carried out on the time series of *G. ruber* (w) and *Universa senticosa* $\delta^{13}C$ show similar distributions of spectral power, except for the period of 29,000 yr, where variance is more pronounced in the $\delta^{13}C$ signal of *G. ruber* (w) (Figure 3a). Cross-spectral analysis indicates that both $\delta^{13}C$ records are coherent and in phase with each other at the primary frequency bands of eccentricity, obliquity, and precession. Thus, both time series seem to be controlled equally by the same mechanisms.

To explain the similarities of the two foraminiferal $\delta^{13}C$ records constant nutrient concentrations are required at both sites. With accordance to the modern calibration [*Moos et al.*, submitted] *G. ruber* (w) seems to display nutrient depleted surface waters during the past

307,000 yr, which is also supported by results of *Cayre and Bard* [1999]. Thus, the carbon isotope variations of *G. ruber* (w) indicate changes of Arabian Sea surface water masses and can be used as reference to evaluate nutrient dependent $\delta^{13}C_{\Sigma CO2}$ variations.

Neogloboquadrina dutertrei

The $\delta^{13}C$ values of *N. dutertrei* range from about -0.2 ‰ to 1.1 ‰ and show a higher variability than the *Universa senticosa* record (Figure 2a), which is additionally revealed by cross-spectral analyses (Figure 3b). While *Universa senticosa* shows a high variance in the main orbital periods, *N. dutertrei* has extra spectral power superimposed in the precessional frequency bands of 23,000 yr and 19,000 yr and in sub-Milankovitch periods. The phase relationship between both records indicates a more differentiated timing than found for *Universa senticosa* and *G. ruber* (w). These differences are interpreted in terms of regional $\delta^{13}C_{\Sigma CO2}$ variations superimposed on the global signal in the carbon isotope record of *N. dutertrei*.

$\Delta\delta^{13}C$ r-d

While *G. ruber* (w) documents generally $\delta^{13}C_{\Sigma CO2}$ of nutrient depleted surface waters, *N. dutertrei* is strongly adapted to high nutrient conditions during the upwelling season. Thus, the $\Delta\delta^{13}C_{r\text{-}d}$ gradient displays the inter-annual end member of $\delta^{13}C_{\Sigma CO2}$ depending on variations in nutrient concentrations. During glacial periods the calculated down core $\Delta\delta^{13}C_{r\text{-}d}$ gradient is equal or smaller compared to the recent surface sediments indicating higher nutrient gradients at about 6000 yr, 120,000 yr, 205,000 yr, 240,000, and 265,000 yr (Figure 2b).

The spectral peaks found in the $\Delta\delta^{13}C_{r\text{-}d}$ spectrum allow a clear relation to the $\delta^{13}C$ spectra of *N. dutertrei* and *G. ruber* (w). The spectral power of the $\Delta\delta^{13}C_{r\text{-}d}$ record that is concentrated near the period of Earth's eccentricity depends on the phase angle between $\delta^{13}C$ of *G. ruber* (w) and *N. dutertrei* as derived from the different phase relationships relative to the $\delta^{13}C$ record of *Universa senticosa*. The variance concentrated at the precessional periods as well as in the sub-Milankovitch frequency bands is related to the *N. dutertrei* spectrum with spectral power concentrated at 12,500 yr and 7,700 yr (Figure 3c). Only the period of 29,000 yr is related to *G. ruber* (w). A 29,0000 yr component is neither observed for *N. dutertrei*, nor for the global variations of ΣCO_2. However, this period is also found in a sea

surface temperature record of the southern Indian Ocean and interpreted as a component of monsoon variation related to latent heat transport [*Clemens and Prell*, 1991]. Nevertheless, we found no clear relationship to monsoonal upwelling variations for *G. ruber* (w).

Comparison of Nutrients, Productivity, and Upwelling Intensity

To determine the varying influence of nutrient concentrations and upwelling intensity on the productivity signal we compared the $\Delta\delta^{13}C_{r\text{-}d}$ record of core GeoB 3005 with the relative abundance of *G. bulloides* from ODP Site 723B from the coastal upwelling region off Oman [*Anderson and Prell*, 1991] and with the record of lithogenic grain size of core RC 27-61 [*Clemens and Prell*, 1990] indicating upwelling related productivity and SW monsoon wind strength, respectively. Due to its elevated location on the Owen Ridge the lithogenic component of site RC27-61 depends on eolian dust alone and is unaffected by sediments from the Oman margin and the Indus Fan [*Clemens et al.*, 1991; *Clemens and Prell*, 1990].

Nutrient variations and upwelling related productivity ($\Delta\delta^{13}C_{r\text{-}d}$ - % G. bulloides)

A visual comparison of the $\Delta\delta^{13}C_{r\text{-}d}$ record of core GeoB 3005 with the abundance of *G. bulloides* of ODP Site 723B suggests a general agreement in long-term variations (Figure 2b). In accordance to a confidence level of 80 % the results show a significant coherence for the periods of highest variance in the eccentricity and precessional frequency band (120,000 yr and 23,000 yr) as revealed in Figure 4a. Coherence and phase relationship close to zero indicate the same control mechanisms with similar timing for eccentricity and to a slightly lower degree for precession. In contrast, close to the coherence between both records at 26,000 yr the time of highest *G. bulloides* abundance leads the maximum of $\Delta\delta^{13}C_{r\text{-}d}$ by approximately ¼ cycle.

The results of cross-spectral analyses show a relationship between $\Delta\delta^{13}C_{r\text{-}d}$ and *G. bulloides* abundance at frequencies close to the eccentricity and the precession band indicating that productivity is mainly affected by nutrient variations at these periods. Nevertheless, some differences exist in the distribution of spectral power, and coherence as well as phase angles, indicating changes of productivity (% *G. bulloides*) independent of nutrient variations at periods of 41,000 yr, 26,000, and 17,000 yr. These variations might be controlled by the intensity of upwelling and related monsoonal wind strength. On the other hand, there are nutrient variations at periods of 29,000 yr and 19,000 yr that do not affect

productivity. Possibly these nutrient variations compensated by opposite changes of upwelling intensity.

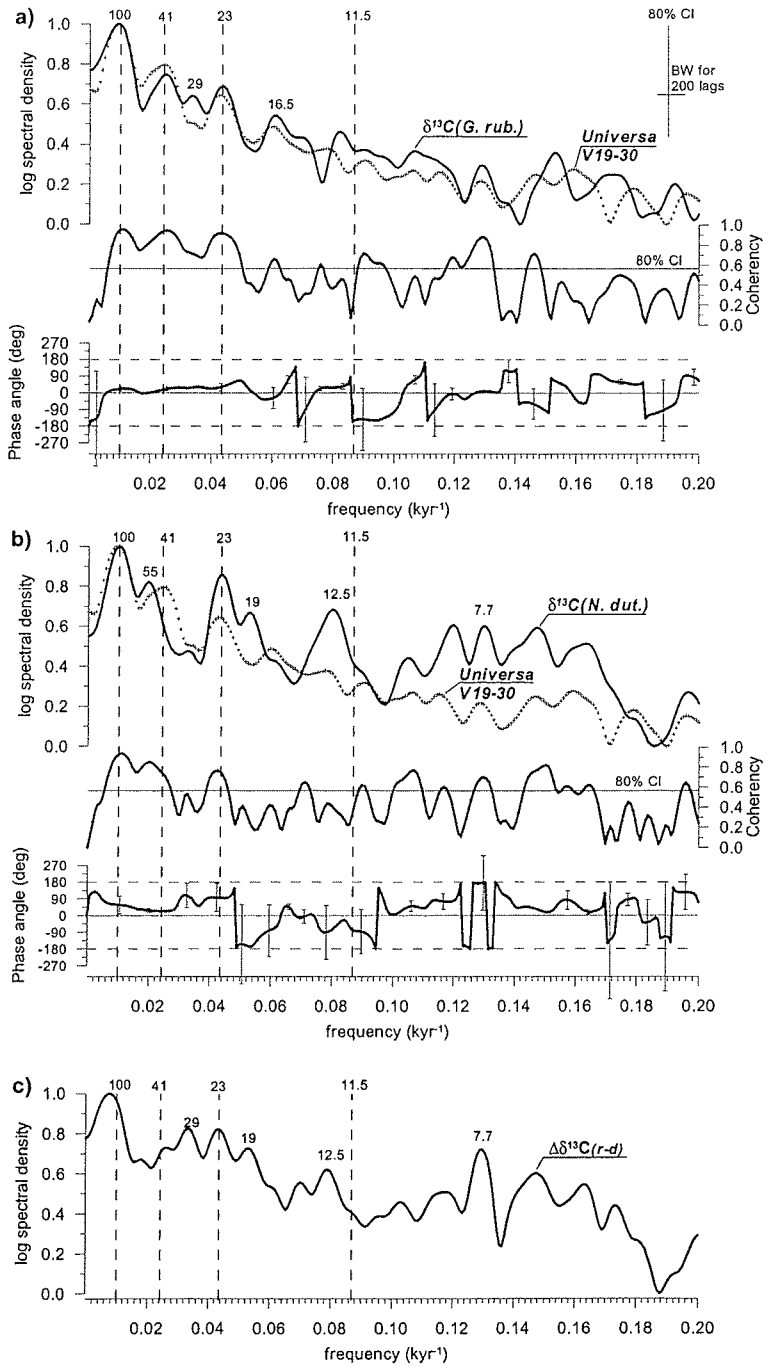

Figure 3: Spectral density, cross-coherency, and phase angles versus frequency. Time series interpolated at 750 yr from 0-307,000 yr. a) $\delta^{13}C$ of *G. ruber* (w) and *Universa senticosa*, b) $\delta^{13}C$ of *N. dutertrei* and *Universa senticosa*, c) carbon isotope difference between *G. ruber* (w) and *N. dutertrei* ($\Delta\delta^{13}C_{r\text{-}d}$).

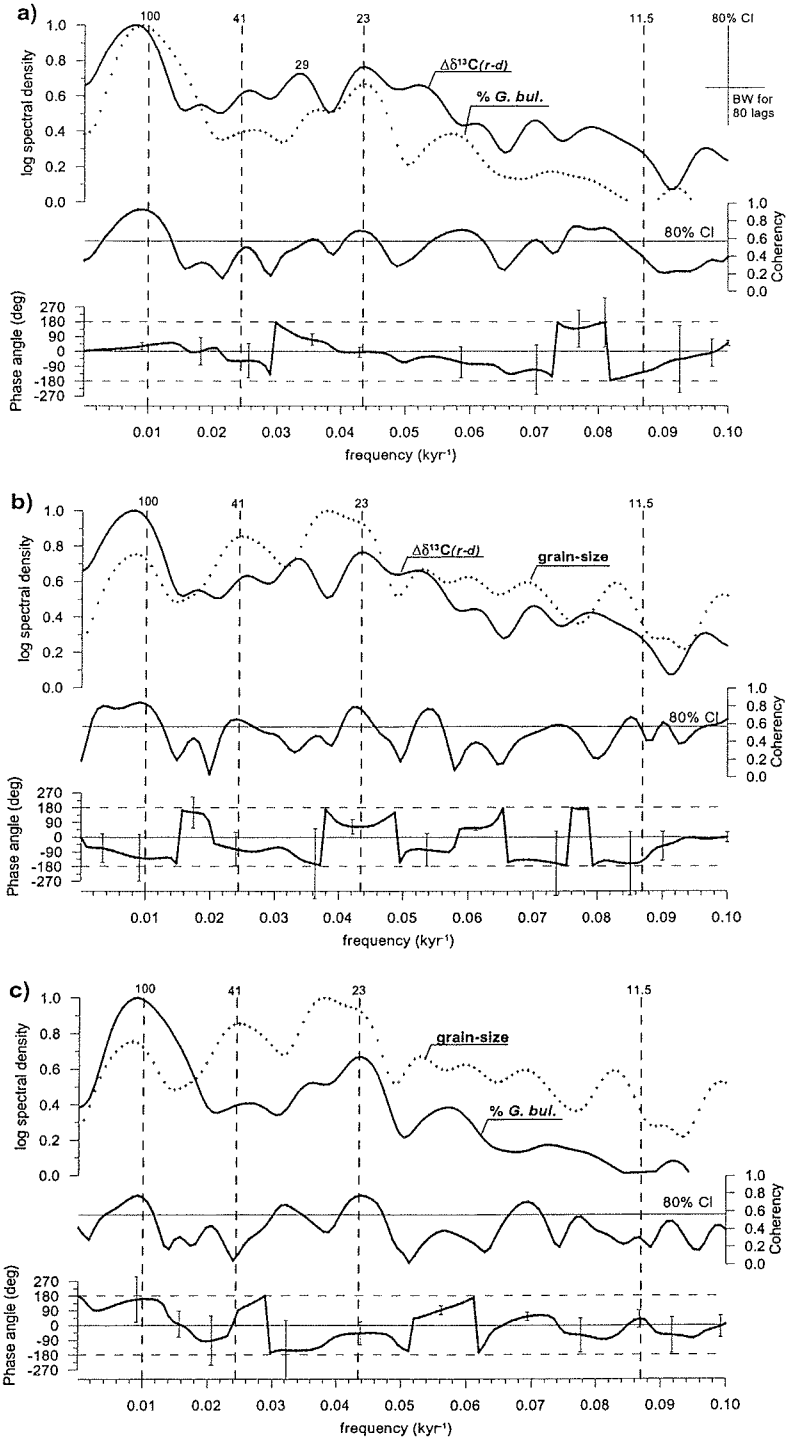

Figure 4. Spectral density, cross-coherency, and phase angles versus frequency. Time series were interpolated at 2000 yr from 4-306,000 yr. a) $\Delta\delta^{13}C_{r\text{-}d}$ (GeoB 3005) and abundance of *G. bulloides* (ODP Site 723B), b), $\Delta\delta^{13}C_{r\text{-}d}$ (GeoB 3005) and lithogenic grain size (RC27-61), c) lithogenic grain size (RC27-61) and the abundance of *G. bulloides* (ODP Site 723B). Note, that the differences of the $\delta^{13}C_{r\text{-}d}$ spectra illustrated in Figure 3 and 4 depend on the different statistical parameters and resolutions of the time series (750 yr and 2000 yr).

Nutrient variations and monsoon wind strength ($\Delta\delta^{13}C_{r\text{-}d}$ - grain size)

The distribution of spectral variance, coherence, and the phase relationship between the records of $\Delta\delta^{13}C_{r\text{-}d}$ and lithogenic grain size, indicating nutrients and monsoon wind strength, respectively, should help to explain the primary features of productivity variations. The results of cross-spectral analyses show significant coherence at the three primary orbital periods including the 19,000 yr component of precession (Figure 4b). The lithogenic grain size contains highest variance at periods from 23,000 yr to 25,000 yr and close to 41,000 yr. Concentration of spectral power in the frequency band of eccentricity is obviously lower compared to $\Delta\delta^{13}C_{r\text{-}d}$ or % *G. bulloides*. The phase angles between $\Delta\delta^{13}C_{r\text{-}d}$ and lithogenic grain size range from a quarter to a half cycle and suggest that enhanced productivity is not driven by these two mechanisms at the same time. The coherence at 19,000 yr and average phase angle of a quarter cycle combined with a large phase uncertainty (indicating instability of the phase relation) might explain the absence of the 19,000 yr component in the productivity record of *G. bulloides*. This could also be true for the frequency band of Earth's obliquity.

Upwelling related productivity and monsoon wind strength (G. bulloides - grain size)

To complete the evaluation of productivity we additionally compared the strength of monsoon winds with productivity intensity, indicated by lithogenic grain size and the relative abundance of *G. bulloides*, respectively. The records are coherent at periods of 23,000 yr and 100,000 yr. The low spectral density of the grain size record and the phase angle in the low frequency domain versus *G. bulloides* suggests low variations of upwelling intensity and a minor influence on productivity for the frequency band of eccentricity. For the frequency band of precession the phase relationship suggests a time lag of about 3,000 yr.

Conclusions

A comparison of the planktic foraminifera *G. ruber* (w) $\delta^{13}C$ with global variations of $\delta^{13}C_{\Sigma CO2}$ derived from the benthic foraminiferal species *Universa senticosa* indicates that *G. ruber* (w) preferred nutrient depleted surface water conditions during the past 307,000 yr. This is also supported by results of *Cayre and Bard* [1999]. Based on a recent calibration and additionally suggested by the strong deviations of *N. dutertrei* versus the global $\delta^{13}C_{\Sigma CO2}$

signal, *N. dutertrei* displays highest nutrient levels of sub-surface water masses affected by upwelling. The carbon isotope difference between *G. ruber* (w) and *N. dutertrei* can be used to trace nutrient gradients in the northwestern Arabian Sea.

The $\Delta\delta^{13}C_{r\text{-}d}$ gradient indicates strong nutrient variations in the upwelling area of the northwestern Arabian Sea during the past 307,000 yr. Variations show significant periodicities close to the primary orbital periods of Earth's eccentricity and precessional components of 23,000 yr and 19,000 yr. Additionally, the distribution of spectral variance indicates variations near the half cycle of precession at 12,500 yr as well as at 7,700 yr.

In a simplified system variations of productivity are interpreted as the residuum of the superimposition of nutrient concentration and upwelling intensity. Geological records of foraminiferal carbon isotope gradients and lithogenic grain size were used to investigate the influence of nutrient availability and monsoon wind strength to productivity as indicated by the relative abundance of *G. bulloides*. The results of cross-spectral analyses suggest that variations of *G. bulloides* are more affected by nutrient availability than by changes in upwelling intensity. Especially at the frequency band of eccentricity and the 23,000 yr component of precession the *G. bulloides* and $\Delta\delta^{13}C_{r\text{-}d}$ records are coherent and in phase with each other. In contrast, the phase relationship between the time series of *G. bulloides* and lithogenic grain size indicates a different timing of productivity and monsoon wind strength. Wind strength and nutrient records seem to be coherent with one another at all significant periods, but are out of phase. Additionally large phase errors might suggest a more differentiated superimposition of both control mechanisms on productivity.

Acknowledgements

We thank captain and crew of R/V *Meteor* for the excellent cooperation during the cruises. The research was funded by the Bundesministerium für Bildung, Wissenschaft, Forschung und Technologie (BMBF) and is part of the NEtherlands BRemen OCeanography (NEBROC) cooperation.

The data presented in this paper are archived in the Pangea database (http://www.pangaea.de).

5. Conclusions

The intention of this thesis is to give a generalised picture of the temporal and regional variations in primary productivity as well as SSTs in the Arabian Sea. The reconstruction of past productivity and SST changes is based on the sedimentary content of TOC and C_{37} alkenones, as well as on the stable carbon isotope composition of planktonic foraminifera, and the ketone unsaturation ratio UK'37, respectively. From this investigation the following conclusions can be drawn:

1. TOC/C_{37} alkenone records indicate periods of high productivity in tune with precessional forcing all over the Arabian Sea. Based on their phase relationship to indicators of monsoonal upwelling as well as boreal summer insolation it is suggested that variations in past primary productivity document a combined signal of moderate SW monsoon and related upwelling intensity and of strengthened and prolonged NE monsoon winds in the western Arabian Sea. In the eastern Arabian Sea the phasing implies maximum productivity due to stronger NE monsoon winds associated with precession-related maxima in ice volume.
2. At the Owen Ridge precession-related changes in past productivity are of only secondary importance as compared to the western Arabian Sea open ocean upwelling region. Here, higher productivity levels are indicated during glacial times. This pattern is attributed to NW-SE displacements of the Findlater Jet axis, which separates the region of upwelling to the northwest from downwelling to the southeast, in tune with glacial-interglacial climate changes.
3. Results of the stable carbon isotope ratio $\delta^{13}C$ of the planktonic foraminifera *G. ruber* (w) and *N. dutertrei* indicate a dissociation of productivity from monsoonal upwelling intensity. Instead, productivity depends mainly on the availability of nutrients, while upwelling intensity of sub-surface water masses itself seems to be of only secondary importance.
4. The alkenone SST signal is not affected by the seasonal productivity pattern in the western Arabian Sea. Alkenone-derived SSTs reflect an annually integrated temperature signal of all seasons and not preferentially the season of upwelling when concomitant highest biogenic fluxes occur.
5. Late Quaternary SST changes are very similar all over the Arabian Sea paralleling the global pattern of glacial-interglacial climate changes. According to the alkenone temperatures MIS 6 remained relatively warm and was not as cold as MIS 3 to 4 and 8,

which is in good agreement with the modulation of precessional insolation by eccentricity.

6. A close comparison between past SSTs in the western and in the eastern Arabian Sea revealed larger differences between both sites during cold periods. Prolonged NE monsoon winds during times of expanded Northern Hemisphere ice-sheets were probably more effective in cooling the winter SSTs in the western Arabian Sea, thereby lowering the annual mean temperature stronger than in the eastern Arabian Sea.

6. References

Altabet, M. A., and W. B. Curry, Testing models of past ocean chemistry using foraminifera $^{15}N/^{14}N$, *Global Biogeochem. Cycles, 3,* 107-119, 1989.

Altabet, M. A., R. Francois, D. W. Murray, and W. L. Prell, Climate-related variations in denitrification in the Arabian Sea from sediment $^{15}N/^{14}N$ ratios, *Nature, 373,* 506-509, 1995.

Anderson, D. M., and W. L. Prell, Coastal upwelling gradient during the late Pleistocene, *Poc. Ocean Drill. Program, Sci. Results, 117,* 265-276, 1991.

Anderson, D. M., J. C. Brock, and W. L. Prell, Physical upwelling processes, upper ocean environment and the sediment record of the southwest monsoon, in *Upwelling Systems: Evolution since the Early Miocene,* edited by C. P. Summerhayes, W. L. Prell, and K.-C. Emeis, *Geol. Soc. Publ., 64,* 121-129, 1992.

Anderson, D. M., and W. L. Prell, The structure of the Southwest Monsoon Winds over the Arabian Sea during the late Quaternary: Observations, simulations, and marine geologic evidence, *J. Geophys. Res., 97,* 15481-15487, 1992.

Anderson, D. M., and W. L. Prell, A 300 kyr record of upwelling off Oman during the late Quaternary: Evidence of the Asian southwest monsoon, *Paleoceanography, 8,* 193-208, 1993.

Antoine, D., and A. Morel, Oceanic primary production 1. Adaption of a spectral light-photosynthesis model in view of application to satellite chlorophyll observations, *Global Biogeochem. Cycles, 10,* 43-55, 1996.

Antoine, D., J.-M. André, and A. Morel, Oceanic primary production 2. Estimation at global scale from satellite (coastal zone color scanner) chlorophyll, *Global Biogeochem. Cycles, 10,* 57-69, 1996.

Bassinot, F. C., L. Beaufort, E. Vincent, L. D. Labeyrie, F. Rostek, P. J. Müller, X. Quidelleur, and Y. Lancelot, Coarse fraction fluctuations in pelagic carbonate sediments from the tropical Indian Ocean: A 1500-kyr record of carbonate dissolution, *Paleoceanography, 9,* 579-600, 1994.

Beaufort, L., Y. Lancelot, P. Camberlain, O. Cayre, E. Vincent, F. Bassinot, and L. Labeyrie, Insolation changes as a major control of equatorial Indian Ocean primary productivity, *Science, 278,* 1451-1454, 1997.

Berger, A. L., Long-term variations of daily insolation and Quaternary climatic change. *J. Atmos. Sci., 35,* 2362-2367, 1978.

Berger, W. H., V. S. Smetacek, and G. Wefer, Ocean productivity and paleoproductivity - an overview, in *Productivity of the Ocean: Present and Past,* edited by W. H. Berger, V. S. Smetacek, and G. Wefer, 1-34, John Wiley & Sons Limited, 1989.

Bigg, G. R., *The Oceans and Climate,* Cambridge University Press, pp. 266, 1996.

Boyle, E. A., Cadmium and $\delta^{13}C$ paleochemical ocean distributions during the stage 2 glacial maximum, *Annu. Rev. Earth Planet. Sci., 20,* 245-287, 1992.

Brassell, S. C., G. Eglinton, I. T. Marlowe, U. Pflaumann, and M. Sarnthein, Molecular stratigraphy: A new tool for climatic assessment, *Nature, 320*, 129-133, 1986.

Brassell, S. C., Applications of biomarkers for delineating marine paleoclimatic fluctuations during the Pleistocene, in *Organic Geochemistry: Principles and Applications* edited by M. H. Engel and S. A. Macko, 699-738, Plenum Press, 1993.

Brock, J. C., and C. R. McClain, Interannual variability in phytoplankton blooms observed in the northwestern Arabian Sea during the Southwest Monsoon, *J. Geophys. Res., 97,* 733-750, 1992.

Brock, J. C., C. R. McClain, D. M. Anderson, W. L. Prell, and W. W. Hay, Southwest monsoon circulation and environments of recent planktonic foraminifera in the northwestern Arabian Sea, *Paleoceanography, 7*, 799-813, 1992.

Brock, J., S. Sathyendranath, and T. Platt, A model study of seasonal mixed-layer primary production in the Arabian Sea, in *Biogeochemistry of the Arabian Sea, 103*, edited by D. Lal, pp. 65-78, Indian Academy of Sciences, 1994.

Brown, J., A. Colling, D. Park, J. Phillips, D. Rothery, and J. Wright, *Ocean Circulation*, The Open University, pp. 238, 1998.

Budziak, D., R. R. Schneider, F. Rostek, P. J. Müller, E. Bard, and G. Wefer, Late Quaternary insolation forcing on total organic carbon and C_{37} alkenone variations in the Arabian Sea, *Paleoceanography, 15*, 307-321, 2000.

Budziak, D., R. R. Schneider, F. Rostek, P. J. Müller, E. Bard, and G. Wefer, Variations of alkenone-derived sea surface temperatures and productivity patterns of C_{37} alkenones in the Arabian Sea during the Late Quaternary, to be submitted to *Earth and Planetary Science Letters*, in prep.

Burkill, P. H., Arabesque: An overview, *Deep-Sea Res. II, 46*, 529-547, 1999.

Cadet, D., Meteorology of the Indian summer monsoon, *Nature, 279,* 761-767, 1979.

Cayre, O., and E. Bard, Planktonic foraminiferal and alkenone records of the last deglaciation from the Eastern Arabian Sea, *Quat. Res., 52*, 337-342, 1999.

Cayre, O., L. Beaufort, and E. Vincent, Paleoproductivity in the equatorial Indian Ocean for the last 260,000 yr: A transfer function based on planktonic foraminifera, *Quat. Sci. Rev., 18,* 839-857, 1999.

Clemens, S. T., and W. L. Prell, Late Pleistocene variability of Arabian Sea summer monsoon winds and continental aridity: Eolian records from the lithogenic component of deep-sea sediments, *Paleoceanography, 5,* 109-145, 1990.

Clemens, S. C., and W. L. Prell, One million year record of summer monsoon winds and continental aridity from the Owen Ridge (Site 722), northwest Arabian Sea, *Proc. Ocean Drill. Program, Sci. Results, 117,* 365-388, 1991.

Clemens, S. C., and W. L. Prell, 1991, Late Quaternary Forcing of Indian Ocean Summer-Monsoon Winds: A comparison of Fourier Model and General Circulation Model Results, *J. Geophys. Res., 96*, 22683-22700, 1991.

Clemens, S., W. Prell, D. Murray, G. Shimmield, and G. Weedon, Forcing mechanisms of the Indian Ocean monsoon, *Nature, 353,* 720-725, 1991.

Colborn, J., The thermal structure of the Indian Ocean, The University Press of Hawaii, 1976.

Conte, M. H., G. Eglinton, and L. A. S. Madureira, Long-chain alkenones and alkyl alkenoates as palaeotemperature indicators: Their production, flux and early sedimentary diagenesis in the Eastern North Atlantic, *Org. Geochem.*, *19*, 287-298, 1992.

Conte, M. H., and G. Eglinton, Alkenone and alkenoate distributions within the euphotic zone of the eastern North Atlantic: Correlation with production temperature, *Deep-Sea Res. I, 40*, 1935-1961, 1993.

Curry, W. B., D. R. Ostermann, M. V. S. Guptha, and V. Ittekkot, Foraminiferal production and monsoonal upwelling in the Arabian Sea: Evidence from sediment traps, in *Upwelling systems: Evolution Since the Early Miocene,* edited by C. P. Summerhayes, W. L. Prell, and K.-C. Emeis, *64, Geol. Soc. Publ.*, 93-106, 1992.

de Leeuw J. W., F. W. van den Meer, W. E. C. Rijpstra, and P. A. Schenk, On the occurence and structural identification of long chain unsaturated ketones and hydrocarbons in sediments, in *Advances in Organic Geochemistry 1979,* edited by A. G. Douglas and J. R. Maxwell), pp. 211-217, Pergamon, 1980.

DeMenocal P., J. Bloemendal, and J. King, A rock-magnetic record of monsoonal dust deposition to the Arabian Sea: Evidence for a shift in the mode of deposition at 2.4 Ma, *Proc. Ocean Drill. Progr., Sci. Res., 117*, 389-407, 1991.

DeMenocal, P. B., and D. Rind, Sensitivity of Asian and African climate to variations in seasonal insolation, glacial ice cover, sea surface temperature, and Asian orography, *J. Geophys. Res., 98*, 7265-7287, 1993.

Duplessy, J.-C., L. D. Labeyrie, N. Kallel, and A. Juillet-Leclerc, Intermediate and deep water characteristics during the last glacial maximum, in *Climate and Geo-Sciences*, edited by A. Berger, Kluwer Academic Publishers, 105-120, 1989.

Emeis, K.-C., Geochemische Auftriebsindikatoren in Sedimenten des Nordwestlichen Arabischen Meeres. Habilarbeit, Christian-Albrechts-Universität, Kiel, Germany, 1993.

Emeis, K.-C., D. M. Anderson, H. Doose, D. Kroon, and D. Schulz-Bull, Sea-surface temperatures and the history of monsoon upwelling in the northwestern Arabian Sea during the last 500,000 years, *Quat. Res.,N.Y., 43,* 355-361, 1995.

Farrimond P., G. Eglinton, and S. C. Brassell, Alkenones in Cretaceous black shales, Blake-Bahama Basin, western North Atlantic, *Org. Geochem., 10*, 897-903, 1987.

Findlater, J., A major low level air current near the Indian Ocean during the northern summer, *Q. J. R. Meteorol. Soc., 95*, 362-380, 1969.

Findlater, J., Mean monthly airflow at low levels over the Indian Ocean, Geophys. Memoirs. Her Majesty's Stationary Office, London, 53 pp, 1971.

Findlater, J., Observational aspects of the low-level cross-equatorial jet stream of the western Indian Ocean, in T.N. Krishnamurti (Editor), *Monsoon Dynamics*. Birkhäuser Verlag, Basel, 1251-1262, 1978.

Gross M. G., and E. Gross, *Oceanography - A view of Earth.* Prentice Hall, pp. 472, 1996.

Haake, B., V. Ittekkot, T. Rixen, V. Ramaswamy, R. R. Nair, and W. B. Curry, Seasonality and interannual variability of particle fluxes to the deep Arabian Sea, *Deep Sea Res., Part I, 40,* 1323-1344, 1993.

Hansell, D. A., and E. T. Peltzer, Spatial and temporal variations of total organic carbon in the Arabian Sea, *Deep Sea Res. Part II, 45,* 2171-2193, 1998.

Hastenrath, S., and P. J. Lamb, *Climatic Atlas of the Indian Ocean*, Univ. of Wisc. Press, Madison, 1979.

Hays J. D., J. A. Lozano, N. Shackleton, and G. Irving, Reconstruction of the Atlantic and western Indian Ocean sectors of the 18,000 B.P Antarctic Ocean, *Geol. Soc. Am. Mem., 145*, 337-374, 1976.

Hemleben, C., W. Roether, and P. Stoffers, *Östliches Mittelmeer, Rotes Meer, Arabisches Meer, Cruise No. 31, 30 December 1994 - 22 March 1995, METEOR-Berichte* 96-4, 282 pp., Universität Hamburg, Hamburg, Germany, 1996.

Imbrie, J., J. D. Hays, D. G. Martinson, A. McIntyre, A. C. Mix, J. J. Morley, N. G. Pisias, W. L. Prell, and N. J. Shackleton, The orbital theory of Pleistocene climate: Support from a revised chronology of the marine $\delta^{18}O$ record, in *Milankovitch and Climate, NATO ASI Ser., Ser. C, 126*, part 1, edited by A. L. Berger, pp. 269-305, D. Reidel, Norwell, Mass., 1984.

Imbrie, J., A. McIntyre, and A. C. Mix, Oceanic response to orbital forcing in the Late Quaternary: Observational and experimental strategies, in *Climate and Geosciences,* edited by A. L. Berger et al., pp. 121-164, Kluwer Acad., Norwell, Mass., 1989.

Ittekkot, V., B. Haake, M. Bartsch, R. R. Nair, and V. Ramaswamy, Organic carbon removal in the sea: The continental connection, in *Upwelling System: Evolution Since the Early Miocene*, edited by C. P. Summerhayes et al., *Geol. Soc. Spec. Pub., 64*, 167-176, 1992.

Jenkins, G. M., and D. G. Watts, *Spectral Analysis and Its Application*, Holden-Day, San Francisco, Ca., 1968.

Kallel, N., L. D. Labeyrie, A. Juillet-Leclerc, and J.-C. Duplessy, A deep hydrological front between intermediate and deep-water masses in the glacial Indian Ocean, *Nature, 333*, 651-655, 1988.

Kutzbach, G., Concepts of monsoon physics in historical perspective: the Indian Monsoon (seventeenth to early twentieth century), in *Monsoons,* edited by J. S. Fein and P. L. Stephens, 159-209, John Wiley & Sons, 1987.

Levitus, S., and T. Boyer, World Ocean Atlas, Vol. 4: Temperature. NOAA Atlas NESDIS 4, U.S.Govt. Printing Office, 1994.

Lourens, L. J., A. Antonarakou, F. J. Hilgen, A. A. M. Van Hoof, C. Vergnaud-Grazzini, and W. J. Zachariasse, Evaluation of the Plio-Pleistocene astronomical timescale, *Paleoceanography, 11,* 391-413, 1996.

Luther, M. E., and J. J. O'Brien, A model of the seasonal circulation in the Arabian Sea forced by observed winds, *Progr. in Oceanogr., 14*, 353-385, 1985.

Luther, M. E., J. J. O'Brien, and W. L. Prell, Variability in upwelling fields in the northwestern Indian Ocean, 1, Model experiments for the past 18,000 years, *Paleoceanography, 5,* 433-445, 1990.

Moos, C. A., G.-J. A. Brummer, G. Ganssen, W. Helder, A. Hupe, R. Kloosterhuis, R. Lendt, R. R. Schneider, and G. Wefer, Seasonal and decadal changes in carbon isotope composition of the north western Arabian Sea, *Deep-Sea Res. I*, in press.

Moos, C., R. Schiebel, R. R. Schneider, and G. Wefer, Stable isotopes in planktic foraminifera recording monsoonal upwelling in the northwestern Arabian Sea, *Mar. Micropal.*, submitted.

Müller, P. J., and E. Suess, Productivity, sedimentation rate, and sedimentary organic matter in the oceans, I, Organic carbon preservation, *Deep Sea Res., Part A, 26*, 1347-1362, 1979.

Müller, P. J., R. Schneider, and G. Ruhland, Late Quaternary PCO_2 variations in the Angola Current: Evidence from organic $\delta^{13}C$ and alkenone temperatures, in *Carbon Cycling in the Glacial Ocean: Constrains on the Ocean's Role in Global Change,* edited by R. Zahn et al., *NATO ASI Ser., Ser. I, 17*, 343-366, 1994.

Müller, P. J., G. Kirst, G. Ruhland, I. von Storch and A. Rosell-Melé, Calibration of the alkenone paleotemperature index UK'37 based on core tops from the eastern South Atlantic and the global ocean (60°N-60°S), *Geochim. et Cosmochim. Acta, 62*, 1757-1772, 1998.

Mulitza, S., H. Arz, S. Kemle-von Mücke, C. Moos, H.-S. Niebler, J. Pätzold, and M. Segl, The South Atlantic carbon isotope record of planktic foraminifera, in *Use Of Proxies In Paleoceanography,* edited by G. Fischer, and G. Wefer, Berlin, New York, Springer, 427-445, 1999.

Murray, D. W., and W. L. Prell, Late Pliocene and Pleistocene climatic oscillations and monsoon upwelling recorded in sediments from the Owen Ridge, northwestern Arabian Sea, in *Upwelling Systems: Evolution Since the Early Miocene*, edited by C. P. Summerhayes W. L., Prell, and K.-C. Emeis, *Geol. Soc. Publ., 64*, 301-321, 1992.

Naidu, P. D., and B. A. Malmgren, A high-resolution record of late Quaternary upwelling along the Oman Margin, Arabian Sea based on planktonic foraminifera, *Paleoceanography, 11,* 129-140, 1996.

Nair, R. R., V. Ittekkot, S. J. Manganini, V. Ramaswamy, B. Haake, E. T. Degens, B. N. Desai, and S. Honjo, Increased particle flux to the deep ocean related to monsoons, *Nature, 338,* 749-751, 1989.

Niitsuma, N., T. Oba, and M. Okada, Oxygen and carbon isotope stratigraphy at Site 723, Oman Margin, *Proc. Ocean Drill. Program, Sci. Results, 117,* 321-341, 1991.

Paillard, D., L. Labeyrie, and P. Yiou, Macintosh program performs time series analysis, *Eos Trans. AGU, 77* (39), 379, 1996.

Pailler, D., F. Rostek, E. Bard, A. van Geen, R. Mortlock, and Y. Zheng, Precession control on sedimentary burial of organic matter and redox sensitive metals in the tropical Indian Ocean, *Mineral. Mag., 62A,* 1122-1123, 1998.

Paropkari, A. L., C. Prakash Babu, and A. Mascarenhas, A critical evaluation of depositional parameters controlling the variability of organic carbon in Arabian Sea sediments, *Mar. Geol., 107*, 213-226, 1992.

Paropkari, A. L., A. Mascarenhas and C. Prakash Babu, Comment on "Lack of enhanced preservation of organic matter in sediments under the oxygen minimum on the Oman Margin" by T. F. Pedersen, G. B. Shimmmield, and N. B. Price, *Geochim. et Cosmochim. Acta*, 57, 2399-2401, 1993.

Pedersen, T. F., G. B. Shimmield, and N. B. Price, Lack of enhanced preservation of organic matter in sediments under the oxygen minimum on the Oman Margin, *Geochim. Cosmochim. Acta, 56,* 545-551,1992.

Peeters, F., E. Ivanova, S. Conan, G.-J. Brummer, G. Ganssen, S. Troelstra, and J. v. Hinte, A size analysis of planktic foraminifera from the Arabian Sea, *Mar. Micropal., 36*, 31-63, 1999.

Petit, J. R., J. Jouzel, D. Raynaud, N. I. Barkov, J.-M. Barnola, I. Basile, M. Bender, J. Chappellaz, M. Davis, G. Delaygue, M. Delmotte, V. M. Kotlyakov, M. Legrand, V. Y. Lipenkov, C. Lorius, L. Pépin, C. Ritz, E. Saltzman, and M. Stievenard, Climate and atmospheric history of the past 420,000 years from the Vostok ice core, Antarctica, *Nature, 399*, 429-436, 1999.

Pisias, N. G., W. Prell, F. Prahl, M. Delaney, D. Lea, J. Jasper, B. Popp, G. Rau, R. Murray, D. McCorkle, D. Rea, L. Derry, and Workshop Participants, Marine aspects of Earth System History (MESH), *Proxy Development Workshop Report,* Corvallis, Oregon, pp. 1-75, 1995.

Prahl, F. G., and S. G. Wakeham, Calibration of unsaturated patterns in long-chain ketone composition for paleotemperature assessment, *Nature, 330*, 367-369, 1987.

Prahl, F. G., L. A. Muehlhausen, and D. L. Zahnle, Further evaluation of long-chain alkenones as indicators of paleoceanographic conditions, *Geochim. et Cosmochim. Acta, 52*, 2303-2310, 1988.

Prell, W. L., and H. F. Streeter, Temporal and spatial patterns of monsoonal upwelling along Arabia: A modern analogue for the interpretation of Quaternary SST anomalies, *J. Mar. Res., 40*, 143-155, 1982.

Prell, W. L., Monsoonal climate of the Arabian Sea during the late Quaternary: A response to changing solar radiation, in *Milankovitch and Climate, NATO ASI Ser., Ser. C, 126*, part 1, edited by A. L. Berger et al., pp. 349-366, D. Reidel, Norwell, Mass., 1984a.

Prell, W. L., Variation of monsoonal upwelling: A response to changing solar radiation, in *Geophysical Monograph Series*, edited by J. E. Hansen, and T. Takahasi, T., Washington, D.C., American Geophysical Union, *29*, 48-57, 1984b.

Prell, W. L., and J. E. Kutzbach, Monsoon variability over the past 150,000 years, *J. Geophys. Res., 92,* 8411-8425, 1987.

Prell, W. L., and J. E. Kutzbach, Sensitivity of the Indian monsoon to forcing parameters and implications for its evolution, *Nature, 360,* 647-652, 1992.

Prell, W. L., and E. Van Campo, Coherent response of Arabian Sea upwelling and pollen transport to late Quaternary monsoonal winds, *Nature, 323*, 526-528, 1986.

Rao, R. R., R. L. Molinari, and J. F. Festa, Evolution of the climatological near-surface thermal structure of the tropical Indian Ocean, 1, Description of mean monthly layer depth, and sea surface temperature, surface current, and surface meteorological fields, *J. Geophys. Res., 94,* 10,801-10,815, 1989.

Reichart, G. J., L. J. Lourens, and W. J. Zachariasse, Temporal variability in the northern Arabian Sea oxygen minimum zone (OMZ) during the last 225,000 years, *Paleoceanography, 13,* 607-621, 1998.

Rixen, T., B. Haake, and V. Ittekkot, Coupling between SW monsoon-related surface and deep ocean processes as discerned from continuous particle flux measurements and correlated satellite data, *J. Geophys. Res., 101,* 28569-28582, 1996.

Rostek, F., G. Ruhland, F. C. Bassinot, P. J. Müller, L. D. Labeyrie, Y. Lancelot, and E. Bard, Reconstructing sea surface temperature and salinity using $\delta^{18}O$ and alkenone records, *Nature, 364,* 319-321, 1993.

Rostek, F., G. Ruhland, F. C. Bassinot, L. Beaufort, P. J. Müller, and E. Bard, Fluctuations of the Indian monsoon regime during the last 170,000 years: Evidence from sea surface temperature, salinity and organic carbon records, in *Global Change and Precipitation,* edited by M. Debois and F. Desalmand, *NATO ASI Ser., Ser. I, 26,* 27-51, 1994.

Rostek, F., E. Bard, L. Beaufort, C. Sonzogni, and G. Ganssen, Sea surface temperature and productivity records for the past 240 kyr in the Arabian Sea, *Deep Sea Res. Part II, 44,* 1461-1480, 1997.

Sarnthein, M., U. Pflaumann, R. Ross, R. Tiedemann, and K. Winn, Transfer functions to reconstruct ocean palaeoproductivity: A comparison, in *Upwelling Systems: Evolution Since the Early Miocene*, edited by C. S. Summerhayes, W. L. Prell, and K.-C. Emeis, *Geol. Soc. Spec. Publ., 64,* 411-427, 1992.

Schneider, R., P. J. Müller, and G. Ruhland, Late Quaternary surface circulation in the east equatorial South Atlantic: Evidence from alkenone sea surface temperatures, *Paleoceanogr., 10,* 197-219, 1995.

Schneider, R. R. P. J. Müller, G. Ruhland, G. Meinecke, H. Schmidt, and G. Wefer, Late Quaternary surface temperatures and productivity in the east-equatorial South Atlantic: Response to changes in trade/monsoon wind forcing and surface water advection, in: *The South Atlantic: Present and Past*, edited by G. Wefer, W. H. Berger, G. Siedler and D. J. Webb, Springer-Verlag, Heidelberg, pp. 527-551, 1996.

Schneider, R. R., P. J. Müller, and R. Acheson, Atlantic alkenone sea-surface temperature records - Low versus mid latitudes and differences between Hemispheres, in *Reconstructing Ocean History: A Window into the Future*, edited by F. Abrantes and A. Mix, pp. 33-55, Kluwer Academic / Plenum Publishers, 1999.

Schott, F., Monsoon response of the Somali Current and associated upwelling, *Prog. Oceanogr., 12*, 357-381, 1983.

Schubert, C. J., J. Villanueva, S. E. Calvert, G. L. Cowie, U. von Rad, H. Schulz, U. Berner, and H. Erlenkeuser, Stable phytoplankton community structure in the Arabian Sea over the past 200,000 years, *Nature, 394,* 563-566, 1998.

Schulte, S., F. Rostek, E. Bard, J. Rullkötter, and O. Marchal, Variations of oxygen-minimum and primary productivity recorded in sediments of the Arabian Sea, *Earth Planet. Sci. Lett., 173*, 205-221, 1999.

Schulz, M., and K. Stattegger, Spectrum: Spectral analysis of unevenly spaced paleoclimatic time series, *Comput. & Geosci., 23,* 929-945, 1997.

Schulz, H., U. von Rad, and H. Erlenkeuser, Correlation between Arabian Sea and Greenland climate oscillations of the past 110,000 years. *Nature, 393,* 54-57, 1998.

Seibold E., and W. H. Berger, *The sea floor - an introduction to marine geology*, Springer, pp. 356, 1993.

Shackleton, N. J., J. Imbrie, and M. A. Hall, Oxygen and carbon isotope record of East Pacific core V19-30: Implications for the formation of deep water in the late Pleistocene North Atlantic, *Earth Plan. Sci. Lett., 65*, 233-244, 1983.

Shetye, S. R., A model study of the seasonal cycle of the Arabian Sea surface temperature, *J. Mar. Res., 44,* 242-251, 1986.

Shimmield, G. B., S. R. Mowbray, and G. P. Weedon, A 350 ka history of the Indian Southwest Monsoon: Evidence from deep-sea cores, northwest Arabian Sea, *Trans. Roy. Soc. Edingburgh Earth Sci., 81,* 289-299, 1990.

Sirocko, F., M. Sarnthein, H. Erlenkeuser, H. Lange, M. Arnold, and J.-C. Duplessy, Century-scale events in monsoonal climate over the past 24,000 years, *Nature, 364,* 322-324, 1993.

Sirocko, F., Deep-sea sediments of the Arabian Sea: A paleoclimatic record of the Southwest-Asian summer monsoon, *Geologische Rundschau, 80/3*, 557-566, 1997.

Smith, S. L., L. A. Codispoti, J. M. Morrison, and R. T. Barber, The 1994-1996 Arabian Sea Expedition: An integrated, interdisciplinary investigation of the response of the northwestern Indian Ocean to monsoonal forcing, *Deep-Sea Res. II, 45*, 1905-1915, 1998.

Sonzogni, C., E. Bard, F. Rostek, and D. Dollfus, Temperature and salinity effects on alkenone ratios measured in surface sediments from the Indian Ocean, *Quat. Res., 47*, 344-355, 1997,a.

Sonzogni, C., E. Bard, F. Rostek, R. Lafont, A. Rosell-Melé, and G. Eglinton, Core-top calibration of the alkenone index vs sea surface temperature in the Indian ocean, *Deep Sea Res., Part II, 44,* 1445-1460, 1997,b.

Steens, T. N. F., G. Ganssen, and D. Kroon, Oxygen and carbon isotopes in planktonic foraminifera as indicators of upwelling intensity and upwelling-induced high productivity in sediments from the northwestern Arabian Sea, in *Upwelling Systems: Evolution Since the Early Miocene,* edited by C. P. Summerhayes, W. L. Prell, and K.-C. Emeis, *Geol. Soc. Spec. Pub., 64*, 107-119, 1992.

Swallow, J. C., and M. Fieux, Historical evidence for two gyres in the Somali Current, *J. of Mar. Res., 40*, 747-755, 1982.

Swallow, J. C., Some aspects of the physical oceanography of the Indian Ocean, *Deep Sea Res., 31,* 639-650, 1984.

Tomczak, M., and J. S. Godfrey, *Regional Oceanography: An Introduction*, Pergamon Press, 1994.

Van Campo, E., J.-C. Duplessy, and M. Rossignol-Strick, Climatic conditions deduced from a 150-kyr oxygen isotope-pollen record from the Arabian Sea, *Nature, 296,* 56-59, 1982.

Verardo, D. J., P. N. Froelich, and A. McIntyre, Determination of organic carbon and nitrogen in marine sediments using the Carlo Erba NA-1500 Analyzer, *Deep Sea Res., 37,* 157-165, 1990.

Volkman, J. K., G. Eglinton, E. D. S. Corner, and J. R. Sargent, Novel unsaturated straight-chain C_{37}-C_{39} methyl and ethyl ketones in marine sediments and a coccolithophore *Emiliania huxleyi, Advances in Organic Geochemistry 1979, 12*, 219 - 227, 1980.

Volkman, J. K., S. M. Barrett, S. I. Blackburn, and E. L. Sikes, Alkenones in Gephyrocapsa oceanica: Implications for studies of paleoclimate, *Geochim. Cosmochim. Acta, 59*, 513-520, 1995

Warren, B. A., Ancient and medieval records of the monsoon winds and currents of the Indian Ocean, in *Monsoons* edited by J. S. Fein and P. L. Stephens,135-158, John Wiley & Sons, 1987.

Weaver P. P. E., M. R. Chapman, G. Eglinton, M. Zhao, D. Rutledge, and G. Read, Combined coccolith, foraminiferal, and biomarker reconstruction of the paleoceanographic conditions over the past 120 kyr in the northern North Atlantic (59°N, 23°W), *Paleoceanogr., 14*, 336-349, 1999.

Webster, P. J., The elementary monsoon, in *Monsoons,* edited by J. S. Fein and P. L. Stephens, pp. 3-32, John Wiley, New York, 1987.

Wefer G., W. H. Berger, J. Bijma, and G. Fischer, Clues to ocean history: a brief overview of proxies, in *Use of Proxies in Paleoceanography - Examples from the South Atlantic* edited by G. Fischer and G. Wefer, pp. 1-68, Springer, Berlin, 1999.

Wyrtki, K., *Oceanographic Atlas of the International Indian Ocean Expedition,* 531 pp., U.S. Govt. Print. Off., Washington D.C., 531 pp, 1971.

Wyrtki, K., Physical oceanography of the Indian Ocean, in *The Biology of the Indian Ocean* edited by B. Zeitschel and S. A. Gerlach, 18-36, Springer-Verlag, New York, 1973.

Young, J. A., Physics of monsoons: the current view, in *Monsoons,* edited by J. S. Fein and P. L. Stephens, 211-243, John Wiley & Sons, 1987.